Protein kinase D2 drives chylomicron-mediate lipid transport in the intestine and promotes obesity

♦♦♦♦♦

Die Proteinkinase D2 treibt den Chylomicron-vermittelten Lipidtransport im Darm an und fördert Fettleibigkeit

Doctoral thesis for a doctoral degree

at the Graduate School of Life Sciences,

Julius-Maximilians-Universität Würzburg,

Section Biomedicine

Submitted by

Jonathan Trujillo Viera

from Sogamoso, Colombia

Würzburg, June 2021

Submitted on: _____

Office stamp

Members of the Thesis Commiitee:

Chairperson:	Prof. Dr. med. Manfred Gessler
Primary Supervisor:	Dr. Grzegorz Sumara
Supervisor (Second):	Prof. Dr. Hermann Schindelin
Supervisor (Third):	Dr. rer nat. Mohamed Hankir
Supervisor (Fourth):	

Date of Public Defence: _____

Date of Receipt of Certificates: _____

ABSTRACT

Obesity and associated metabolic syndrome are growing concerns in modern society due to the negative consequences for human health and well-being. Cardiovascular diseases and type 2 diabetes are only some of the pathologies associated to overweight. Among the main causes are decreased physical activity and food availability and composition. Diets with high content of fat are energy-dense and their overconsumption leads to an energy imbalance, which ultimately promotes energy storage as fat and obesity. Aberrant activation of signalling cascades and hormonal imbalances are characteristic of this disease and members of the Protein Kinase D (PKD) family have been found to be involved in several mechanisms mediating metabolic homeostasis. Therefore, we aimed to investigate the role of Protein Kinase D2 (PKD2) in the regulation of metabolism. Our investigation initiated with a mice model for global PKD2 inactivation, which allowed us to prove a direct involvement of this kinase in lipids homeostasis and obesity. Inactivation of PKD2 protected the mice from high-fat diet-induced obesity and improved their response to glucose, insulin and lipids. Furthermore, the results indicated that, even though there were no changes in energy intake or expenditure, inactivation of PKD2 limited the absorption of fat from the intestine and promoted energy excretion in feces. These results were verified in a mice model for specific deletion of intestinal PKD2. These mice not only displayed an improved metabolic fitness but also a healthier gut microbiome profile. In addition, we made use of a small-molecule inhibitor of PKD in order to prove that local inhibition of PKD2 in the intestine was sufficient to inhibit lipid absorption. The usage of the inhibitor not only protected the mice from obesity but also was efficient in avoiding additional body-weight gain after obesity was pre-established in mice. Mechanistically, we determined that PKD2 regulates lipids uptake in enterocytes by phosphorylation of Apolipoprotein A4 (APOA4) and regulation of chylomicron-mediated triglyceride absorption. PKD2 deletion or inactivation increased abundance of APOA4 and decreased the size of chylomicrons and therefore lipids absorption from the diet. Moreover, intestinal activation of PKD2 in human obese patients correlated with higher levels of triglycerides in circulation and a detrimental blood profile. In conclusion, we demonstrated that PKD2 is a key regulator of dietary fat absorption in murine and human context, and its inhibition might contribute to the treatment of obesity.

ZUSAMMENFASSUNG

Fettleibigkeit und das damit verbundene metabolische Syndrom stellt in der modernen Gesellschaft aufgrund der negativen Folgen für die menschliche Gesundheit und das Wohlbefinden ein zunehmendes Problem dar. Herz-Kreislauf-Erkrankungen und Typ-2-Diabetes sind nur einige der mit Übergewicht verbundenen Pathologien. Zu den Hauptursachen zählen eine verminderte körperliche Aktivität sowie die Verfügbarkeit und Zusammensetzung von Nahrungsmitteln. Diäten mit hohem Fettgehalt haben eine hohe Energiedichte und ihr übermäßiger Konsum führt zu einem Energieungleichgewicht, das letztendlich die Energiespeicherung als Fett und Fettleibigkeit fördert. Aberrante Aktivierung von Signalkaskaden und hormonelle Ungleichgewichte sind charakteristisch für diese Krankheit, und es wurde festgestellt, dass Mitglieder der Protein Kinase D (PKD) -Familie an mehreren Mechanismen der metabolischen Homöostase beteiligt sind. Daher zielten wir darauf ab die Rolle der Proteinkinase D2 (PKD2) bei der Regulation des Stoffwechsels zu untersuchen. Unsere Untersuchung begann mit einem Mäusemodell für die globale PKD2-Inaktivierung, welches es uns ermöglichte, eine direkte Beteiligung dieser Kinase an der Lipidhomöostase und Fettleibigkeit nachzuweisen. Die Inaktivierung von PKD2 schützte die Mäuse vor fettreicher diätbedingter Fettleibigkeit und verbesserte ihre Reaktion auf Glukose, Insulin und Lipide. Darüber hinaus zeigten die Ergebnisse, dass die Inaktivierung von PKD2 die Absorption von Fett über den Darm begrenzte und die Energieausscheidung im Kot förderte, obwohl sich die Energieaufnahme oder der Energieverbrauch nicht änderten. Diese Ergebnisse wurden in einem Mäusemodell mit spezifischer Deletion von intestinaler PKD2 verifiziert. Diese Mäuse zeigten nicht nur eine verbesserte metabolische Fitness, sondern auch ein gesünderes Darmmikrobiomprofil. Zusätzlich verwendeten wir einen niedermolekularen PKD-Inhibitor, um zu beweisen, dass die lokale Hemmung von PKD2 im Darm ausreicht, um die Lipidabsorption zu hemmen. Die Verwendung des Inhibitors schützte die Mäuse nicht nur vor Fettleibigkeit, sondern verhinderte auch wirksam eine zusätzliche Gewichtszunahme, nachdem bei Mäusen bereits Fettleibigkeit festgestellt worden war. Mechanistisch haben wir festgestellt, dass PKD2 die Lipidaufnahme in Enterozyten durch Phosphorylierung von Apolipoprotein A4 (APOA4) und Regulation der Chylomicron-vermittelten Triglyceridabsorption reguliert. Die Deletion oder

Inaktivierung von PKD2 erhöhte die Häufigkeit von APOA4 und verringerte die Größe der Chylomikronen und damit die Lipidabsorption aus der Nahrung. Darüber hinaus korrelierte die intestinale Aktivierung von PKD2 bei adipösen Patienten mit höheren Triglyceridspiegeln im Kreislauf und einem schädlichen Blutprofil. Zusammenfassend haben wir gezeigt, dass PKD2 ein Schlüsselregulator für die Aufnahme von Nahrungsfett im murinen und menschlichen Kontext ist und seine Hemmung zur Behandlung von Fettleibigkeit beitragen könnte.

TABLE OF CONTENTS

1. INTRODUCTION

1.1. Obesity and different organs involved in metabolism.

Excessive calorie intake and decreased energy expenditure have led to the overwhelming epidemic of obesity and overweight. Recent data from the World Health Organization calculates that around 40% of the adult population are overweight, including a significant number of 650 million of adults classified as obese (WHO 2020). The consequences of excessive weight accumulation are detrimental for the whole organism since overweight and obesity are directly related to the development of cardiovascular diseases, dyslipidemia, musculoskeletal problems, insulin resistance and type 2 diabetes, fatty liver disease, and some types of cancer. Metabolic syndrome (a combination of several of the previously mentioned diseases) is highly due to excessive fat accumulation and, therefore, weight loss is the direct target for the treatment of metabolic syndrome (Bagchi and Preuss 2007).

The maintenance of an energy and nutrients balance is influenced by several aspects including hormones, diet content, fitness status, genetic predisposition and social environment (Brahmbhatt 2017). Physiologically, this balance is orchestrated by the cross talk of several organs, which together control the uptake, processing, storage, usage and excretion of nutrients (Kim 2016). The hypothalamus in the brain responds to several stimuli (including leptin secreted by adipose tissue and blood sugar levels) to control appetite and energy homeostasis. The white adipose tissue works as a storage organ for accumulation of energy as triglycerides (TG) that are released during fasting periods or under a high-energy demand like exercise. Furthermore, adipose tissue maintains an active interaction with other organs via the release of adipokines, the sensing of insulin and free fatty acids in circulation, and the neural innervation. The brown adipose tissue accumulates energy likewise white adipose tissue but with a different purpose: to convert triglycerides into heat in the process of non-shivering thermogenesis. The skeletal muscle also plays an important role in energy metabolism since it utilizes high amounts of energy in order to produce ATP, especially during exercise. Other important organ involved in energy homeostasis is the liver because of its plasticity regarding the anabolism and catabolism of all types of nutrients,

specially carbohydrates and lipids. The liver not only regulates nutrients levels in circulation but also contributes to the storage, synthesis and degradation of different substances and metabolites (Kahn and Flier 2000, Kim 2016). Finally, another organ, which has been underestimated in the energy homeostasis equation, is the small intestine. However, it is a determinant organ since it controls nutrients absorption, excretion and signaling to other organs including pancreas and brain (Bradley, Zwingelstein et al. 2011, Kraus, Yang et al. 2015).

In conclusion, energy homeostasis comprises a series of structured, complex and crucial process, which depend on a correct functioning of several organs. Imbalances in the components of this network might lead to the development of overweight and the associated metabolic consequences.

1.1.1. Energy balance / Metabolizable energy.

During the metabolic studies, several factors need to be quantified in order to explore different pathways that might be affected by pharmacological treatments, genetic modifications or as a response to stimuli. Metabolic phenotyping of mice is used to assess the energy balance and it opens up different metabolic pathways that might be affected by these modifications and, consequently, the predisposition to the development of obesity (Tschöp, Speakman et al. 2012).

On one side of the energy equation, the energy consumption quantifies not only the energy consumed but also the efficiency in the absorption. The food consumed can be easily measured and converted into energy with the caloric content of the food whereas the absorption efficiency measures urinary and fecal energy content to calculate how much of the energy consumed was actually absorbed and it is available as metabolizable energy (reviewed in (Grobe 2017) and (Rozman, Klingenspor et al. 2014)).

On the other hand, it is necessary to measure the energy output/expenditure. This measurement includes basal metabolic rate, thermoregulation, diet-induced thermogenesis, and physical activity. The complete set of elements contributing to energy expenditure are mostly measured by the method of indirect calorimetry in metabolic cages. The quantification is made from rates of oxygen consumption and

carbon dioxide production measured as changes in the concentration in the respirometry chamber. Indirect calorimetry also allows to calculate the respiratory exchange rate as an indicator of fuel selection (carbohydrate or lipids). The metabolic cages also offer the possibility to quantify physical activity by measuring photoelectric beam interruptions or running wheel revolutions. See Fig 1. (reviewed in (Grobe 2017) and (Rozman, Klingenspor et al. 2014)).

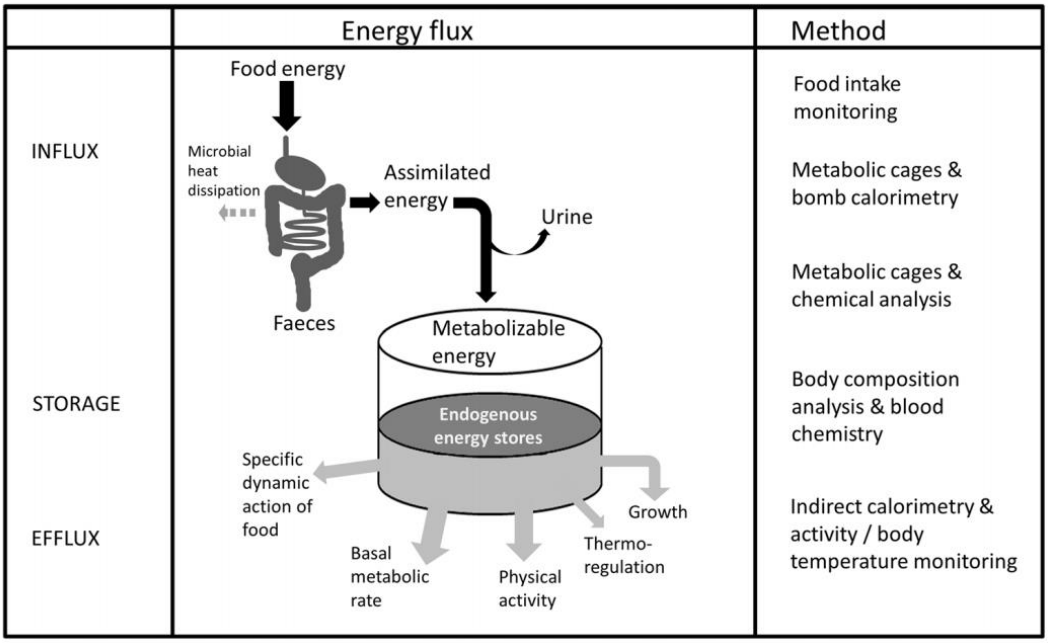

Fig 1. Components of the energy balance equation.

From: (Rozman, Klingenspor et al. 2014)

To sum up, the processes involved in energy uptake and metabolization might be affected by specific conditions or gene alterations. The use of metabolic cages, bomb calorimeter and food analysis enable the metabolic phenotyping and identification of possible mechanisms of action.

1.2. Intestine as a metabolically active organ.

The small intestine is best known for its function in the absorption of nutrients. However, growing evidence suggests that it plays an important role in the whole body energy homeostasis (Bradley, Zwingelstein et al. 2011). Anatomically, the small intestine can be divided in three main sections: duodenum, jejunum and ileum. They

are very similar and anatomically difficult to distinguish. However, their functions make them different from each other. The small intestine is attached by the mesentery and it is connected to the superior mesenteric artery, superior mesenteric vein, lacteals, biliary and pancreatic ducts and nerves (DeSesso and Jacobson 2001). Four layers compose the intestinal wall (from outermost to innermost): serosa, which envelops the intestine; muscularis, in charge of contractibility; submucosa, which is a connective tissue containing vessels, nerves and immune cells; and mucosa (DeSesso and Jacobson 2001, Bass and Wershil 2016) see Fig 2. The mucosa is the most active part of the intestine. It contains projections and insertions denominated villi and crypts respectively. The crypts are particular in the sense that they contain Paneth cells and stem cells. Paneth cells produce antimicrobial proteins while stem cells have an intense mitotic activity, which allows them to replenish the constant renewal of epithelial cells. On the other hand, the villi contain a variety of cells with several functions including enterocytes, goblet cells and enteroendocrine cells. The enterocytes or absorptive cells contain the microvilli in the brush border. These are micro protuberances (only visible by electron microscopy) that increase up to 40-fold the absorptive surface of the villi (Bass and Wershil 2016). Goblet cells are dispersed in between the absorptive cells and produce mucin and other mucus components to protect and lubricate the intestinal lumen (Pelaseyed, Bergström et al. 2014). The last group of cells in the mucosa are the enteroendocrine cells which produce peptides with paracrine and endocrine effects (Bass and Wershil 2016).

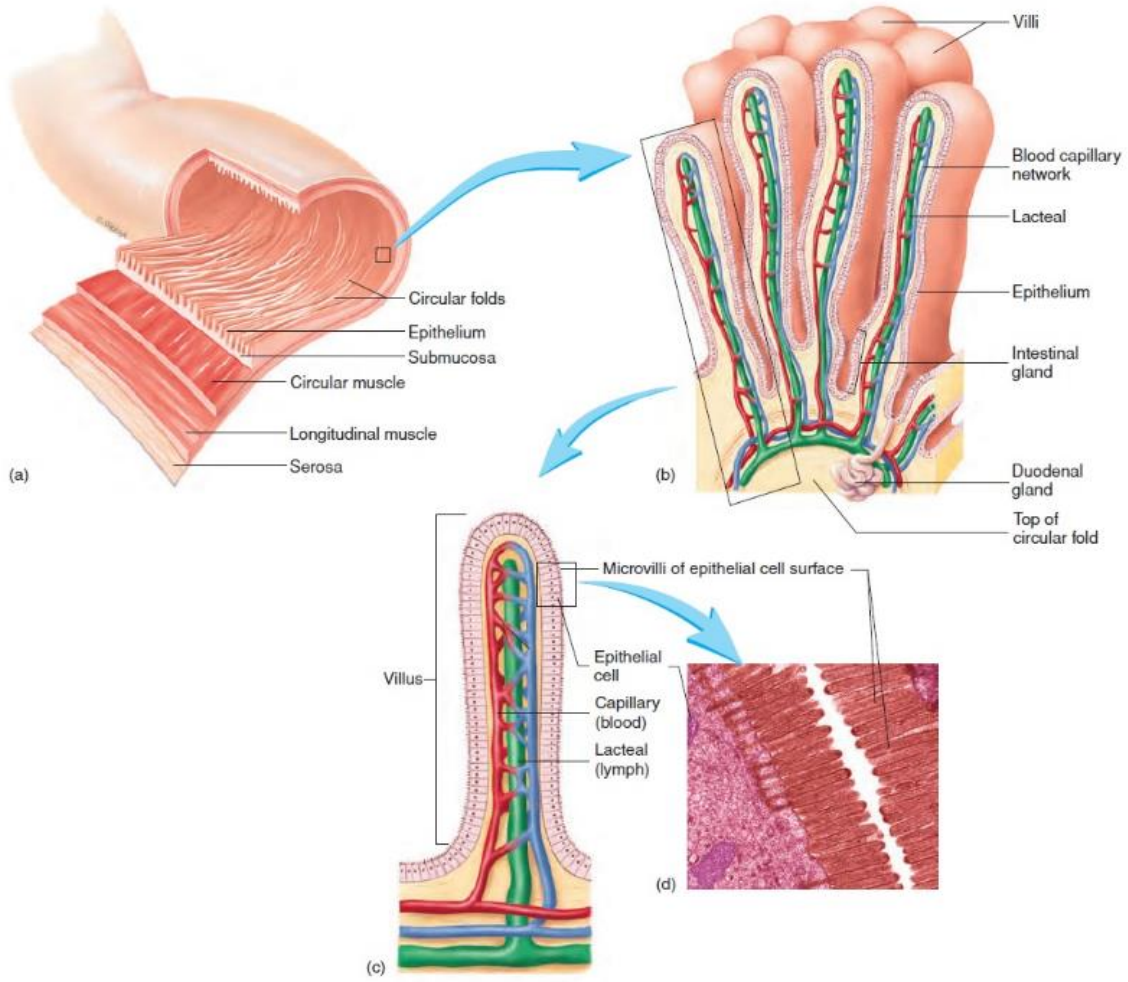

Fig 2. Intestinal anatomy.

From: (Brainkart 2021)

The release of several peptides (including incretins) allows the intestine to interact with the pancreas, brain, liver, and adipose tissue among others (see Fig 3). In response to food ingestion, several incretins like GLP-1 and GIP are released from enteroendocrine L-cells in the distal intestine and in the proximal intestine respectively. Incretins have shown an inverse correlation with obesity and glucose intolerance by promoting insulin secretion, β-cell proliferation and protection, and suppressing appetite. The release of peptide YY (PYY) by enteroendocrine L-cells is also stimulated by feeding. This peptide reduces acute food consumption by inhibiting gastro-intestinal functions, which delays digestion and increases satiation (Reviewed in (Wren and Bloom 2007)). In addition, microbiota is another important regulator of energy metabolism. There are millions of microorganisms located in the small and

large intestines (Bäckhed, Ley et al. 2005). Human and mice data have shown the central role of the diet in the regulation of microbiota composition but also a regulation of adiposity by the microbiota (Ley, Turnbaugh et al. 2006). Genomic analysis have shown an increase in the proportion of *Firmicutes* and a decrease in the case of *Bacteroidetes* in different models of obesity (Turnbaugh, Ley et al. 2006) . Microbiota composition determines the bioavailability of complex carbohydrates, vitamin synthesis and maturation of the immune system (Mazmanian, Liu et al. 2005). Development of inflammatory bowel disease, gastric carcinoma and obesity are also highly dependent on a healthy and balanced microbiota (Bäckhed, Ley et al. 2005).

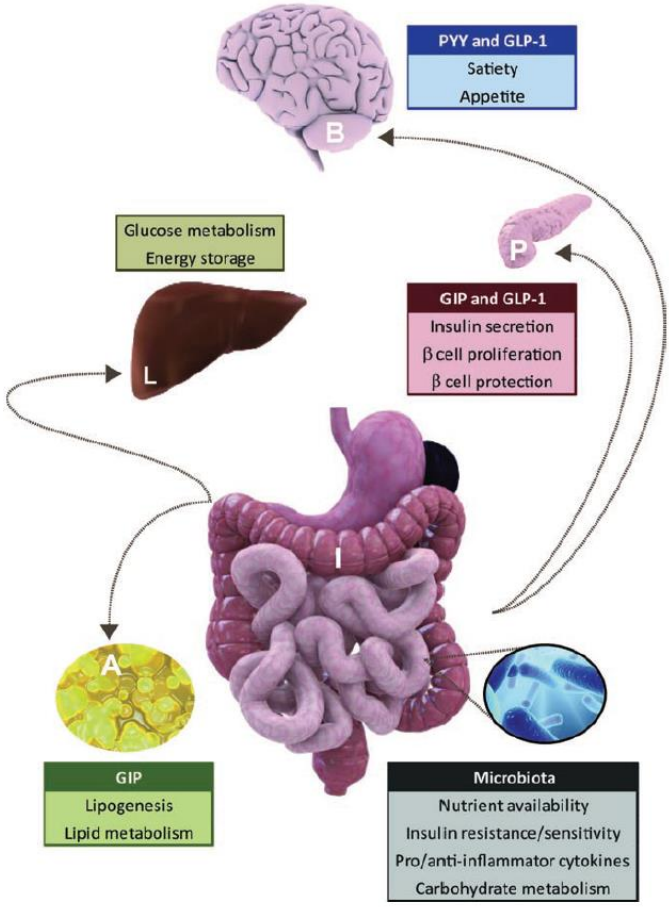

Fig 3. Intestinal cross-talk with other organs.

From: (Bradley, Zwingelstein et al. 2011)

In conclusion, the intestine is a specialized organ, which is in charge of not only nutrients processing and absorption but also regulates energy metabolism mainly by

two mechanisms: by the secretion of peptides (which signal several organs) and by hosting and maintaining an adequate balance of the microbiota.

1.3. The process of nutrients digestion and absorption.

After food ingestion, the digestion begins in different steps involving mechanical (mouth, stomach and small intestine) and chemical processing of nutrients (stomach and small intestine). Digestion of big pieces of food guarantees that small pieces reach the small intestine and can be absorbed into the blood or lymphatic system. The stomach secretes gastric juice containing hydrochloric acid and pepsin, which start breaking up food particles. Bile acids (produced by the liver) and pancreatic juice (produced by pancreas) are released into the first part of duodenum and contribute with nutrients extraction from food and preparation for absorption (reviewed in (DeSesso and Jacobson 2001)) (Bass and Wershil 2016). Bile acids solubilize lipid substances by emulsification of big fat droplets and formation of micelles, which facilitate hydrolysis of triglycerides and cholesterol esters and interaction with the brush border. The pancreatic juice includes a variety of digestive enzymes in charge of breaking down polysaccharides (α-amylase), proteins (trypsin, chymotrypsin, elastase), lipids (pancreatic lipase, colipase, cholesterol esterase) and nucleic acids (ribonuclease, deoxyribonuclease). Epithelial cells in the intestine also contain or release α-amylase, peptidases, lipases and nucleases (reviewed in (DeSesso and Jacobson 2001)).

Different mechanisms are involved in nutrients and water absorption including passive and facilitated diffusion, active transport and through osmotic gradient (DeSesso and Jacobson 2001). Glucose utilizes an active transport through the Na^+-dependent glucose transporter (SGLT1) and there is evidence of other mechanisms involving glucose transporter type 2 (GLUT2). In the case of fructose, its absorption is done through GLUT5. Glucose and sodium absorption generates an osmotic gradient which is the responsible mechanism for water diffusion and therefore absorption (Kellett, Brot-Laroche et al. 2008). In the case of proteins, they must be hydrolyzed by pepsin and other pancreatic proteases before absorption since only free aminoacids, dipeptides and tripeptides are transported from the lumen into the blood vessels.

Sodium-dependent amino acid transporters and PepT1 are responsible for the active transport of these nutrients (reviewed in (Keohane, Grimble et al. 1985, Webb 1990)).

Furthermore, the absorption of lipid species is a more complex process which depends on the type of lipid (triglyceride, cholesterol, phospholipid or vitamin) and involves a series of steps (see Fig 4). Initially, lipids must be emulsified in order to make them soluble and reachable for enzymatic digestion. Emulsification is possible due to bile acids secreted in the bile. The bile is secreted by the liver into the gall bladder, where it is concentrated, and it contains not only bile acids but also cholesterol and bilirubin (reviewed in (Nordskog, Phan et al. 2001)). Cholesterol 7α-hydroxylase (*Cyp7a1*) is the rate-limiting enzyme in the biosynthesis of bile acids but there are several genes involved in the regulation of bile acids metabolism and transport (*Cyp8b1, Asbt, Ostα, Ostβ, Taut, Csd*), cholesterol efflux transport (*Abcg5, Abcg8*), fatty acid β-oxidation (*Pparα, Acad1, Ehhadh, Acaa1*), and bile acid conjugation (*Bacs and Baat*) (Qi, Jiang et al. 2015).

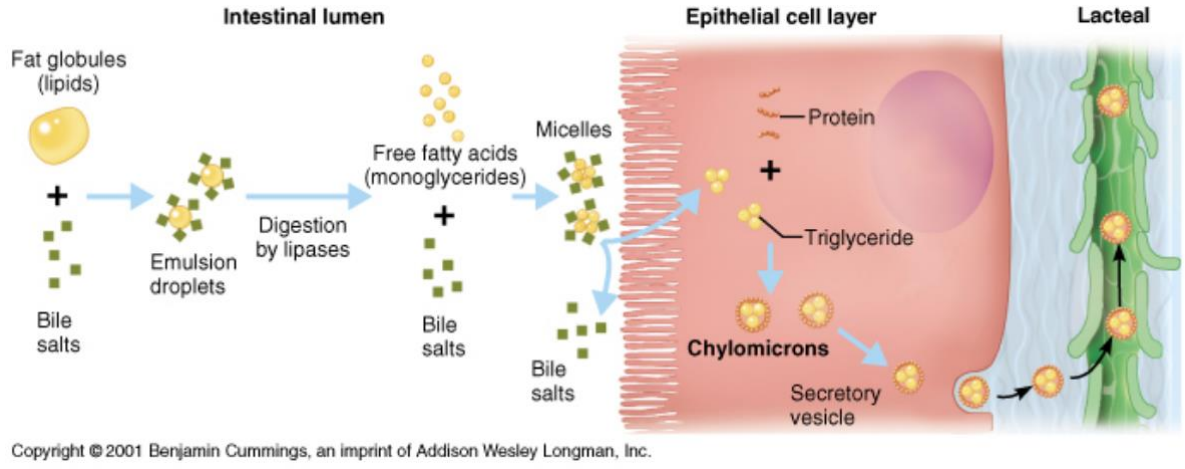

Fig 4. Steps in the process of intestinal lipids absorption.

From: (Cummings 2001)

After emulsification of big lipid droplets into smaller ones, a process of enzymatic digestion of triglycerides is carried out by pancreatic lipase and colipase. In this process, the fatty acids in positions 1 and 3 are hydrolyzed and, therefore, two free fatty acids (FFA) and one monoglyceride are generated per molecule of triglyceride (reviewed in (Hussain 2014) (Nordskog, Phan et al. 2001)). Phospholipids are

degraded by phospholipase A2 (PLA2) and other lipases. Cholesterol, FFA, monoglycerides and phospholipids aggregate with the help of bile acids into smaller particles denominated micelles, which facilitates that the hydrophobic lipids reach the hydrophilic unstirred water layer and therefore the enterocytes (reviewed in (Nordskog, Phan et al. 2001)).

The process of absorption into the enterocytes is also dependent on the type of lipid. In the case of cholesterol, Niemann-Pick C1-Like 1 (NPC1L1) receptor mediates the intracellular transport of cholesterol in enterocytes where cholesterol is esterified by the action of acyl-CoA cholesterol acyltransferase (ACAT) before packaging (Hussain 2014). Phospholipids components either diffuse or are flipped into the inner membrane of enterocytes. Free fatty acids (FFA) and monoglycerides (MG) enter the enterocyte mainly by diffusion, although there is evidence of the importance of transporters like cluster of differentiation 36 (CD36) and fatty acid transporter proteins (specifically FATP4) (Stahl, Hirsch et al. 1999) (reviewed in (Tso, Nauli et al. 2004, Hussain 2014)). Once inside the enterocytes, FFA and monoglycerides are reesterified into triglycerides by the action of monoacylglycerol acyltransferase 2 (MOGAT2) and diacylglycerol O-Acyltransferase 1 (DGAT1) in the endoplasmic reticulum (ER) (reviewed in (Hussain 2014)). The absorbed lipids need to be properly packed and transported along the cell before being released into the basolateral side of the cell for distribution to other tissues.

1.4. Insights into lipids repackaging and distribution.

Cholesterol and triglycerides cannot be transported in a free form through the body because of their hydrophobicity. Therefore, lipid transport has to be mediated by lipoproteins composed of a core of triglycerides and cholesteryl esters surrounded by a layer of phospholipids and apolipoproteins. The lipoproteins are classified according to their size, from bigger to smaller into: chylomicrons, chylomicrons remnants, very low density lipoprotein (VLDL), low density lipoprotein (LDL), Lipoprotein a (Lp(a)) and high density lipoprotein (HDL). Chylomicrons are produced in the enterocytes of the small intestine while the liver hepatocytes produce VLDL. Furthermore, LDL are the final product of VLDL catabolism and HDL are mostly produced by liver (70-80%) and up to some extent by the small intestine. All these lipoproteins are pro-atherogenic,

except for HDL, which is anti-atherogenic due to its ability to promote reverse cholesterol transport via ABCG1, SR-B1 and passive diffusion. HDL transfers excessive cholesterol to the liver for further processing or elimination as bile acids in the bile. However, more important than the size, the content of lipids and apolipoproteins define the lipoproteins. The content of TG decreases with the size of the lipoproteins, while the portion of cholesterol and apolipoproteins increases. In addition, the type of apolipoproteins controls the interaction between lipoproteins (which helps with the exchange of lipids and apolipoproteins) and the activation or inhibition of enzymes controlling the metabolism of lipoproteins (reviewed in (Gotto 1990) and (Feingold 2021)).

The process of fat absorption from the intestine starts when the enterocytes deliver lipids into the body in the form of chylomicrons. The process is initiated in the lumen of the ER, by the recruitment of Apolipoprotein B48 (APOB48). Whether APOB48 is initially attached to a small TG-rich lipid droplet or a dense particle (mostly made up of phospholipids and cholesterol) is still controversial. This nascent lipoprotein is known as prechylomicron and contains only one molecule of APOB48. The translocation of APOB48 into the lumen of the ER and initial interaction with lipid droplets is facilitated by microsomal triglyceride transfer protein (MTTP) (Hesse, Jaschke et al. 2013, Mansbach and Siddiqi 2016). MTTP is essential for the initial formation of lipoproteins and the number of APOB-containing particles in circulation. Mutations in MTTP cause abetalipoproteinemia with complete absence of apolipoproteins B48 and B100 (the full-length variant of APOB48 expressed by liver) and gross defects in fat absorption (Hussain, Nijstad et al. 2011). Another important component of the nascent prechylomicron is Apolipoprotein A4 (APOA4). APOA4 is also attached in the ER and its importance in chylomicron maturation/lipidation will be discussed in the next section.

After the prechylomicron is formed in the ER, it needs to be transferred via prechylomicron transport vesicles (PCTV) into the *cis*-Golgi through processes involving membranes fusion, budding and fission. These process are orchestrated by a series of proteins belonging to v-SNARE family like vesicle associated membrane protein 7 (VAMP7) and syntaxin. During the transport from *cis* to *trans*-Golgi and, prechylomicrons mature into chylomicrons by the addition of apolipoprotein A1 (APOA1) and increased lipidation. Some other proteins belonging to the small GTP-

ases family (ARFRP1 and ARL1) have been investigated because of their role in the regulation of chylomicrons transport in the *trans*-Golgi network before their release into the lymphatic system (Charles 2009, Mansbach and Siddiqi 2016).

Lymphatic vessels are found in the middle of each villi. They are composed by a single layer of endothelial cells which are permeable to larger and hydrophobic particles like chylomicrons. The lymphatic content travels via the thoracic duct and joins venous blood circulation at the subclavian vein (DeSesso and Jacobson 2001). Once chylomicrons are in circulation their content is uptaken by the action of an extracellular enzyme in the luminal surface of the vascular endothelium: lipoprotein lipase (LPL). Therefore, LPL provides substrates (FFA and glycerol) for energy supply and TG-reesterification to different tissues including adipose tissue, cardiac and skeletal muscles and macrophages. Lipoprotein lipase is regulated by a wide variety of physiological factors including hormones, apolipoproteins, exercise and feeding state. Due to its importance and very sensitive balance, alterations in LPL activity imply dysregulated lipoproteins metabolism and the development of correlated diseases including dyslipidemia, obesity, type 2 diabetes, non-alcoholic fatty liver disease (Merkel, Eckel et al. 2002, de Andrade Júnior 2018).

In conclusion, specific features of lipids including size and hydrophobicity make them a complex substrate in need of particular processes before they can be delivered to cells. Lipids need to be digested, resuspended, hydrolyzed, repacked, transported and delivered in ways that involve complex cellular processes and are orchestrated by a series of proteins and enzymatic reactions. Each step plays a role in the homeostasis of lipids metabolism.

1.4.1. Apolipoprotein A4.

One of the main components of chylomicrons is Apolipoprotein A4 (APOA4). This protein is mostly synthesized in the intestine and widely distributed in circulation. However, it can also be produced in hypothalamus and liver. APOA4 can be found, not only in the surface of chylomicrons, but it is also transferred into HDL, VLDL and released from chylomicrons in high amounts as a lipid-free protein (up to 50%). Although the function of APOA4 is not fully characterized, it is well-known that it plays

an important role in lipids absorption and reverse cholesterol transport (reviewed in (Wang, Kohan et al. 2015) and (Qu, Ko et al. 2019)).

APOA4 is part of a cluster of apolipoproteins (including APOA1, APOC, APOE, APOB) that regulate the transport and metabolization of lipoproteins. These related apolipoproteins are exchangable during the different processes of uptake and clearance of lipoproteins (Wang, Kohan et al. 2015). However, APOA4 is the only one which production is directly stimulated by lipids consumption. Levels of APOA4 in jejunum raise after acute lipid consumption or as a response to refeeding after fasting with either low fat diet or high fat diet (Kalogeris, Fukagawa et al. 1994). However, hypothalamic levels of APOA4 do not increase after refeeding with low fat diet and the stimulation of production decreases after chronic ingestion of high fat diet (Liu, Shen et al. 2004).

The specific function and mechanism of action of APOA4 have not been completely unraveled. Plasma levels of APOA4 correlate with TG during fasting and after a lipid-rich meal (Ferrer, Bigot-Corbel et al. 2002). Overexpression of APOA4 seems to protect from diet-induced atherosclerosis by mechanisms involving an increase in HDL, improved reverse cholesterol transport and decreased inflammation. APOA4, together with APOCII, promotes the activity of Lipoprotein lipase and therefore the hydrolysis of TG-rich lipoproteins like chylomicrons (reviewed in (Kersten 2014). Moreover, the removal of excessive cholesterol from peripheral tissues by HDL seems to be improved by the interaction of HDL particles with APOA4 (Stein, Stein et al. 1986) (Steinmetz, Barbaras et al. 1990) (see Fig 5). The injection of APOA4 improves insulin secretion and glucose sensitivity in *Apoa4* knockout mice after high-fat diet (HFD). Supporting previous results implying APOA4 as a regulator of appetite and satiety (reviewed in (Wang, Kohan et al. 2015) and (Qu, Ko et al. 2019)). This shows that APOA4 is a versatile regulator of energy homeostasis and response to lipids ingestion.

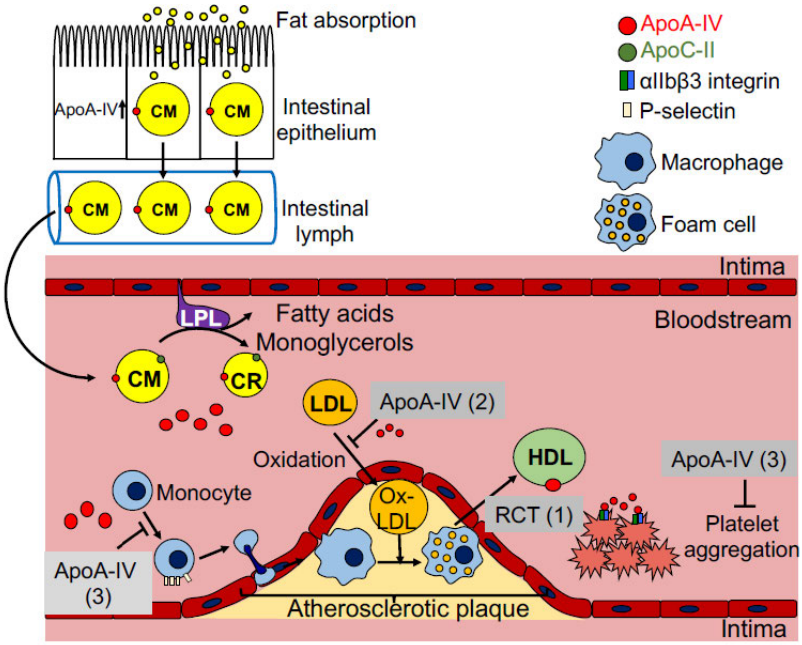

Fig 5. APOA4 is involved in lipoproteins and lipids metabolism.

From: (Qu, Ko et al. 2019)

In human association studies, high levels of APOA4 also represent a good prognosis and it has even been proposed as a biomarker of fat intake, obesity and diabetes. Low circulating APOA4 correlates with coronary artery disease in men (Kronenberg, Stühlinger et al. 2000). Furthermore, high levels of this protein before Roux-en-Y bypass surgery is correlated to improved insulin sensitivity after surgery (Rao, Roche et al. 2017). However, this human data should be read with cautiousness since APOA4 is highly responsive to fat ingestion and the data was taken either after fasting or after refeeding with low fat meal. In addition, fat-stimulated production of APOA4 fades upon obesity in animals and humans (Kalogeris and Painter 2001, Weinberg, Gallagher et al. 2012) and that also limits the use of APOA4 as a marker for metabolic diseases.

Although, it is well accepted that APOA4 has a protective function and it is an indicator of metabolic fitness, the studies on knockout models of APOA4 have contradictory results regarding the specific interaction between this protein and chylomicrons. Firstly, several studies in cell lines, mice and rats directly correlate APOA4 abundance with increased lipids absorption. Inhibition of chylomicron formation decreases APOA4 secretion, which is reversed by removal of the inhibitor (Hayashi, Nutting et al. 1990).

It was also shown that higher expression of APOA4 increased fat absorption by increasing chylomicron size (Gonzalez-Vallina, Wang et al. 1996, Simon, Cook et al. 2011) and that APOA4 stabilizes the surface of newly formed prechylomicrons in order to facilitate the incorporation of more triglycerides (Simon, Cook et al. 2011). However, there is also evidence in the opposite direction. In a different study, knockout mice secreted larger chylomicrons, which are uptaken slower than controls. The decrease in chylomicrons uptake was shown to be dependent on the source of chylomicrons (wildtype or *ApoA4* knockout animals) and not the recipient animals, suggesting another role for APOA4 (Kohan, Wang et al. 2012, Kohan, Wang et al. 2013). Clearly, there is no agreement on the effects of APOA4 abundance on chylomicron size or mechanism of action; it is likely that studies on post-translational modifications would help clarify the role of APOA4 on dietary fat absorption.

The current knowledge on APOA4 demonstrates its importance as a regulator of metabolism. This intestinal protein is a main component of chylomicrons and other lipoproteins, which plays a pivotal role in lipids absorption, accumulation and metabolization. However, more research is needed in order to answer the diverse, and sometimes contradictory, effects of APOA4 in the complex metabolic pathways in which it might be involved.

1.5. Caco2 cell line as a tool for intestinal research.

Caco2 cells are epithelial cells derived from a human-male colorectal adenocarcinoma. These cells have been utilized as a model of intestinal epithelial barrier because of their ability to behave as small intestine enterocytes in terms of absorption and cellular transport (Hidalgo, Raub et al. 1989, Lea 2015).

An important characteristic of this cell line is the formation of monolayers of cells that spontaneously differentiate after confluency by generating tight junctions that replicate the intestinal barrier. Moreover, Caco2 cells express not only membrane transporters for all types of nutrients, but also the digestive enzymes normally present in the small intestine (Sambuy, De Angelis et al. 2005, Lea 2015).

Caco2 cells are used in pharmaceutical companies and research laboratories as an in-vitro model for drugs and/or nutrients absorption. For that purpose, the cells must be cultured in filtered membranes where they differentiate and polarize and, simulating

physiological conditions, the cells are able to cross metabolites from the apical to the basal side of the membrane (Meunier, Bourrie et al. 1995, Lea 2015).

Different models involving the usage of Caco2 cells and equations to measure kinetic parameters have been developed. However, Caco2 models lack several components from the normal epithelium, including Paneth cells, goblet cells and enteroendocrine cells. Furthermore, solubilization, and therefore absorption, of lipids might be affected by the lack of mucus, bile acids, pancreatic lipases and peristalsis (Sun, Chow et al. 2008, Lea 2015). Caco2 cells have proved to be very useful in basic research and in studies of drugs and food metabolization. However, the analysis of results and in-vivo extrapolation of those must be done cautiously.

1.6. Protein Kinase D2.

1.6.1. PKD structure and activation.

The family of Protein Kinase D consists of three highly homologous serine/threonine kinases (PKD1, 2 and 3). They are part of the group of Ca^{2+}/calmodulin-dependent kinases. Structurally, PKDs contain an N-terminal regulatory domain which contains: a) tandem cysteine-rich zinc-finger motifs (C1a and C1b) for interaction with diacylglycerol (DAG) and b) pleckstrin homology (PH) domain for autoinhibition. The catalytic domain is located at the C-terminal and involves several serines that need to be phosphorylated for PKDs to be active (Kolczynska, Loza-Valdes et al. 2020). (see Fig 6).

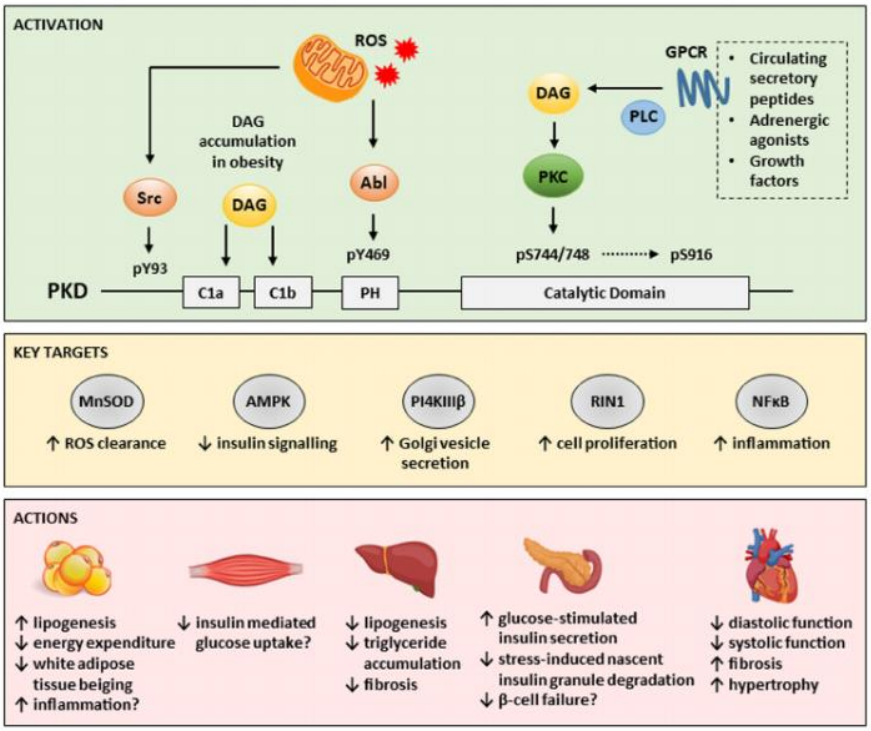

Fig 6. PKD activation and action in different organs.

From: (Renton, McGee et al. 2020)

Different mechanisms for PKD activation have been proposed. In the canonical pathway, different stimuli (adrenergic agonists, growth factors, circulating peptides) activate GPCRs which activate phospholipase C, increasing DAG levels as a consequence. DAG not only activates Protein kinase C (PKC) but also anchors PKD to the cell membrane next to activated PKC. As a consequence PKC transphosphorylates PKD in the activation loop (Zugaza, Sinnett-Smith et al. 1996). In the case of human PKD2, the phosphorylation occurs specifically at serines 706 and 710 (707 and 711 in murine). PKD2 also increase catalytic activity via autophosphorylation of serine 876 (873 in murine) at the C-terminal. Other less studied mechanisms have shown spatiotemporal dynamics, stimuli-specific responses and differences regarding the PKC dependency for activation (Renton, McGee et al. 2020). (see Fig 6).

PKD activity in organs like adipose tissue, liver and heart is elevated upon refeeding of fasted animals, implying a connection between PKD activity and nutrient sensing (Venardos, De Jong et al. 2015, Löffler, Mayer et al. 2018, Mayer, Löffler et al. 2019).

Even though, PKD activity has been studied in different organs and pathologies, the downstream targets of PKDs are still under debate and mostly unknown. Some of the known targets of PKDs involve manganese superoxide dismutase (MnSOD), 5' AMP-activated protein kinase (AMPK), phosphatidylinositol 4-kinase III β (PI4kIIIβ), Ras and Rab interactor 1 (RIN1) and nuclear factor kappa-light-chain-enhancer of activated B cells (NFκB). It is important to mention that these targets seem to be organ and stimuli-specific and have been mostly attributed to one or the other PKD members (Reviewed in (Renton, McGee et al. 2020)).

Currently, inhibitors of PKD proteins are used for research mainly regarding their potential use to suppress cancer growth in-vitro and in animal studies. On the one hand, CID755673 inhibits more efficiently PKD1 and it has proved to inhibit prostate cancer cell proliferation, migration and invasion (Sharlow, Giridhar et al. 2008). Inhibition of PKDs by CID755673 also enhances heart function in diabetic mice (Venardos, De Jong et al. 2015) and helps maintaining pluripotency in embryonic stem cells (Zhu, Zhang et al. 2020), however, CID755673 also inhibits other kinases (PKC, CAK, PLK1, CAMKII) and interferes in cell cycle progression independently of PKD1 expression or activation (Sharlow, Giridhar et al. 2008, Torres-Marquez, Sinnett-Smith et al. 2010). On the other hand, CRT0066101 inhibitor has been used to inhibit pancreatic cancer growth (Harikumar, Kunnumakkara et al. 2010), breast cancer proliferation (Liu, Wang et al. 2019), bladder cancer growth (Li, Hsu et al. 2018) and colorectal cancer growth (Wei, Chu et al. 2014). This inhibitor exhibits higher selectivity for PKDs against panels of kinases. Moreover, CRT0066101 inhibitor is orally bioavailable, water-soluble and there are studies on mouse pharmacokinetics (Harikumar, Kunnumakkara et al. 2010).

1.6.2. PKDs in health and disease.

Distribution and activity of the different members of Protein Kinase D family differ between different tissues. Although the 3 members are virtually expressed in all organs, levels of expression and specificity in the activity have been shown in different studies ((Löffler, Mayer et al. 2018, Mayer, Löffler et al. 2019) also reviewed in (Renton, McGee et al. 2020)).

The first Protein Kinase D described and the most studied is Protein Kinase D1. Deletion of PKD1 in pancreatic β-cells demonstrated the role of this protein in adaptation to high fat diet (HFD) and in the secretion of insulin granules. An increase in PKD1 activity correlates with higher insulin secretion and improved glucose tolerance (Sumara, Formentini et al. 2009, Bergeron, Ghislain et al. 2018). PKD1 regulates adipose tissue by suppressing activation of AMP-activated protein kinase. PKD1 knockout in adipocytes decreased lipogenesis, increased energy dissipation and overall improved the metabolic fitness of mice under HFD (Löffler, Mayer et al. 2018). An in-vitro study has also shown that AMPK inhibition by PKD1 in muscle-like cells (C2C12) promotes insulin resistance (Coughlan, Valentine et al. 2016).

Protein Kinase D3 has been shown to be the predominant PKD in hepatocytes and to control lipids accumulation and insulin signaling in the liver. Specific hepatic deletion of PKD3 improved insulin-dependent glucose tolerance but promoted lipogenesis and therefore TG and cholesterol accumulation under HFD feeding (Mayer, Löffler et al. 2019).

Protein Kinase D2 has been studied in different fields. It is involved in vesicle transport and secretion, cancer invasion and stimulation of cell proliferation (reviewed in (Azoitei, Cobbaut et al. 2018)). One of the first characterizations of PKD2 showed high expression of this protein in human lung, heart, smooth muscle, brain and pancreas (Sturany, Van Lint et al. 2001). The same study found that PKD2 is highly expressed in proliferative tissues like colonic mucosa and testis.

The function of PKD2 has been studied in the context of diabetic cardiomyopathy and heart failure. It was found that PKD2 in heart is activated in T2D *db/db* mice and its inhibition with CID755673 improved indices of heart function (Venardos, De Jong et al. 2015). In the digestive tract, PKD2 activation is induced by gastrin stimulation (Sturany, Van Lint et al. 2001) and it is necessary for the release of secretory vesicles containing chromogranin A in neuroendocrine tumor cells in-vitro (von Wichert, Edenfeld et al. 2008). PKD2 activity also seems to protect against dextran-induced colitis and its expression is reduced in human samples with inflammatory bowel disease (Xiong, Zhou et al. 2016).

PKD2 has been shown to regulate the proliferation and migration of different tumors including myeloid leukemia cells (Mihailovic, Marx et al. 2004), glioblastoma (Azoitei,

Kleger et al. 2011), prostate cancer (Zou, Zeng et al. 2012), breast cancer (Hao, McKenzie et al. 2013) and hepatocellular carcinoma (Zhu, Cheng et al. 2016).

However, there is only one report on the field of metabolism for PKD2 and the results are limited due to the amount of subjects (2 subjects). Here, they show hyperinsulinemia in two rhesus monkeys with nonsense mutations in PKD2. In addition, total knockout mice for PKD2 showed increased insulin levels and insulin resistance (Xiao, Wang et al. 2018).

1.7. Aims of the study.

Due to the fact, that overweight and obesity are the underlying causes of several metabolic-related diseases like atherosclerosis, diabetes, fatty liver, among others, it is highly important to find strategies to prevent the appearance but also to fight this disease. Although several efforts from different approaches have been taken, the obesity epidemic does not stop increasing and the projections for the future do not seem to be better (Hurt, Kulisek et al. 2010).

Theoretically, all the components of the energy equation can be targeted to induce a negative energy balance in pursuit of weight loss. Firstly, enhanced energy expenditure can be used by increasing physical activity or incrementing thermogenic energy dissipation via cold-exposure or activation of mitochondria in brown or beige adipocytes (Ravussin, Xiao et al. 2014, Löffler, Mayer et al. 2018). Other alternative is to target energy intake by increasing satiety, decreasing food intake as in restrictive diets and intermittent fasting, or by limiting nutrients absorption as in gastric bypass surgery or orlistat treatment (Obert, Pearlman et al. 2017, Hankir, Seyfried et al. 2018). Noteworthy, most of the treatments listed before might affect more than one of the components of the energy equation, which might amplify the final effects on body weight loss.

Previous studies in our and other laboratories have demonstrated the significant role of Protein Kinase D family members in a number of metabolically active organs and in pathways controlling the global metabolic homeostasis. Most of that research has been performed in PKD1 and its regulation of adipose tissue biology and insulin secretion and sensitivity (Sumara, Formentini et al. 2009, Löffler, Mayer et al. 2018).

Moreover, PKD3 has also been shown to regulate metabolism by regulating liver functions (Mayer, Löffler et al. 2019). However, the characterization of PKD2 activity in a metabolic context is certainly reduced.

Therefore, we aimed to explore the potential role of PKD2 in metabolism by using, initially, *Pkd2*$^{ki/ki}$ mice model with global point mutations in the catalytic domain (S707A/S711A). Since these mice showed a very strong resistance to high-fat diet-induced obesity, we designed a project that helped us to unravel the mechanisms involved and the organs that might contribute to that phenotype. In order to investigate, we made use of different diets, widely used metabolic tests, and metabolic phenotyping of the energy balance components. Later on, the results led us to focus our research on the small intestine and the mechanisms by which PKD2 regulates intestinal fat absorption. Finally, we intended to mimic our previous observations by using a pharmacological approach in cells systems and mice as a potential translational attempt to use PKD2 inhibition in the treatment of obesity and comorbidities.

2. RESULTS

2.1. *Pkd2*$^{ki/ki}$ mice are resistant to HFD-induced obesity and protected from the metabolical consequences.

2.1.1. Administration of a diet with high fat content induces body fat gain to a lesser extent when PKD2 is inactive.

In the knock-in mice (*Pkd2*$^{ki/ki}$), the 2 most important phosphorylation sites in PKD2 have been mutated (S707A/S711A). *Pkd2*$^{wt/wt}$ and *Pkd2*$^{ki/ki}$ mice (as well as the heterozygous *Pkd2*$^{wt/ki}$) are viable and born at regular Mendelian rate. No gross physical or behavioural disabilities were noticed during the complete study (data not shown) (Matthews, Navarro et al. 2010). These mice, under a regular chow diet (ND), did not show any significant difference in body weight (Fig 7A). However, high-fat diet feeding as a metabolic challenge demonstrated that mice lacking activation of PKD2 are resistant to body weight gain (Fig 7A). This difference in body weight between phenotypes was due to decreased fat mass in *Pkd2*$^{ki/ki}$ mice as analysed by nuclear magnetic resonance (NMR) and corroborated by weighing the organs after dissection (Fig 7B-C). This response to the metabolic challenge uncovered a potential action mediated by PKD2 in metabolism.

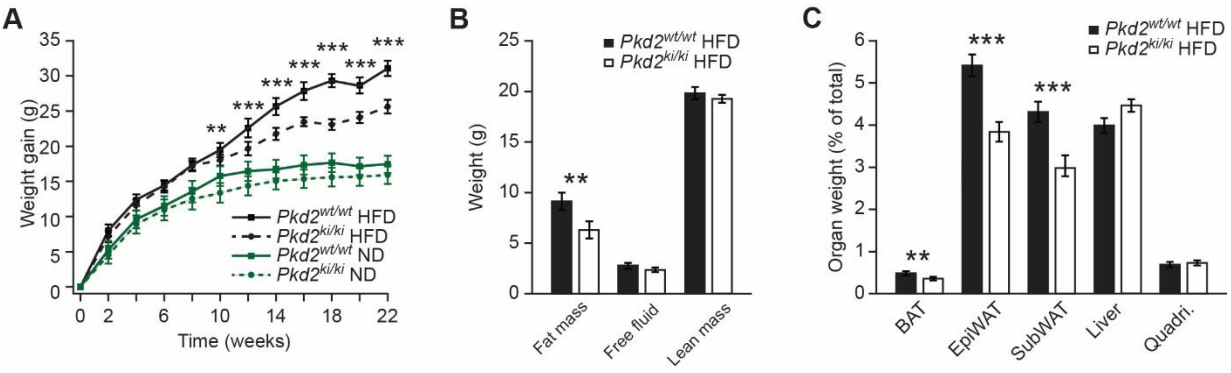

Fig 7. PKD2 inactivation protects from HFD-induced obesity.

A. Body weight gain of male mice with the specified genotypes under normal (ND) or high-fat diet (HFD). B. Quantification of fat, free fluid and lean mass by nuclear magnetic resonance (NMR) of mice in HFD. C. Organ weight of different fat depots (subcutaneous-SubWAT, epididymal-EpiWAT, brown-BAT), liver and quadriceps of *Pkd2*$^{wt/wt}$ and *Pkd2*$^{ki/ki}$ male mice after 22 weeks in HFD. n=7 for ND. In HFD, n=7 for *Pkd2*$^{wt/wt}$ and n=8 for *Pkd2*$^{ki/ki}$.

2.1.2. Glucose and lipids metabolism are affected by PKD2 inactivation.

One of the detrimental consequences of obesity is the inability to properly metabolize and store glucose mostly due to decreased insulin sensitivity by organs like muscles, liver and adipose tissue. Therefore, we performed well-established tests to measure the response of these mice to glucose (GTT) and insulin injection (ITT). The curves in Fig 8 show how mice with inhibition of PKD2 activity have better glucose clearance and insulin sensitivity. The improvement in glucose metabolism was found in *Pkd2*$^{ki/ki}$ mice when compared to control only after feeding them with HFD.

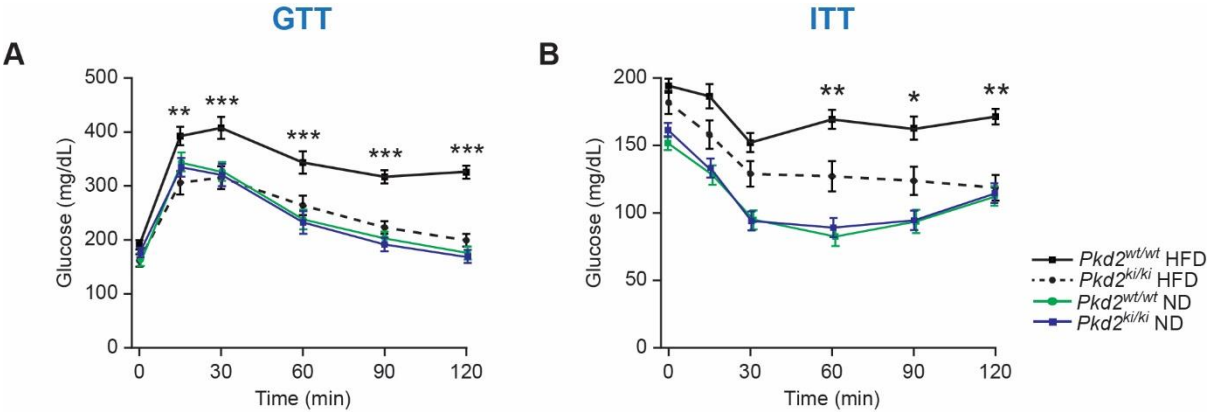

Fig 8. Improved GTT and ITT under PKD2 inactivation.

A. Glucose tolerance test of the specified genotypes after 16 weeks in HFD. B. Insulin tolerance test of *Pkd2*$^{wt/wt}$ and *Pkd2*$^{ki/ki}$ male mice after 18 weeks in HFD. n=7 for *Pkd2*$^{wt/wt}$ and n=8 for *Pkd2*$^{ki/ki}$.

Lipids in circulation are also affected by the development of obesity and are an indicator of dyslipidemias and cardiovascular risk. *Pkd2*$^{ki/ki}$ mice in HFD presented lower levels of triglycerides and free-fatty acids in circulation (Fig 9) which also demonstrates that PKD2 inactivation not only protects from HFD-induced obesity but also from metabolic consequences such as hyperlipidemia.

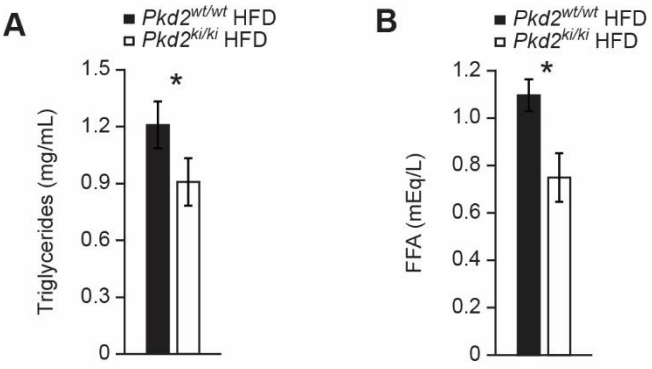

Fig 9. Improved lipid profile in *Pkd2*$^{ki/ki}$ mice under HFD.

A. Triglycerides and B. free fatty acids in circulation of specified mice after 18 weeks in HFD. n=7 for *Pkd2*$^{wt/wt}$ and n=8 for *Pkd2*$^{ki/ki}$.

2.1.3. Response in other organs to PKD2 inactivation

PKD2 inactivation might affect other metabolically active organs. Therefore, we analyzed different depots of adipose tissue. In congruence with the increased mass of adipose tissues shown in Fig 7B-C, histological analysis demonstrated adipocytes' hypertrophy in subcutaneous and epididymal white adipose tissue (SubWAT and EpiWAT) of control mice when compared to *Pkd2*$^{ki/ki}$ mice (Fig 10A-B). This difference was specific for mice receiving HFD and no difference in adipocytes' was observed under normal chow diet (ND) (Fig 10C)

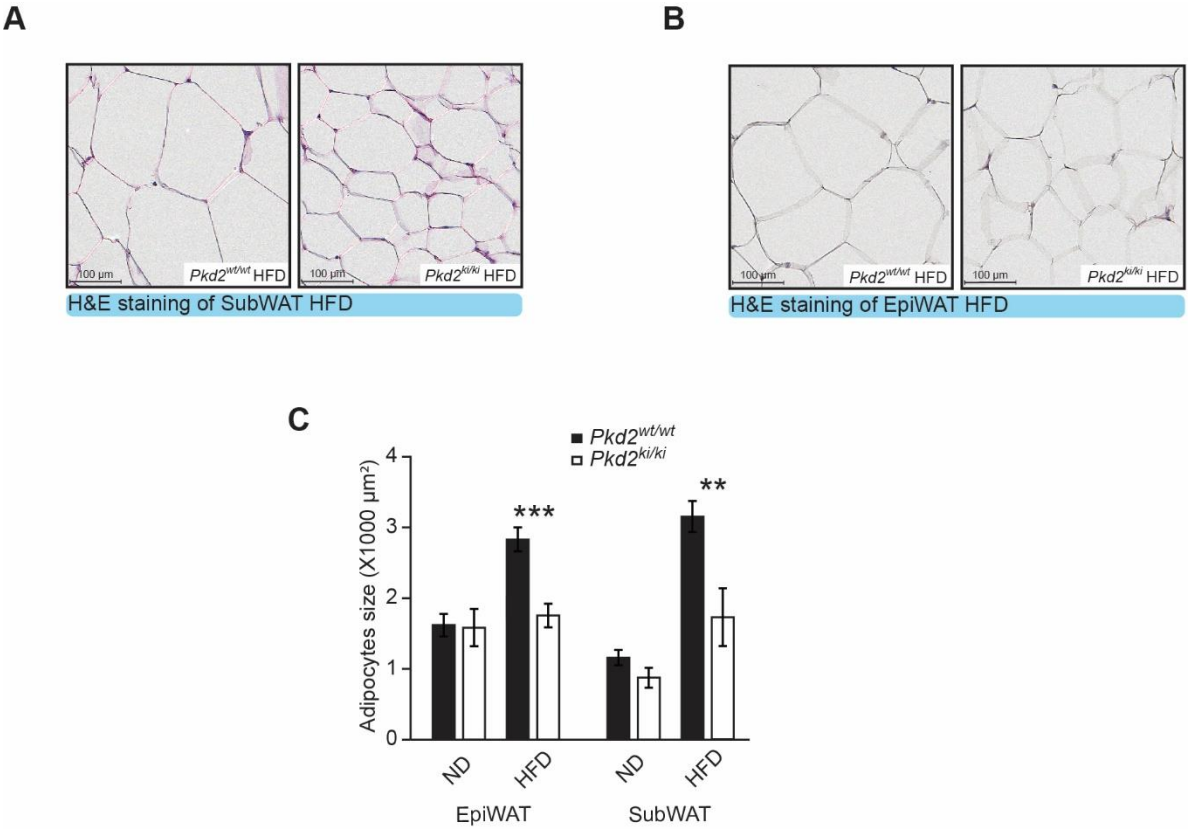

Fig 10. Increased adipocyte size in *Pkd2*$^{wt/wt}$ mice under HFD.

A. Representative pictures of H&E staining of SubWAT and B. EpiWAT of indicated male mice fed HFD. C. Quantification of the average adipocyte size in SubWAT and EpiWAT of male mice of the specified genotypes in normal and high-fat diet. n=7 for *Pkd2*$^{wt/wt}$ and n=8 for *Pkd2*$^{ki/ki}$

According to a previous study (Löffler, Mayer et al. 2018), deletion of PKD1 in adipocytes promotes the expression of beiging markers and energy dissipation. Consequently, these mice also shown decreased adipocytes' size. Due to the similarities between the different members of the PKD family, we tested changes in expression of genes related to energy dissipation and beige adipocyte markers (Fig 11). Analysis of subcutaneous adipose tissue showed no difference in the expression levels of the main markers including Uncoupling Protein 1 (*Ucp1),* Cell Death Inducing DFFA Like Effector A *(Cidea),* Bone Morphogenetic Protein 7 (*Bmp7),* PR domain containing 16 *(Prdm16),* Peroxisome Proliferator Activated Receptor Alpha *(Ppara),* Peroxisome proliferator-activated receptor gamma coactivator 1-alpha (*Pgc1a),* Adrenoceptor Beta 3 *(Adrb3),* Cell Death Inducing DFFA Like Effector C *(Cidec),* Myosin Heavy Chain 2 *(Myh2),* creatine kinase M-type *(Ckm),* Creatine kinase, muscle

(Mck), Solute Carrier Family 6 Member 8 *(Slc6a8),* Solute Carrier Family 27 Member 2 *(Slc27a2),* Uncoupling Protein 3 *(Ucp3)* and Myosin Heavy Chain 1 *(Myh1)*. Only *Slc6a8*, a creatine transporter, was significantly decreased in *Pkd2*$^{ki/ki}$ mice.

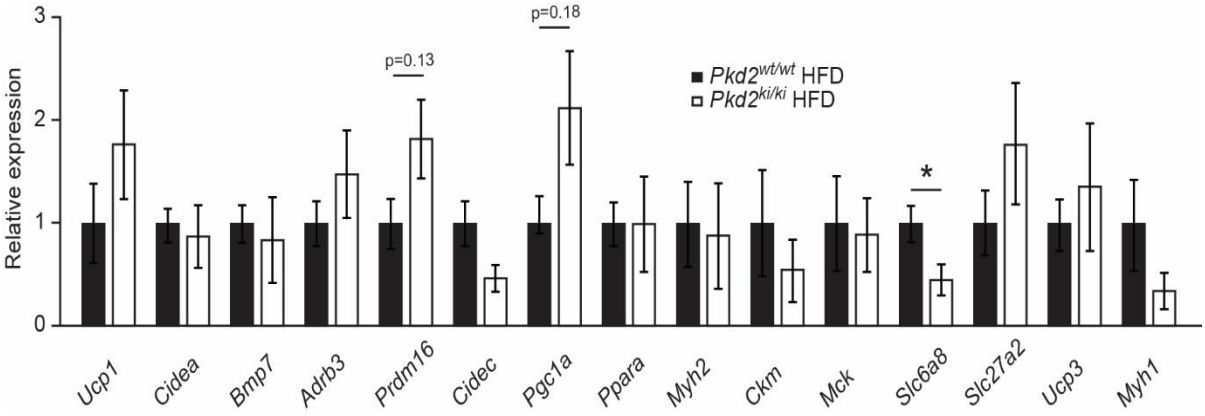

Fig 11. Relative expression of specified browning genes in SubWAT.

Pkd2$^{wt/wt}$ and *Pkd2*$^{ki/ki}$ male mice after 22 weeks in HFD. n=6.

To explore the consequences of PKD2 inactivation in liver, the serum concentration of aspartate transaminase (AST) and alanine transaminase (ALT) were measured as indicators of liver damage or malfunction (Fig 12A). AST and ALT levels showed no significant differences. However, the histological analysis showed increased lipids accumulation in liver of *Pkd2*$^{wt/wt}$ mice, which was later corroborated by lipids extraction from liver tissues and triglycerides quantification (Fig 12B-C).

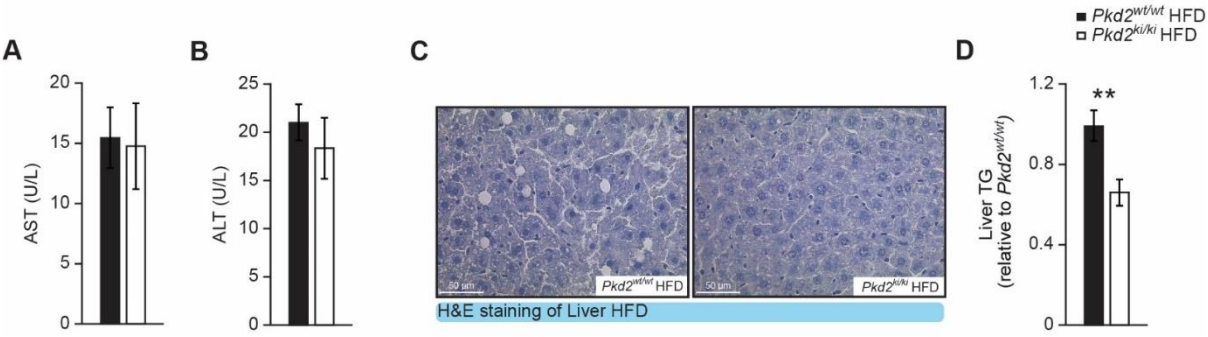

Fig 12. Hepatic alterations in *Pkd2*$^{ki/ki}$ and control mice under HFD.

After 22 weeks in HFD, *Pkd2*$^{wt/wt}$ and *Pkd2*$^{ki/ki}$ male mice were analysed for parameters of hepatic function. A. Aspartate aminotransferase and B. alanine aminotransferase levels in serum. C. Representative pictures of H&E staining of liver. D. Triglycerides content of liver. n=5 in A. and B. In D. n=7 for *Pkd2*$^{wt/wt}$ and n=8 for *Pkd2*$^{ki/ki}$.

Studies on insulin regulation by Protein Kinases D have linked these proteins to altered secretion and sensitivity (Sumara, Formentini et al. 2009, Xiao, Wang et al. 2018). For that reason, a glucose stimulated insulin secretion test (GSIS) was performed to *Pkd2*$^{wt/wt}$ and *Pkd2*$^{ki/ki}$ after 8 weeks in HFD (Fig 13). Even though, higher levels of insulin were observed at the beginning and at the end of the experiment, the differences were not significant. Furthermore, confocal microscopy revealed that the ratio islet size to pancreas size is increased in *Pkd2*$^{ki/ki}$ mice, however, insulin quantification was unchanged.

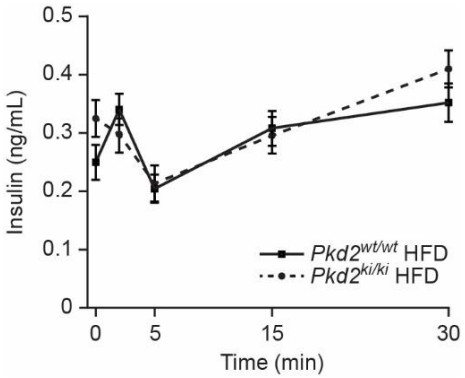

Fig 13. Glucose stimulated insulin secretion of *Pkd2*$^{wt/wt}$ and *Pkd2*$^{ki/ki}$ male mice.

Performed after 8 weeks in HFD. n=8.

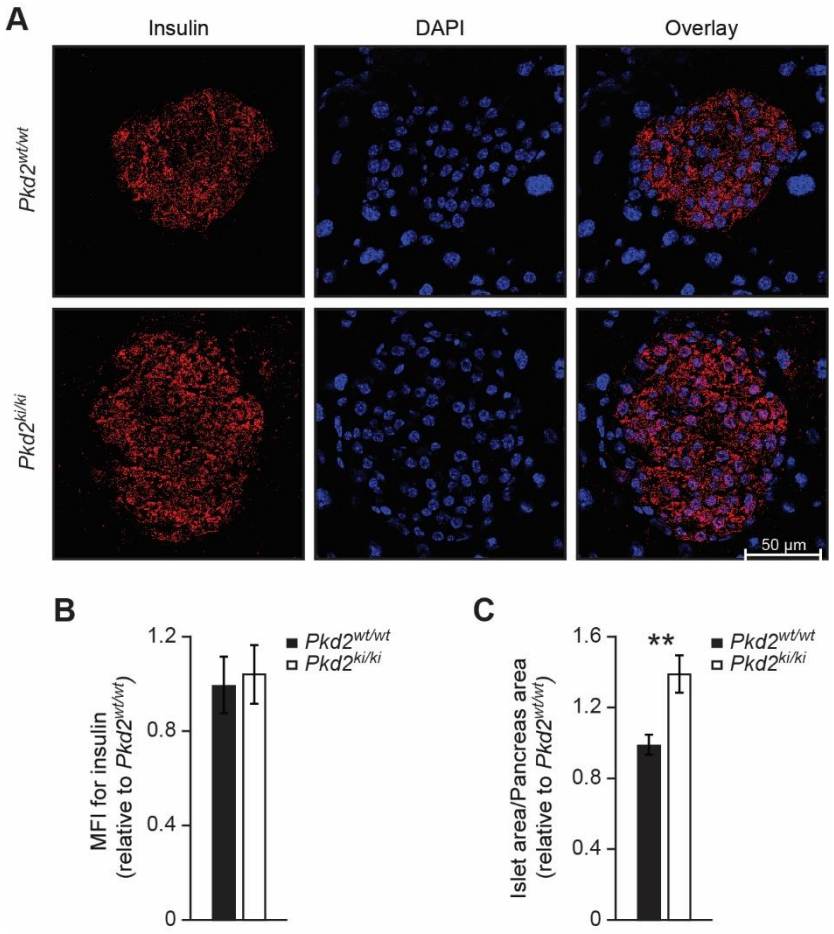

Fig 14. Pancreas studies after PKD2 inactivation.

A. Representative pictures of immunofluorescent staining for insulin (red) and DAPI (blue) of *Pkd2*$^{wt/wt}$ and *Pkd2*$^{ki/ki}$ male mice. n=3. For each subject, three different sections of the pancreas were taken and a distance of 50 micrometers was kept between the sections. B. Mean fluorescence intensity (MFI) for insulin of mice in A. (relative to *Pkd2*$^{wt/wt}$). n=3. MFI was quantified from all the islets found in each of the three sections per experimental subject. C. Islet area compared to pancreas area of mice in A. (relative to *Pkd2*$^{wt/wt}$). All the islets found in each of the three sections per mouse were quantified.

These results show that global inactivation of PKD2 has important metabolic consequences, which are finally reflected as a reduced body weight and a better metabolic fitness of mice regarding responses to lipids and sugar.

2.1.4. Investigation of energy balance and lipids absorption

The next step was to investigate the component(s) of the energy balance equation that might disrupted and influenced the difference in body weight. For that purpose, after 20 weeks in HFD, *Pkd2*$^{ki/ki}$ and respective control mice were placed in the

Phenomaster for metabolic phenotyping. To our surprise, as shown in Fig 15, there were no significant differences between genotypes regarding energy expenditure, energy/food intake, and activity during day or night intervals. Therefore, we decided to explore the other component of the positive side of energy balance: absorption.

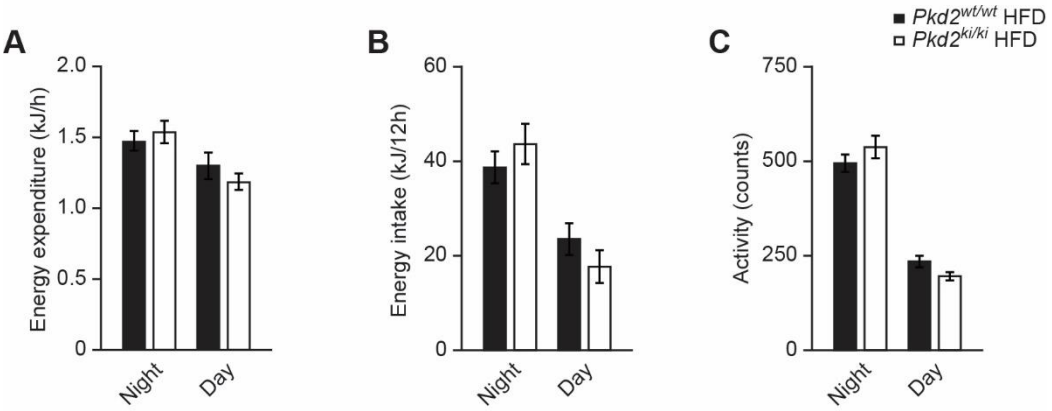

Fig 15. Analysis of *Pkd2*$^{ki/ki}$ and control mice in metabolic cages.

A. Energy expenditure, B. energy intake and C. activity of *Pkd2*$^{wt/wt}$ and *Pkd2*$^{ki/ki}$ male mice after 20 weeks in HFD. Expressed per 12 hours intervals. n=7 for *Pkd2*$^{wt/wt}$ and n=8 for *Pkd2*$^{ki/ki}$.

As a first approach, feces from mice in HFD were collected from individual cages in order to analyse their lipids and energy content. From the collection, it was visible that the amount and characteristics of the feces were altered. Feces from *Pkd2*$^{ki/ki}$ mice presented a yellowish color and floated in water (Fig 16). The amount of feces excreted by *Pkd2*$^{ki/ki}$ mice was higher (Fig 17A) and, when compared to wildtype, more feces were produced per gram of ingested food (Fig 17B). PKD2 inactivation also decreased food efficiency, measured as the weight gained per gram of ingested food (Fig 17C).

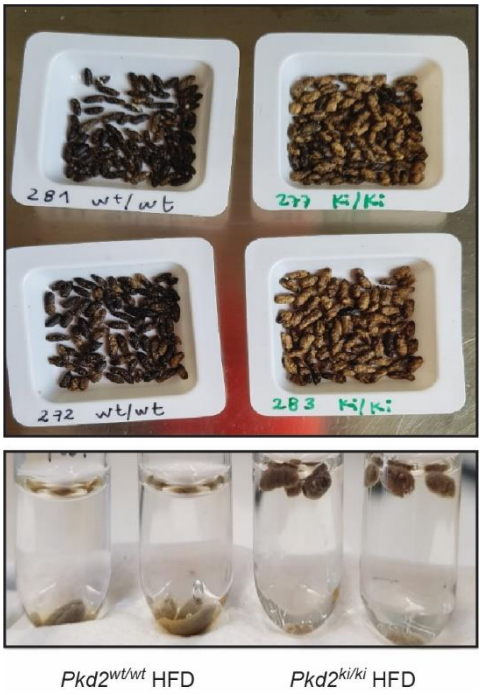

Fig 16. Representative pictures of feces collected from *Pkd2*$^{wt/wt}$ and *Pkd2*$^{ki/ki}$ mice under HFD. Photo of the feces placed in water.

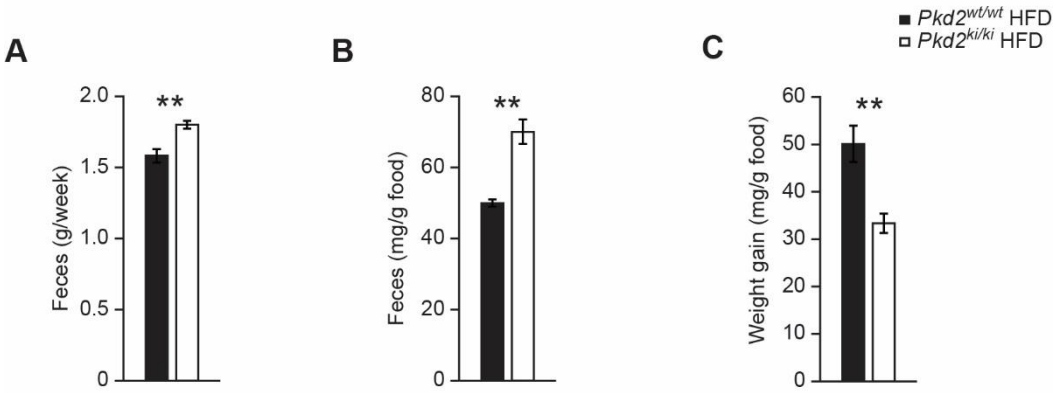

Fig 17. *Pkd2*$^{ki/ki}$ mice excrete more feces and are less food efficient.

A. Weight of feces collected in a week. B. Feces excreted per gram of food consumed. C. Body weight gained per gram of food consumed. n=7 for *Pkd2*$^{wt/wt}$ and n=8 for *Pkd2*$^{ki/ki}$.

The content of feces also differed between genotypes (Fig 18). Lipids extraction and quantification from feces showed that inactivation of PKD2 increased the amount of lipids excreted in the feces. Moreover, bomb calorimetry demonstrated that feces from *Pkd2*$^{ki/ki}$ mice are have a higher energy content compared to those obtained from *Pkd2*$^{wt/wt}$ mice.

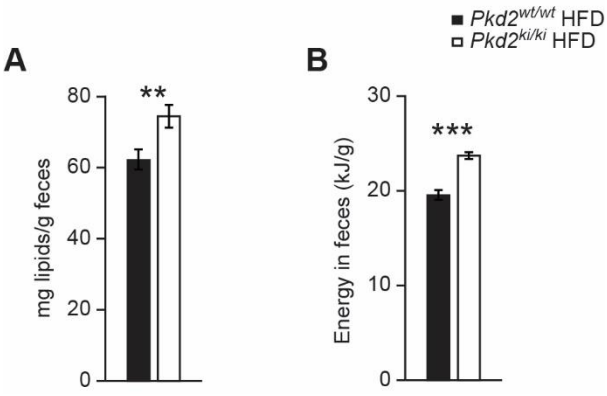

Fig 18. Feces from *Pkd2*$^{ki/ki}$ mice contain more lipids and energy.

A. Lipids content and B. Energy content per gram of feces of mice in HFD. n=7 for *Pkd2*$^{wt/wt}$ and n=8 for *Pkd2*$^{ki/ki}$.

Analysis of data from metabolic cages combined with the analysis of energy content in feces and food, allowed us to quantify the percentage of ingested energy that was excreted by the mice (Fig 19A). This result showed that inactivation of PKD2 increased almost 2-folds the excreted energy. Overall, these results translated into a decreased metabolizable energy in the *Pkd2*$^{ki/ki}$ mice responsible for the negative energy balance in these mice when compared to wildtype (Fig 19B).

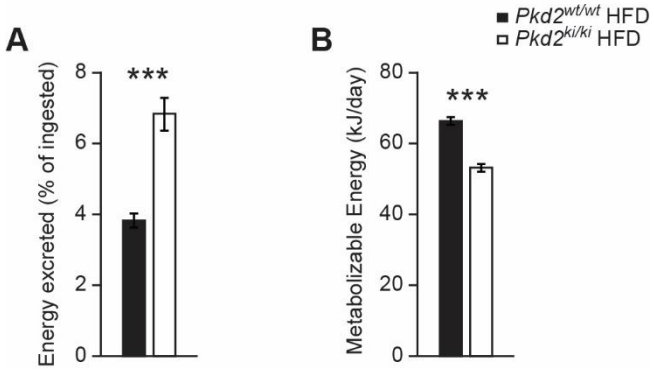

Fig 19. *Pkd2*$^{ki/ki}$ mice under HFD excrete more energy which equals lower metabolizable energy.

A. Percentage of energy excreted in feces from the total energy ingested. B. Metabolizable energy calculated from intake minus excreted and assuming a urinary excretion of 2%. n=7 for *Pkd2*$^{wt/wt}$ and n=8 for *Pkd2*$^{ki/ki}$.

Despite no significant differences in the body weight or metabolic responses between *Pkd2*$^{wt/wt}$ and *Pkd2*$^{ki/ki}$ mice fed normal diet, feces from these mice were collected and no significant differences were found in amount or appearance (Fig 20).

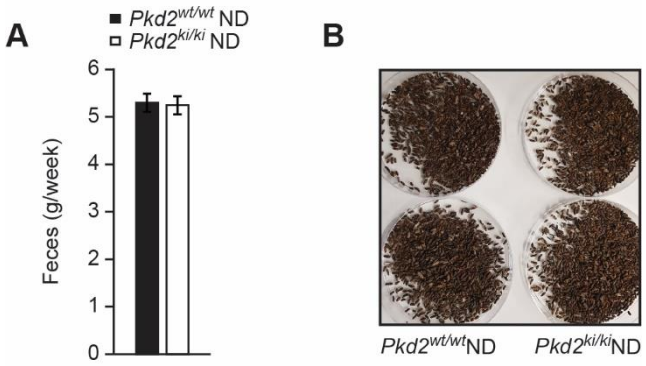

Fig 20. No differences in feces excretion under normal diet.

A. Weight of feces collected from *Pkd2*$^{wt/wt}$ and *Pkd2*$^{ki/ki}$ male mice fed normal diet per week. B. Pictures of feaces from *Pkd2*$^{wt/wt}$ and *Pkd2*$^{ki/ki}$ male mice under normal diet. n=6.

The results from metabolic phenotyping and feces analysis indicated the possibility of decreased lipids' absorption. To study that, a lipids tolerance test (LTT) was performed after acclimating the mice to HFD during 2 weeks. After gavage of olive oil to overnight fasted mice, the concentration of triglycerides in serum of control mice was much higher than in *Pkd2*$^{ki/ki}$ mice (Fig 21A). Furthermore, we blocked the uptake of triglycerides from peripheral tissues by inhibiting lipoprotein lipase with the injection of tyloxapol (LPL inhibitor). In this experiment, *Pkd2*$^{ki/ki}$ mice also responded with lowers levels of triglycerides after olive oil gavage, indicating decreased intestinal absorption is the principal mechanism and not triglycerides uptake by other organs (Fig 21B). Of note, oral gavage of glucose did not alter the glucose concentrations during an oral glucose tolerance test (data not shown).

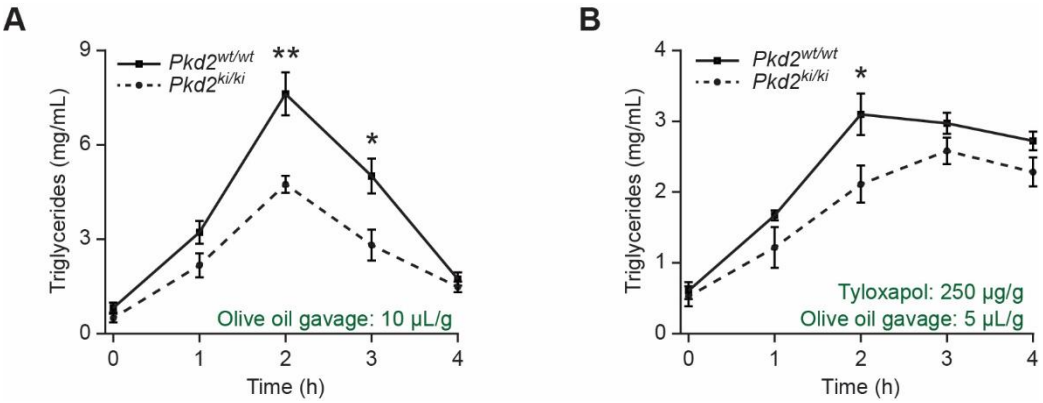

Fig 21. Decreased lipids absorption in *Pkd2*$^{ki/ki}$ mice.

A. Lipids tolerance test after oral gavage of olive oil (10µL per gram of body weight). B. Lipids tolerance test 30 min after tyloxapol i.p. injection (250µg/g body weight) (5µL of olive oil per gram of body weight were gavaged orally). n=6.

2.1.5. Approach into the regulation of intestinal functions by PKD2

2.1.5.1. PKD distribution and activation upon fat ingestion

Currently, there are no studies describing the functions of PKD family members in the small intestine. Therefore, the expression level of PKD1, PKD2 and PKD3 was quantification in wildtype mice. As shown in Fig 22A. *Pkd1* is poorly expressed in the different sections of small intestine and *Pkd2* is the predominant of the three members of PKD.

To test PKD2 activation upon fat ingestion, wildtype mice were gavaged with PBS (control) or olive oil and intestinal samples were taken after 15, 30 and 60 minutes. PKD2 was activated upon fat ingestion demonstrating the responsiveness of this kinase to lipids loading (Fig 22B).

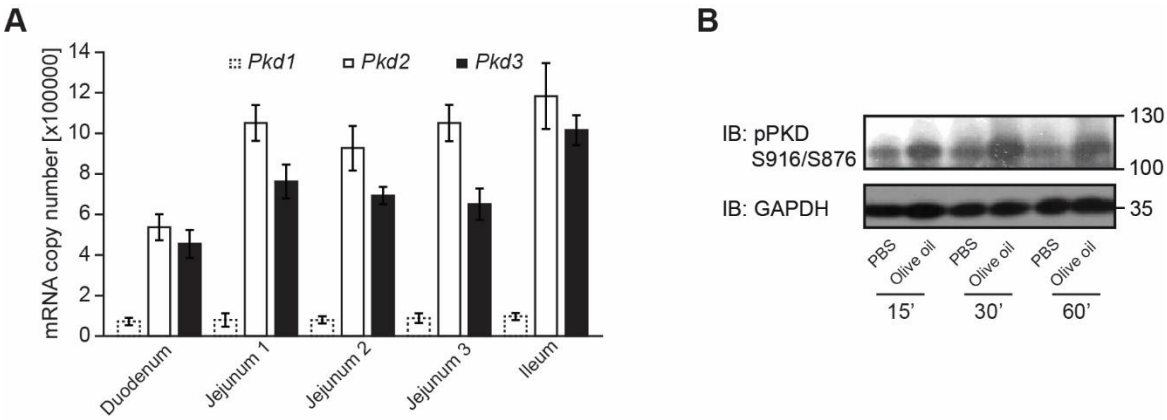

Fig 22. Intestinal quantification of PKDs and activation by lipids.

A. Absolute mRNA quantification of *Pkd1, Pkd2 and Pkd3* in different parts of intestine of C57BL/6 mice. n=4. B. Western blot analysis of phosphorylated PKD (S916/S876) in small intestine of male C57BL/6 mice after overnight fasting, olive oil gavage (or PBS in controls) and dissection at different time-points.

2.1.5.2. Effects of PKD2 inactivation or deletion on other PKD family members.

Given the close relation between the three PKD members and to rule out possible compensatory mechanisms, we analyzed the impact of PKD2 inactivation on the expression and protein levels of PKD1 and PKD3. There were no significant changes on PKD1 and PKD3 expression or total levels as shown in Fig 23. Interestingly, PKD1 was very difficult to detect in WB and PKD2 appeared at a higher molecular weight than PKD1. Two different antibodies verified that PKD2 was effectively inactive in the intestine of *Pkd2*$^{ki/ki}$ mice (Fig 24).

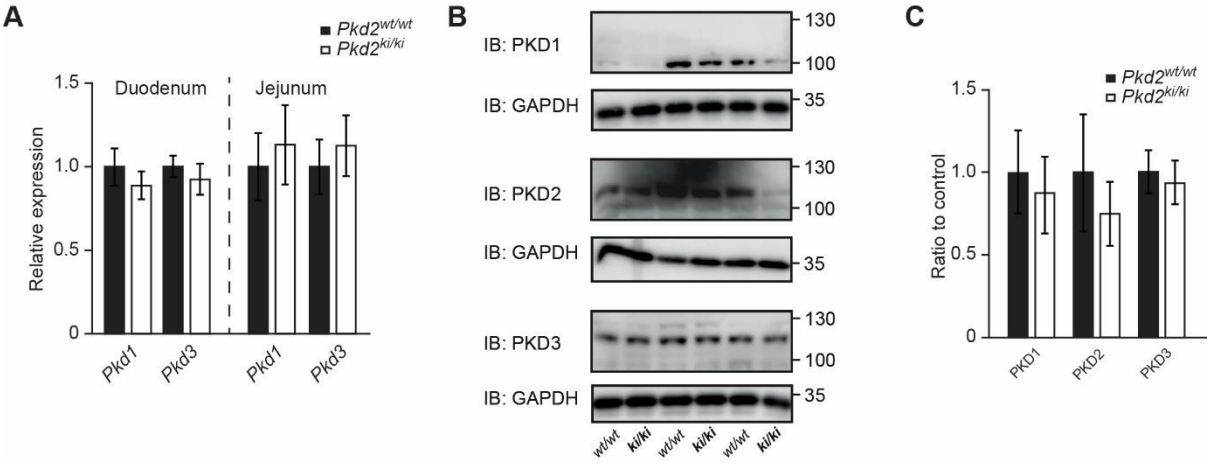

Fig 23. PKDs expression after PKD2 inactivation.

A. *Pkd1* and *Pkd3* expression levels in qPCR in duodenum and jejunum of male mice with indicated genotypes. n=6. B. Western blot analysis of Protein Kinase D1 (PKD1), Protein Kinase D2 (PKD2), and Protein Kinase D3 (PKD3) in small intestine of *Pkd2*$^{wt/wt}$ and *Pkd2*$^{ki/ki}$ male mice. n=3. C. Quantification of the western blots from intestine in B.

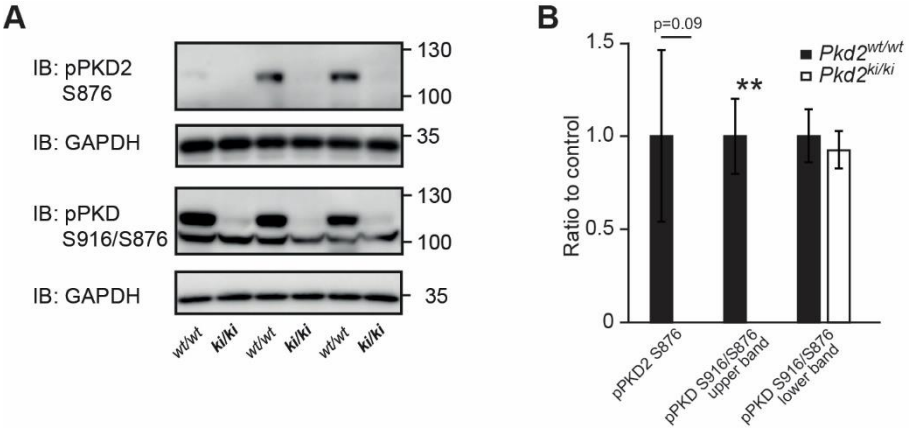

Fig 24. Intestinal PKD2 inactivation is demonstrated by western blot.

A. Western blot analysis and B. quantification of phosphorylated PKD2 (S876) and phosphorylated PKD (S916/S876) in small intestine of *Pkd2*$^{wt/wt}$ and *Pkd2*$^{ki/ki}$ male mice. n=3.

2.1.5.3. In-vitro model confirms PKD2 as a regulator of lipids transport independent of other PKD members.

Caco2 cells were used for the in-vitro studies to test the effects of the deletion of the PKD members. With this purpose, lentivirus were produced in HEK cells and Caco2 cells infected to produce *shRNA* against each of the three proteins. After verifying silencing efficiency, these Caco2 cells were grown in a transwell system which allowed

the study of lipids transport from the apical to the basolateral side of a porous membrane. After overnight stimulation with radioactive ^{14}C-palmitic acid, medium from the apical and the basolateral side, as well as the cell lysates, were quantified in a scintillation counter. Deletion of PKD2 in Caco2 cells significantly reduced the release into the basal medium without affecting the uptake or the retention (Fig 25A). Furthermore, the deletion of other PKDs (PKD1 and PKD3) did not affect the lipids transport, uptake or retention by the Caco2 cells monolayer (Fig 25B-C). These results further proved that PKD2 plays a significant role on lipids transport independently of other PKD members.

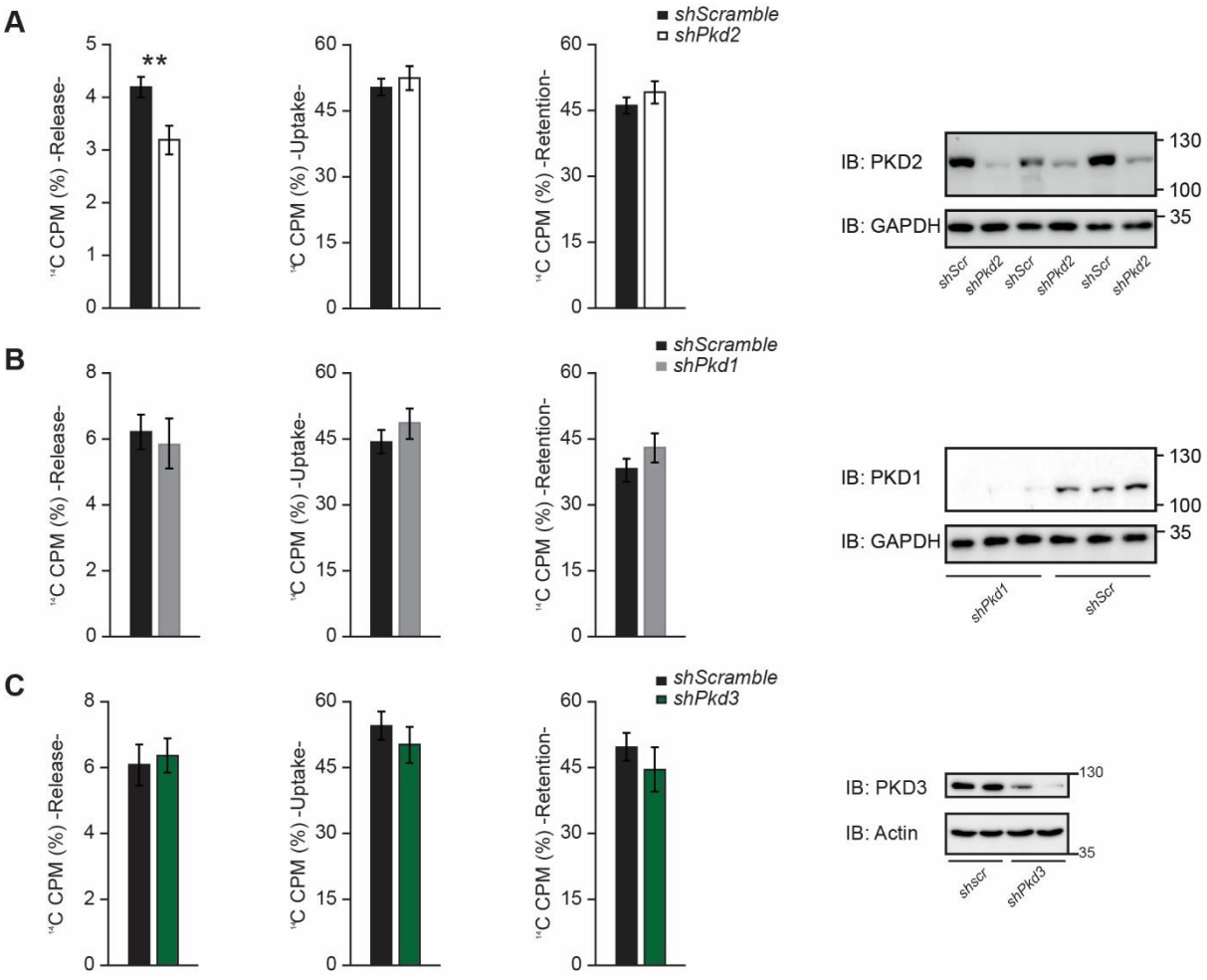

Fig 25. Effect on lipids transport by Caco2 monolayer after deletion of different PKDs.

Percentage of released, uptaken and retained ^{14}C-labeled fatty acids from Caco2 cells expressing *shscramble* or A. *shPkd2,* B. *shPkd1,* C. *shPkd3* in a transwell system. n=6. Western blots for deletion efficiency.

2.1.5.4. Intestine morphology and development are not affected by PKD2 inactivation.

Misregulation of lipids absorption could be associated to several developmental factors in the intestine including: alterations in the corrugations, length, tight junctions or cellular composition (Mazzawi, Gundersen et al. 2015, König, Wells et al. 2016). No alterations were found in the histological studies or the length of the intestine of *Pkd2*$^{ki/ki}$ mice (Fig 26). Moreover, we generated organoids to study possible problems in the proliferation or differentiation of the stem cells of the intestinal crypts (Zietek, Rath et al. 2015). No differences were found between organoids generated from *Pkd2*$^{ki/ki}$ mice and controls regarding development and size, as well as the expression of Villin as a marker of epithelial brush border regulation (Fig 27).

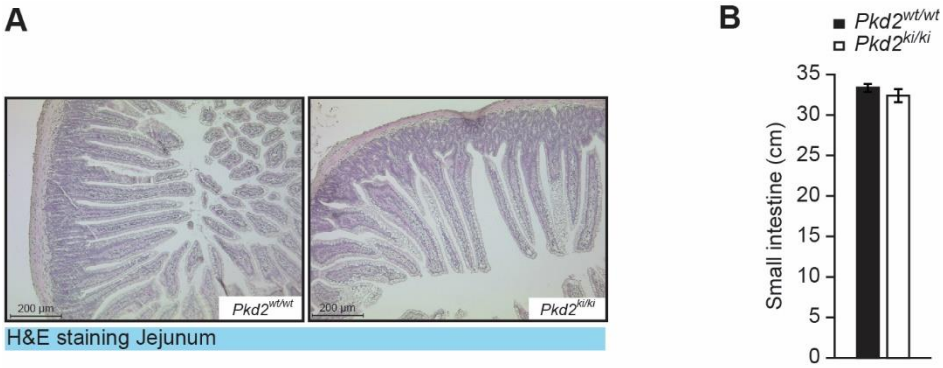

Fig 26. Intestine morphology and length in *Pkd2*$^{ki/ki}$ and control mice.

A. Representative pictures of H&E staining of jejunum of *Pkd2*$^{wt/wt}$ and *Pkd2*$^{ki/ki}$ male mice.

B. Length of small intestine of indicated male mice. n=7 for *Pkd2*$^{wt/wt}$ and n=8 for *Pkd2*$^{ki/ki}$.

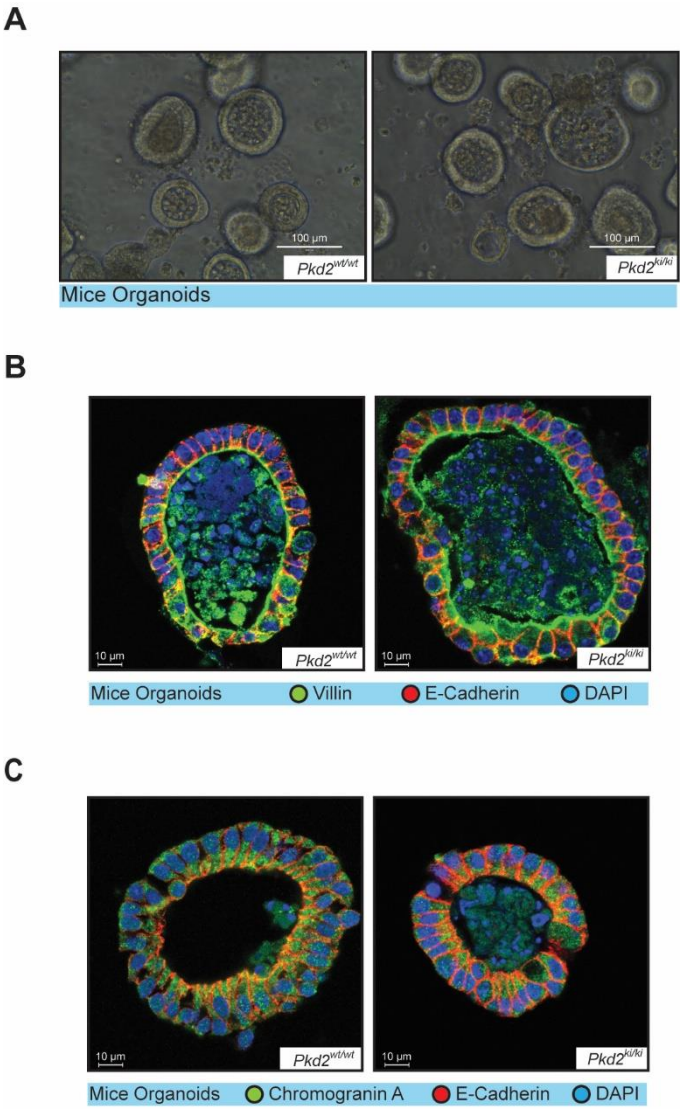

Fig 27. Imaging from organoids derived from intestinal stem cells of *Pkd2*$^{ki/ki}$ and control mice.

A. Representative light microscopy pictures of organoids derived from jejunum crypts of indicated male mice. B. Confocal microscopy images of mice-derived organoids stained for E-cadherin (red), DAPI (blue) and villin (green). C. Confocal microscopy images of mice-derived organoids stained for E-cadherin (red), DAPI (blue) and Chromogranin A (green).

2.2. Specific deletion of PKD2 in intestine reduces fat absorption and protects from obesity.

2.2.1. PKD2 deletion was specific to the intestine and effectively reduced PKD2 activity.

Next, we aimed to prove that specific deletion of PKD2 in intestinal cells confirmed the importance of this kinase in the regulation of lipids absorption. Firstly, we generated genetically modified mice by breeding Villin-Cre mice with *Pkd2 flox/flox* (as specified in the methods section) and the experiments were performed in co-housed littermates knock-out mice (*Pkd2*$^{gut\Delta/\Delta}$) compared to controls (*Pkd2*$^{flox/flox}$). As demonstrated by qPCR and confirmed by Western blot (Fig 28), the deletion of PKD2 was specific to intestinal cells. The deletion also reduced significantly the activation of PKD2 in the intestine as demonstrated by decreased autophosphorylation and activation (Fig 29).

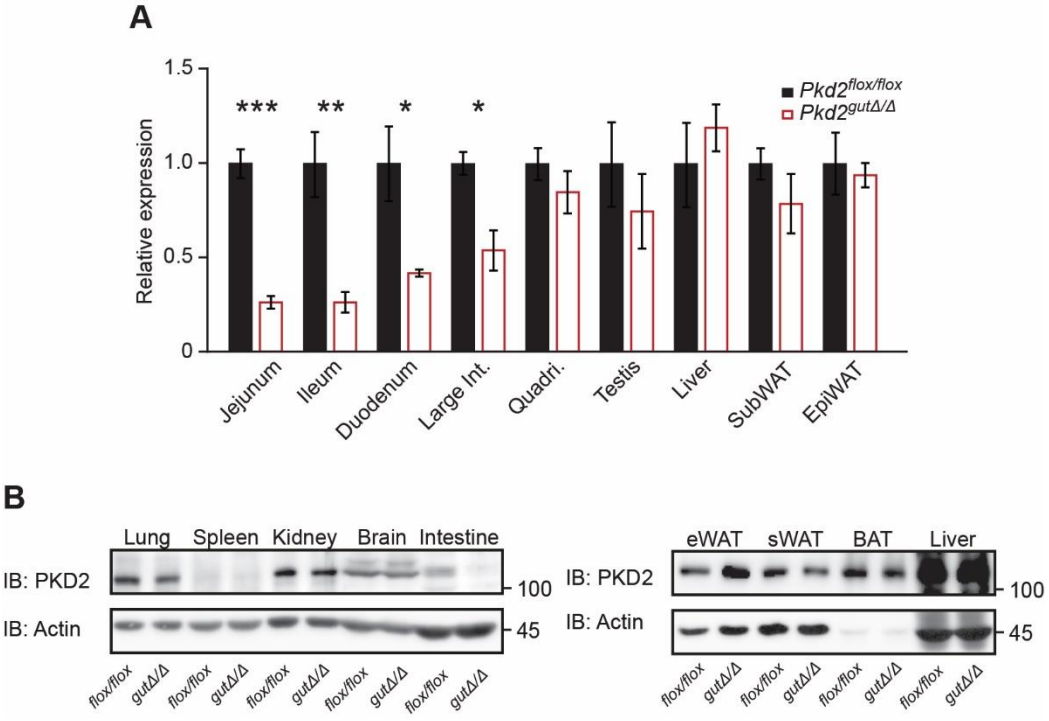

Fig 28. PKD2 is effectively knocked out in the intestine of *Pkd2*$^{gut\Delta/\Delta}$ mice.

A. Relative expression of *Pkd2* in specified organs of *Pkd2*$^{flox/flox}$ and *Pkd2*$^{gut\Delta/\Delta}$ male mice. n=4. B. Western blot of PKD2 in specified organs of *Pkd2*$^{flox/flox}$ and *Pkd2*$^{gut\Delta/\Delta}$ mice.

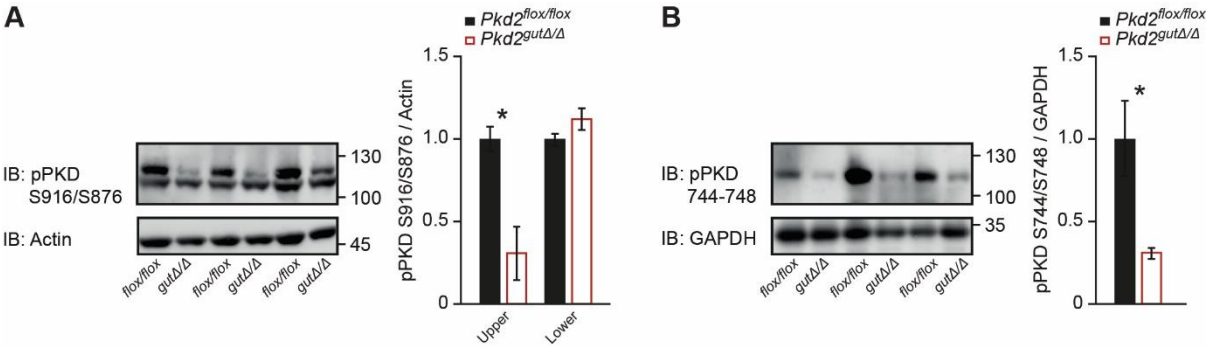

Fig 29. Decreased PKD2 activation in *Pkd2*$^{gut\Delta/\Delta}$ mice.

Western blot and quantification of A. phosphorylated PKD (S916/S876) and B. phosphorylated PKD (S744-748) in small intestine of *Pkd2*$^{flox/flox}$ and *Pkd2*$^{gut\Delta/\Delta}$ male mice. n=3.

2.2.2. Intestinal deletion of PKD2 decreases lipids absorption and protects from HFD-induced obesity.

After an initial adjustment to HFD, *Pkd2*$^{gut\Delta/\Delta}$ and control mice were subjected to a lipids tolerance test. Levels of triglycerides in circulation of *Pkd2*$^{gut\Delta/\Delta}$ were lower at all time-points measured, confirming that intestinal PKD2 is determinant for lipids absorption (Fig 30A). These mice were kept in HFD during 16 weeks and the body weight gain was significantly lower than controls (Fig 30B). The decreased body weight was localized to the adipose tissue as demonstrated by NMR analysis (Fig 30C).

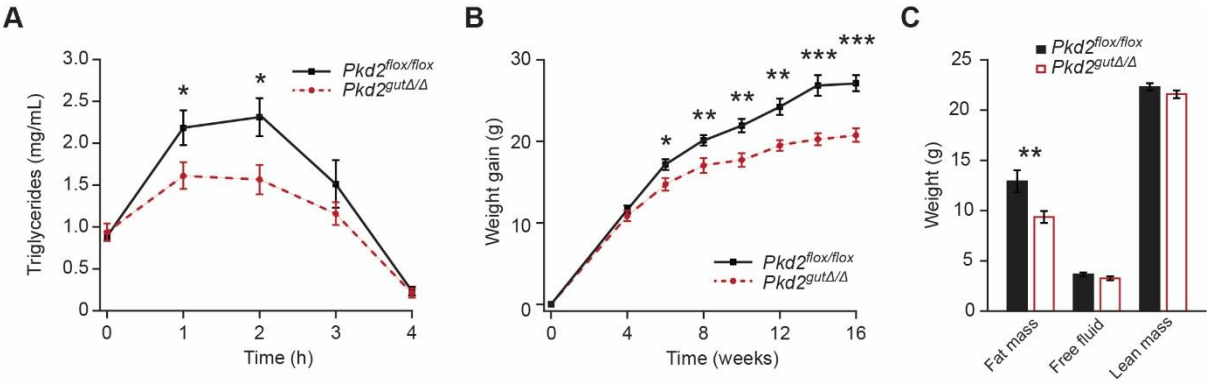

Fig 30. Decreased lipids absorption and body weight gain in *Pkd2*$^{gut\Delta/\Delta}$ mice.

A. Lipids tolerance test after oral gavage of olive oil to *Pkd2*$^{flox/flox}$ and *Pkd2*$^{gut\Delta/\Delta}$ male mice after 6 weeks in HFD. B. Body weight gain of male mice of indicated genotypes in HFD. C. Quantification of fat, free fluid and lean mass by nuclear magnetic resonance of mice in B. n=10.

2.2.3. Improved metabolic profile of *Pkd2*$^{gut\Delta/\Delta}$ mice after challenge with HFD.

As expected, the increased body weight in control animals was detrimental for the management of glucose and lipids when compared to mice lacking intestinal PKD2 (Fig 31). Glucose in circulation of *Pkd2*$^{gut\Delta/\Delta}$ mice was cleared more efficiently than in control animals (Fig 31 A). Moreover, we found a better lipid profile in *Pkd2*$^{gut\Delta/\Delta}$ mice as shown by fasting free-fatty acids and triglycerides in circulation (Fig 31B-C).

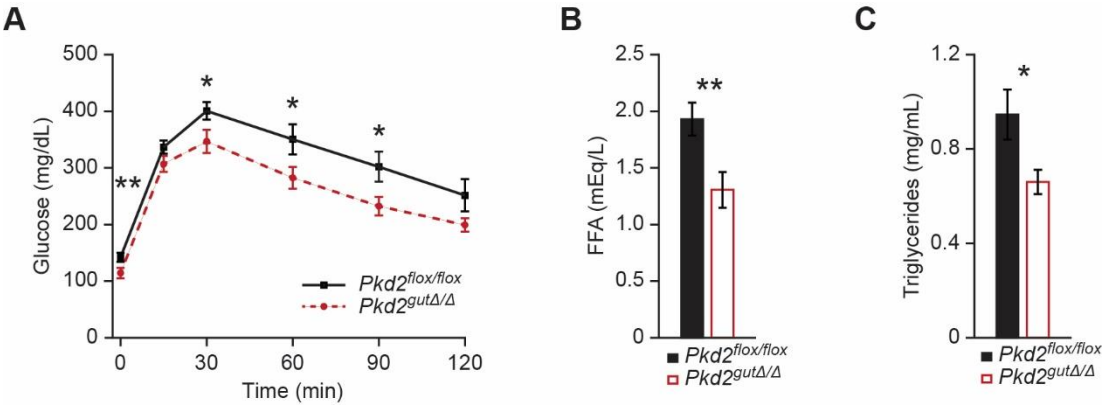

Fig 31. Improved metabolic parameters in *Pkd2*$^{gut\Delta/\Delta}$ mice after HFD.

A. Glucose tolerance test of male mice with indicated genotypes after 16 weeks in HFD. B. Free-fatty acids and C. Triglycerides content in serum of male mice after 17 weeks in HFD. n=10.

2.2.4. Energy balance and morphology of intestine or liver are not affected in *Pkd2*$^{gut\Delta/\Delta}$ mice.

We verified that deletion of PKD2 did not exhibit gross alterations in other organs. For that purpose, we measured the intestinal length and performed H&E staining of intestine and liver (Fig 32) and there were no obvious differences. Similarly, when *Pkd2*$^{gut\Delta/\Delta}$ mice were kept monitored in metabolic cages, they presented no significant differences in food intake or energy expenditure during day or night (Fig 33).

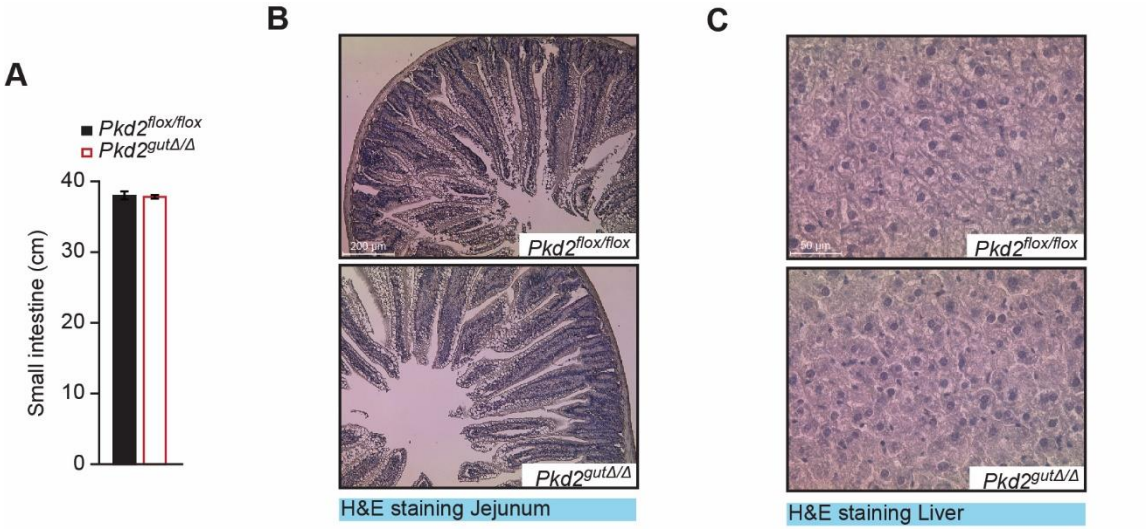

Fig 32. Intestinal and liver morphology of *Pkd2*$^{gut\Delta/\Delta}$ and control mice.

A. Length of small intestine of indicated male mice. n=4. B. Representative H&E pictures of jejunum and C. liver of male mice with indicated genotypes after 17 weeks in HFD.

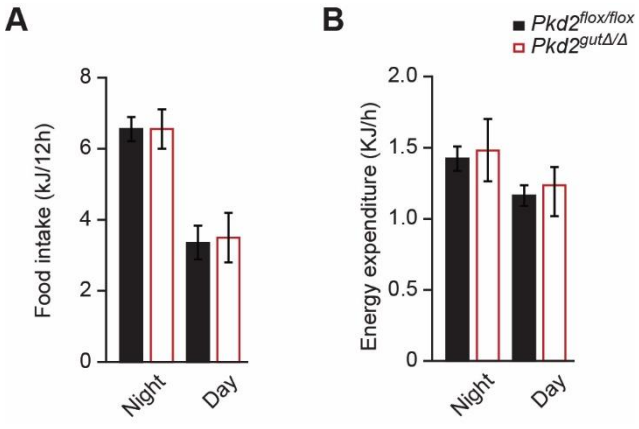

Fig 33. Metabolic cages analysis under PKD2 deletion.

A. Food intake and B. energy expenditure of *Pkd2*$^{flox/flox}$ and *Pkd2*$^{gut\Delta/\Delta}$ male mice after 13 weeks in HFD. n=4.

2.2.5. *Pkd2*$^{gut\Delta/\Delta}$ mice possess a healthier microbiota profile.

Microbiota, diet composition and nutrients absorption are intertwined determinants of metabolic homeostasis. Therefore, we explored into the microbiota composition of *Pkd2*$^{gut\Delta/\Delta}$ and control mice by using 16S rRNA gene sequencing of the intestinal and cecal contents. Firstly, we analyzed the Shannon Index in order to establish the alpha diversity in different sections of the intestine. Fig 34A. shows a significant increase in the diversity of microbiota found in the duodenum of *Pkd2*$^{gut\Delta/\Delta}$ mice. A similar trend was found in the jejunum and ileum but not in the cecum. Next, we analysed specific changes in operational taxonomic units (OTUs). The study of OTUs identified that Bacteroides were present only in the duodenum content of *Pkd2*$^{gut\Delta/\Delta}$ mice and completely absent in respective control animals (Fig 34B). As shown in Fig 34C-D, supervised clustering resulted in similar bacterial composition in jejunum and ileum, which were merged for further analysis. Lastly, the analysis demonstrated significant changes between genotypes in the beta diversity of duodenum and jejunum/ileum but not in the cecum (Fig 34E). In conclusion, the intestinal content of *Pkd2*$^{gut\Delta/\Delta}$ mice showed higher diversity, the presence of Bacteroides and in general an improved microbiota profile.

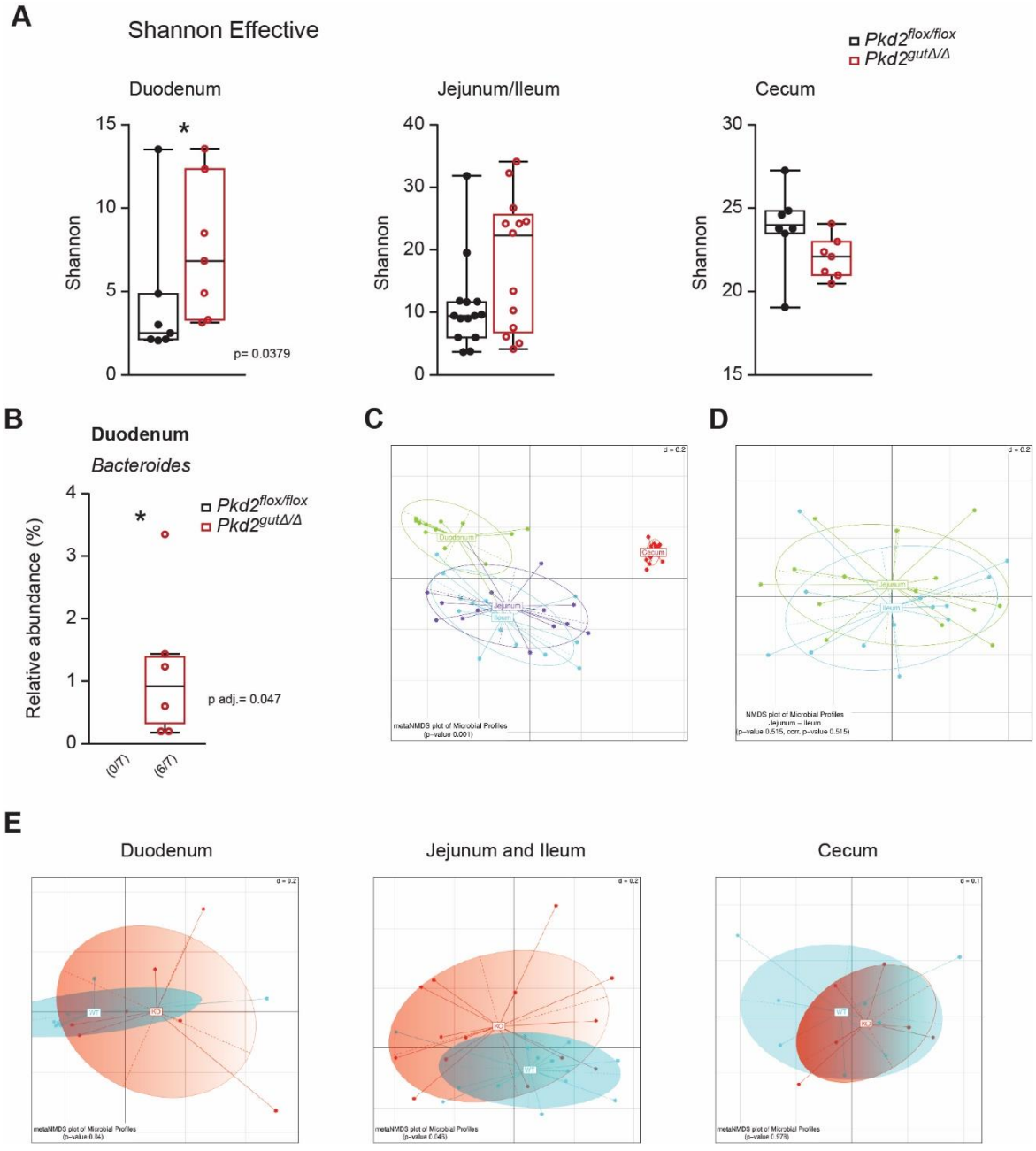

Fig 34. Intestinal deletion of PKD2 promotes a more diverse and healthier microbiome.

A. Differences in bacterial alpha diversity as indicated by Shannon Index. B. Changes in specific Operational taxonomic unit (OTU) in small intestinal samples. C. MetaNMDs plots of bacterial composition show specific differences in small intestinal section. D. Pairwise PERMANOVA indicates no significant differences in compositions of Jejunum & Ileum. E. Beta diversity visualized by metaNMDS plots presents differences in the microbial composition in Duodenum and Jejunum/Ileum. Blue: *Pkd2*$^{flox/flox}$ Red: *Pkd2*$^{gut\Delta/\Delta}$. n=7.

2.3. Pharmacological approach to reduce intestinal lipids absorption via PKD2 inhibition.

2.3.1. In-vitro inhibition of PKD2 reduces lipids transport.

Several PKD inhibitors have been previously tested, therefore, given our results in genetically modified mice, we hypothesized that localized inhibition of PKD2 in intestine with these substances might provide relevant clinical significance.

As a first approach, we utilized Caco2 cells in a transwell system and stimulate these cells with taurocholic acid (bile acid for emulsification), oleic acid and ^{14}C-palmitic acid. The quantification of radioactivity in the basolateral medium proved decreased release of triglycerides in a dose-dependent manner in cells treated with CRT0066101 (Fig 35A). Of note, when the inhibitor was added to cells depleted from PKD2, there was no further reduction in triglycerides transport, demonstrating, once again, that PKD2 is the member of the PKD family members responsible for this phenotype (Fig 35B).

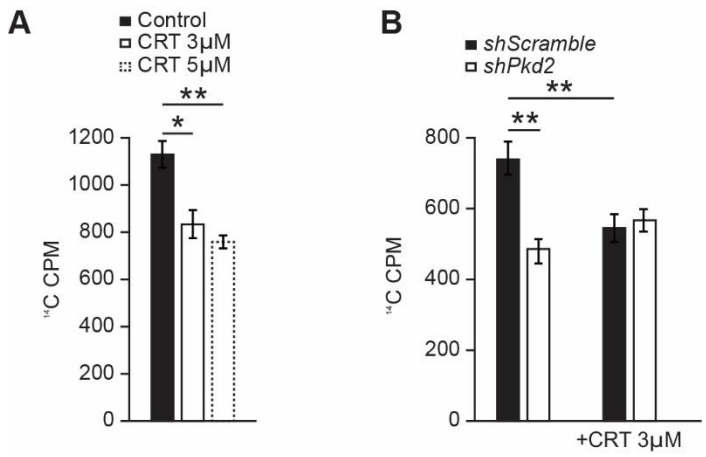

Fig 35. In-vitro inhibition of PKD decreases lipid transport in a PKD2-dependent manner.

Basolateral release of ^{14}C-labeled fatty acids in Caco2 cells grown in a transwell system. A. Cells are treated with CRT0066101 at the indicated concentrations for 24 hours. n=6. B. Caco2 cells expressing *shscramble* or *shPkd2* are treated with CRT0066101 (CRT) or control for 24 hours. n=8.

2.3.2. Small-molecule inhibitor of PKD2 reduces lipids absorption and development of obesity.

2.3.2.1. Oral gavage of CRT0066101 inhibits PKD2 activation in the intestine.

In order to test in-vivo the ability of CRT0066101 to inhibit PKD2 activation and the consequences of such treatment, we administered daily gavage of 10mg/kg of the inhibitor or water to wildtype C57BL/6 mice. As presented in Fig 36, mice receiving the inhibitor showed a significant decreased in the activation of PKD2 in jejunum but not in liver or EpiWAT.

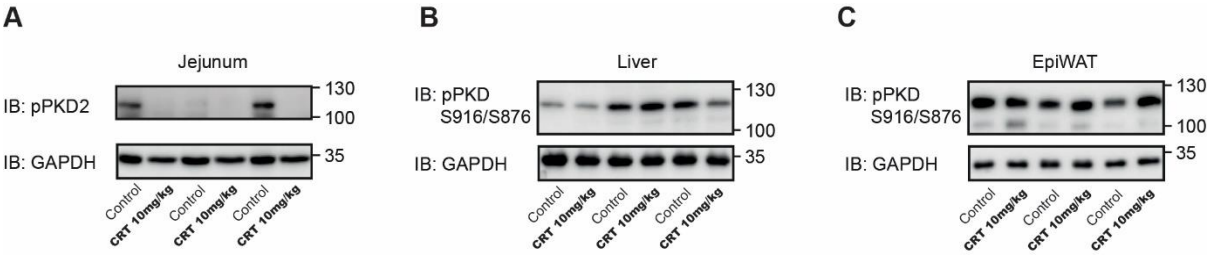

Fig 36. Oral treatment with CRT0066101 inhibits PKD2 activation specifically in intestine.

C57BL/6 mice in HFD were treated with CRT0066101 or control (water) for 13 weeks. A. Western blot analysis of phosphorylated PKD2 in jejunum. B. Western blot of phosphorylated PKD (S916/S876) in liver. C. Western blot of phosphorylated PKD (S916/S876) in EpiWAT. n=3.

2.3.2.2. CRT0066101 treatment reduces lipids uptake, increases energy excretion and reduces body weight.

Mice received 10mg/kg/day of inhibitor (or control) and ad libitum access to HFD. After 9 weeks, the mice were challenged with a lipids tolerance test by gavaging olive oil after overnight fasting. Non-treated mice presented higher levels of triglycerides in circulation after gavage (Fig 37A) demostrating that use of the inhibitor effectively reduces the ability to absorb lipids in the intestine. This result was further supported by the quantification of total energy content in feces by calorimetric bomb (Fig 37B). Mice receiving the inhibitor excreted more energy in feces compared to those receiving water. As a final consequence of the decreased lipids absorption/increased energy

excretion, mice receiving CRT0066101 gained less body weight than their counterparts also in HFD (Fig 37C).

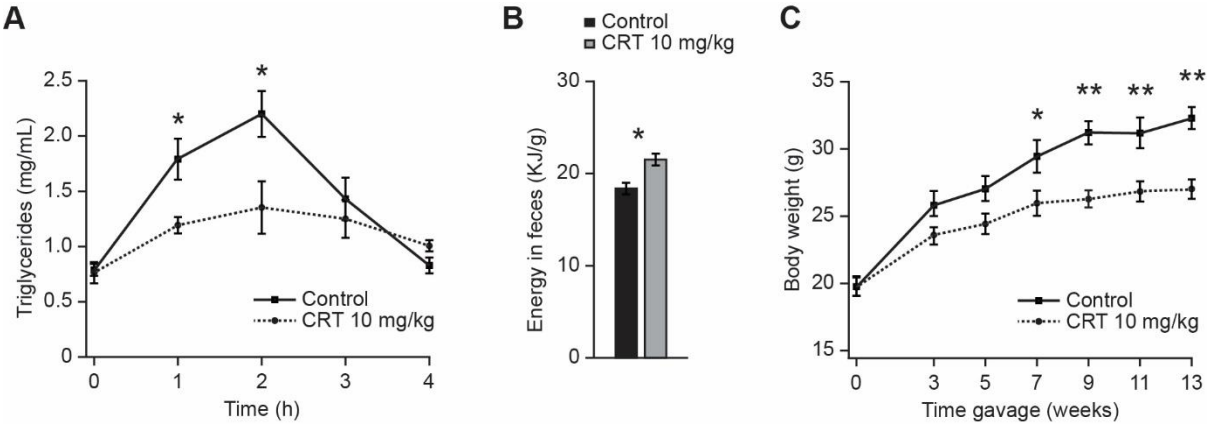

Fig 37. Oral treatment with CRT0066101 decreases lipids absorption, increases excretion and protects from HFD-induced obesity.

Male C57BL/6 mice under HFD were treated with daily gavage of CRT0066101 (10mg/kg) or control (water). A. Lipids tolerance test after oral gavage of olive oil. 9 weeks after starting the experiment. B. Energy content per gram of feces. C. Body weight of mice. n=6 for control and n=5 for CRT0066101.

2.3.2.3. Long-term treatment improved metabolic phenotype of mice under HFD.

Treatment with CRT0066101 not only decreased lipids absorption and body weight gain, but it also improved glucose clearance, insulin sensitivity and decreased insulin levels (Fig 38A-C). There were no changes in hepatic enzymes or triglycerides content (Fig 38D-E). Furthermore, H&E staining showed that mice receiving the inhibitor have a healthier BAT, characterized for being multilocular (Fig 38F). Altogether, these results demonstrate that the decreased body weight under CRT0066101 treatment came along with improved metabolic fitness.

We also utilized metabolic cages to determine whether other components of the energy balance equation were affected when mice received the inhibitor under HFD. However, no significant differences were found in energy intake, energy expenditure or activity of mice (Fig 39A-C).

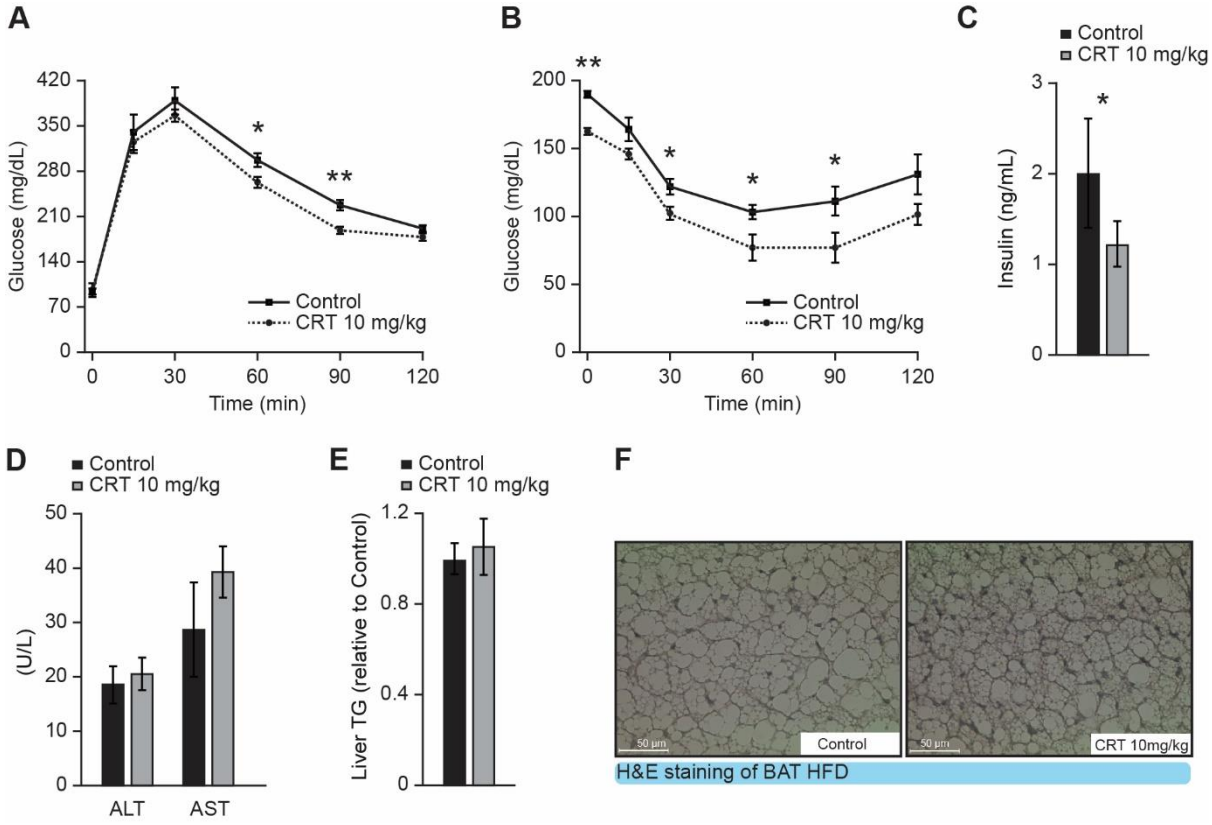

Fig 38. Effects of CRT0066101 treatment on GTT, ITT, insulin levels, liver and BAT.

Male C57BL/6 mice under HFD, which received daily gavage of CRT0066101 or water, were analysed for different metabolic parameters. A. Glucose tolerance test after 10 weeks of treatment. B. Insulin tolerance test after 11 weeks of treatment. C. Insulin levels after 13 weeks. Samples taken after 4 hours fasting and 1 hour refeeding. D. Alanine aminotransferase (ALT) and Aspartate aminotransferase (AST) levels in serum after 13 weeks. E. Triglyceride content in the liver after 13 weeks. Relative to control. F. Representative H&E pictures of brown adipose tissue (BAT) after 13 weeks. n=6 for control and n=5 for CRT0066101.

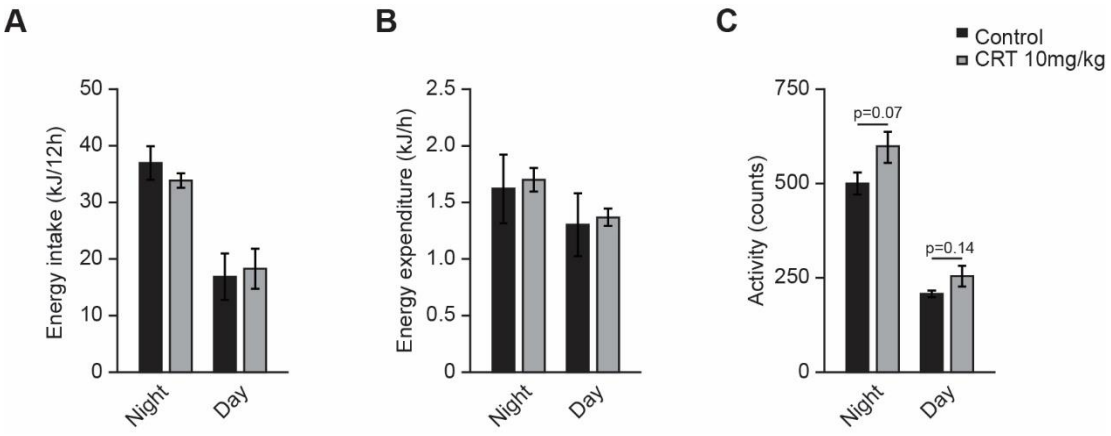

Fig 39. A. Energy intake, B. Energy expenditure, and C. Activity of male C57BL/6 mice under HFD which received CRT0066101 or water (control). Measurements after 7 weeks of treatment and HFD. n=4

2.3.3. Use of PKD2 inhibitor rescues from pre-established obesity and its metabolic consequences.

We demonstrated that oral intake of CRT0066101 efficiently inhibited PKD2 activation specifically in intestine and, as a result, intestinal lipids uptake was impaired. Therefore, we aimed to test the possibility of using this inhibitor after overweight was already induced by high-fat diet. With that purpose, we fed C57BL/6 mice HFD during 7 weeks and then randomly assigned into two different groups. All animals continued receiving HFD but one group started receiving daily gavage of CRT0066101 (10mg/kg) and the other received gavage of water (control). Three weeks after the gavage of inhibitor started, the weight of mice on the control group was already significantly higher that the treated mice (Fig 40A). The difference in body weight continued increasing during the rest of the experiment and it was localized to the adipose depots as calculated by the tissues weights and by nuclear magnetic resonance (Fig 40B-C).

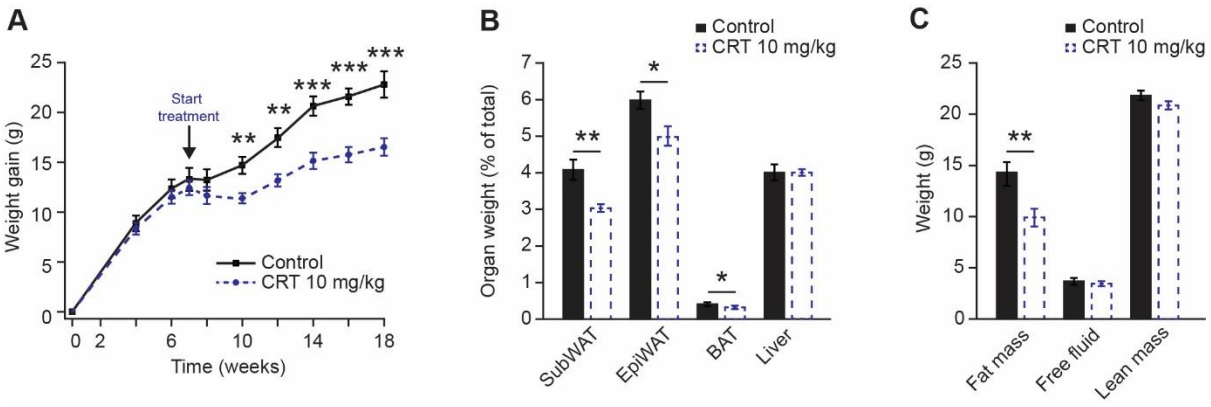

Fig 40. Overweight mice are protected from further body weight gain by treatment with CRT0066101.

In a rescue experiment, C57BL/6 mice received HFD for 7 weeks and then they were randomly split into 2 groups and started receiving gavage of either CRT0066101 or water for 11 weeks. HFD continued along with treatment. A. Body weight gain. B. Organ weight (expressed as percentage of total body weight) of different fat depots and liver. C. Quantification of fat, free fluid and lean mass by nuclear magnetic. n=8.

We also challenged the mice with intraperitoneal injection of glucose (Fig 41A) and insulin (Fig 41B). As expected, mice in the control group demonstrated the obesity-associated glucose and insulin intolerance and performed poorly when compared to

the treated mice. These results reveal that CRT0066101 might be a good candidate in the pursuit of adjuvants for weight control and comorbidities.

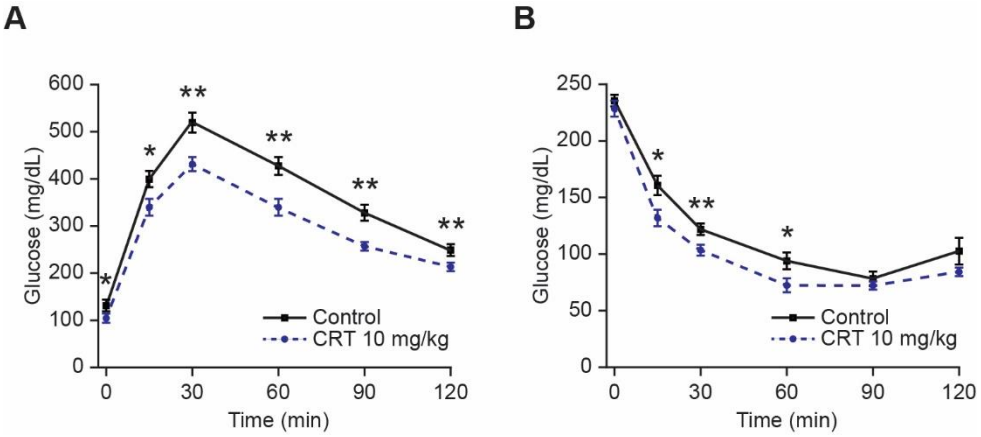

Fig 41. Metabolic tests performed in mice from the rescue experiment.

A. Glucose tolerance test 8 weeks after starting the treatment with CRT0066101 or water. B. Insulin tolerance test 10 weeks after starting the treatment. n=8.

2.4. Studies on the mechanism involved in the PKD2 regulation of lipids absorption.

2.4.1. Intestinal permeability, pancreatic enzymes and bile acids cycle are not affected by PKD2 activity.

Different factors, steps and enzymatic reactions are involved in the whole process of lipids absorption. Chemical digestion, lipids emulsification and transport through the enterocytes are just examples of the complex process of lipids extraction from nutrients and delivery to organs for storage or utilization (Iqbal and Hussain 2009). Therefore, we decided to explore several aspects that could be involved in the decreased lipid transport from the lumen into circulation when PKD2 was genetically inactive, knockout, or chemically inhibited.

Firstly, we measured paracellular permeability of the intestine by gavaging dextran and quantifying serum concentration. We found that *Pkd2*$^{ki/ki}$ mice and those receiving

CRT0066101 inhibitor did not show any significant difference to their respective controls (Fig 42A-B). Furthermore, as demonstrated by the measurement of transepithelial electric resistance, Caco2 cells expressing *shPkd2* in transwells develop in a monolayer with similar barrier integrity to the Caco2 *shScramble* (Fig 42C). Therefore, the reduction in triglycerides crossing in the in-vivo and in-vitro models are not due to changes in epithelial permeability.

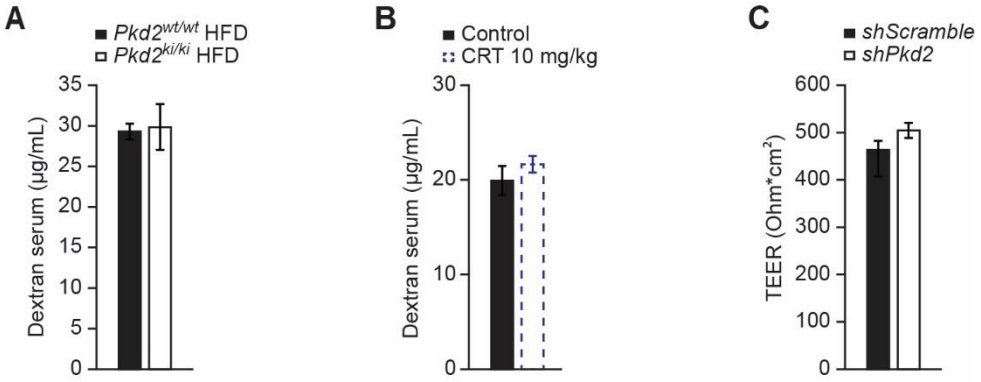

Fig 42. Intestinal permeability in mice and transwell system.

A. Dextran in serum after gavage of *Pkd2*$^{wt/wt}$ and *Pkd2*$^{ki/ki}$ male mice. n=4. B. Dextran concentration in serum after gavage of mice from the rescue experiment. n=8. C. Barrier integrity of *shScramble* and *shPkd2* Caco2 cells in transwells, determined as transepithelial electrical resistance. n=6.

Next, we explored in *Pkd2*$^{ki/ki}$ and control mice if there were changes that might affect lipids digestion or emulsification. Western blot analysis of duodenum showed no differences the secretion of pancreatic lipase between genotypes (Fig 43A). Furthermore, qPCR from the pancreas of these animals also showed no difference in the expression levels of pancreatic lipase and colipase (Fig 43B). Also, bile acids for emulsification are produced and re-absorbed in the liver and ileum, respectively. Therefore, we performed qPCR analysis of those organs. However, the expression levels of different genes involved in the production, metabolism and transport of bile acids were unchanged between *Pkd2*$^{wt/wt}$ and *Pkd2*$^{ki/ki}$ mice (Fig 43C).

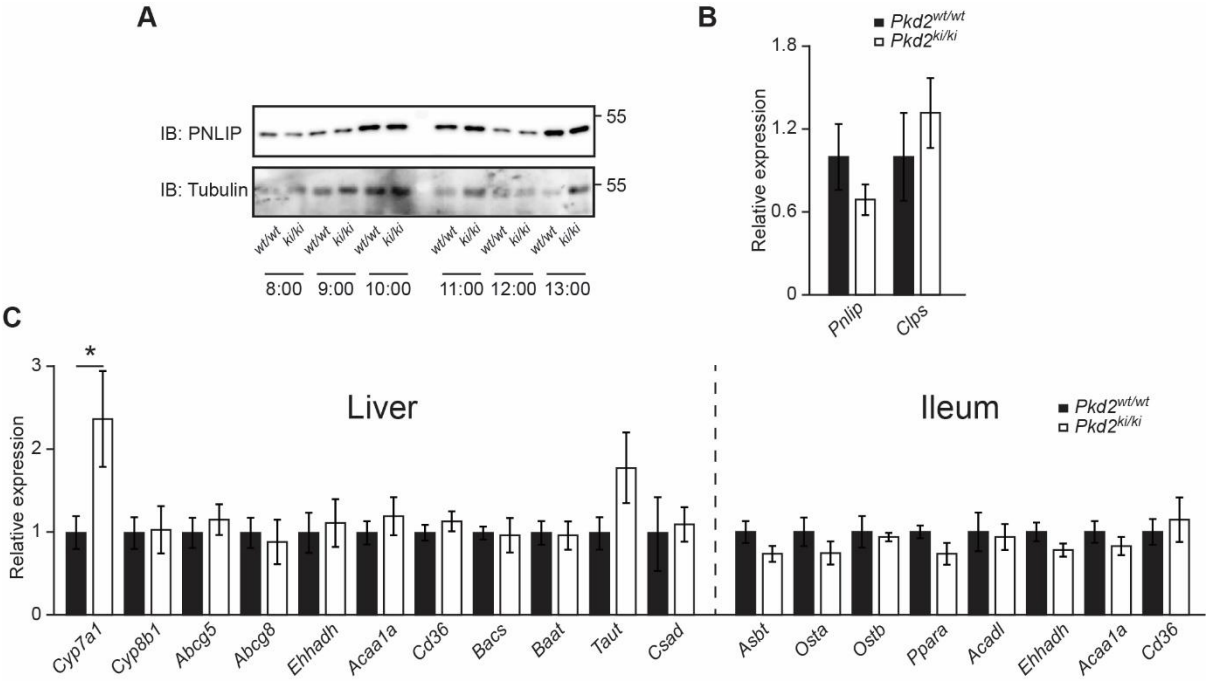

Fig 43. Analysis of proteins involved in lipids digestion and emulsification in the intestine of *Pkd2*$^{wt/wt}$ and *Pkd2*$^{ki/ki}$ male mice.

A. Western blot for pancreatic lipase in duodenum of *Pkd2*$^{wt/wt}$ and *Pkd2*$^{ki/ki}$ male mice 1 hour after olive oil gavage. n=6. The animals were dissected at the indicated time of the day. B. Relative expression of specified genes in pancreas of *Pkd2*$^{wt/wt}$ and *Pkd2*$^{ki/ki}$ male mice. n=6. C. Relative expression of genes involved in bile acids production, metabolism and transport in liver and ileum of male mice with indicated genotypes after 1 week of HFD. n=6.

2.4.2. PKD2 does not affect expression of several proteins involved in uptake, re-esterification and packaging.

Enterocytes are the absorptive cells of the intestine. These cells are in charge of the uptake and re-esterification of FFA and monoglycerides into TG as well as the packaging and release of these lipids, together with cholesterol, into chylomicrons (Demignot, Beilstein et al. 2014). We tested if the expression or protein levels of the main proteins in charge of these processes in the intestine were changed by PKD2 activity. We found that expression levels of transporters like *Fabp2, Fabp4, Fatp2, Fatp4 and Cd36* were unchanged as well as protein levels of CD36 (Fig 44A-C). In addition, expression and protein levels of proteins involved in TG re-esterification or packaging into chylomicrons, including DGAT1, MOGAT2 and MTTP were not affected in the intestine of *Pkd2*$^{ki/ki}$ mice when compared to controls (Fig 44B-C). Moreover, intestinal gene expression of the main apolipoproteins composing chylomicrons (namely *ApoA1, ApoB48* and *ApoA4*) did not differ between genotypes,

as it was the case for the protein quantification of two of them: APOA1 and APOB48 (Fig 44B-C). Taken together, these results indicate that PKD2 activity has no effect on the expression or protein levels of most of the lipids' transport machinery in enterocytes.

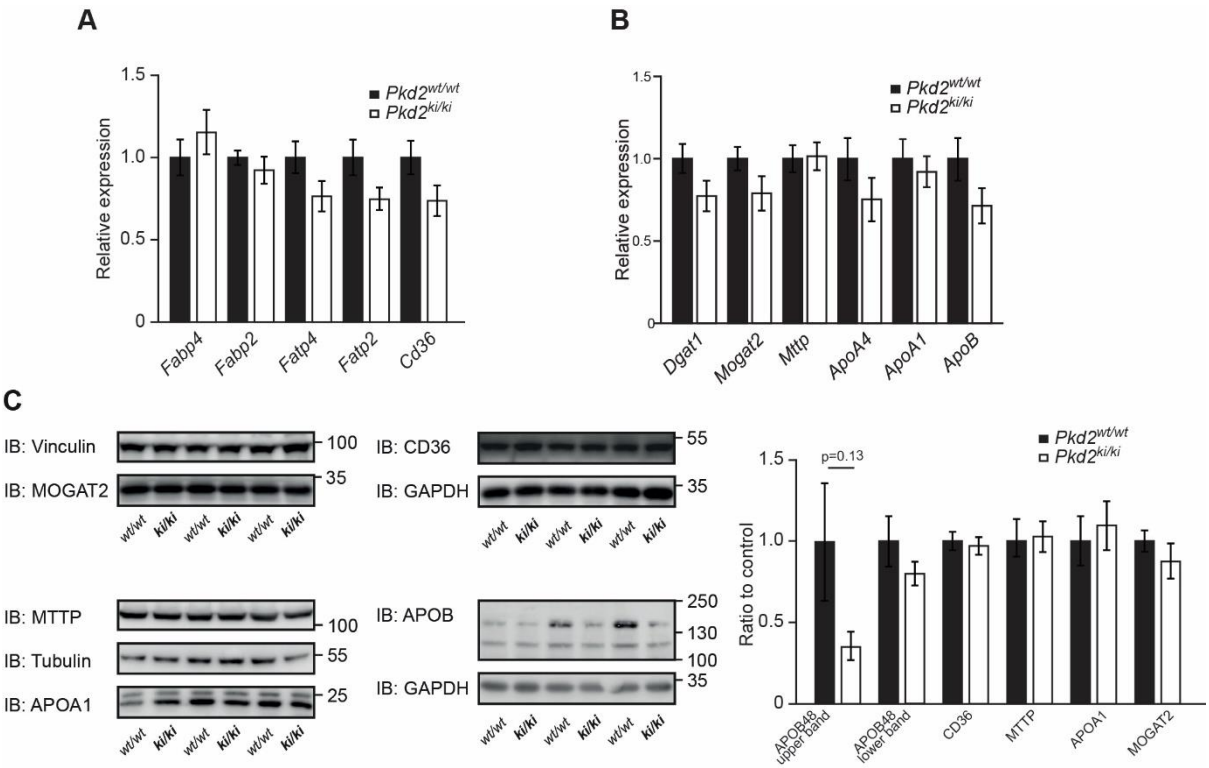

Fig 44. qPCR and western blot analysis of proteins involved in triglycerides metabolism and packaging of chylomicrons in enterocytes.

A. Relative expression of genes involved in fatty acids transport in jejunum of indicated male mice. n=6. B. Relative expression of genes involved in triglycerides and chylomicrons synthesis in jejunum of *Pkd2*$^{wt/wt}$ and *Pkd2*$^{ki/ki}$ male mice after 1 week in HFD. n=7. C. Western blot analysis of proteins involved in triglycerides and chylomicrons synthesis in small intestine of *Pkd2*$^{wt/wt}$ and *Pkd2*$^{ki/ki}$ male mice after one week of HFD. Quantification of the bands for each protein normalized to loading control and relative to *Pkd2*$^{wt/wt}$. n=3.

2.4.3. PKD2 phosphorylates APOA4 and increases chylomicron size

As shown before, inactivation of PKD2 did not affect most of the proteins involved in triglycerides' absorption, repackaging or release from enterocytes. However, the quantification by western blot of protein levels of APOA4 exhibited a significant increase in APOA4 levels in all the models used during this study (Fig 45). Lysates

from jejunum of *Pkd2*$^{ki/ki}$ mice (Fig 45A), *Pkd2*$^{gut\Delta/\Delta}$ mice (Fig 45B) and those treated with CRT0066101 (Fig 45C) showed increased levels of APOA4 when compared to their respective controls. Increased levels of this apolipoprotein were also found in the basolateral medium of Caco2 *shPkd2* cells growing in a transwell system (Fig 45D). Moreover, when the same amount of serum from *Pkd2*$^{wt/wt}$ and *Pkd2*$^{ki/ki}$ mice (overnight fasted, 2 hours refed) were run in a western blot, we confirmed unchanged levels of APOA1 and APOB and a clear increase in APOA4 levels in *Pkd2*$^{ki/ki}$ mice (Fig 46).

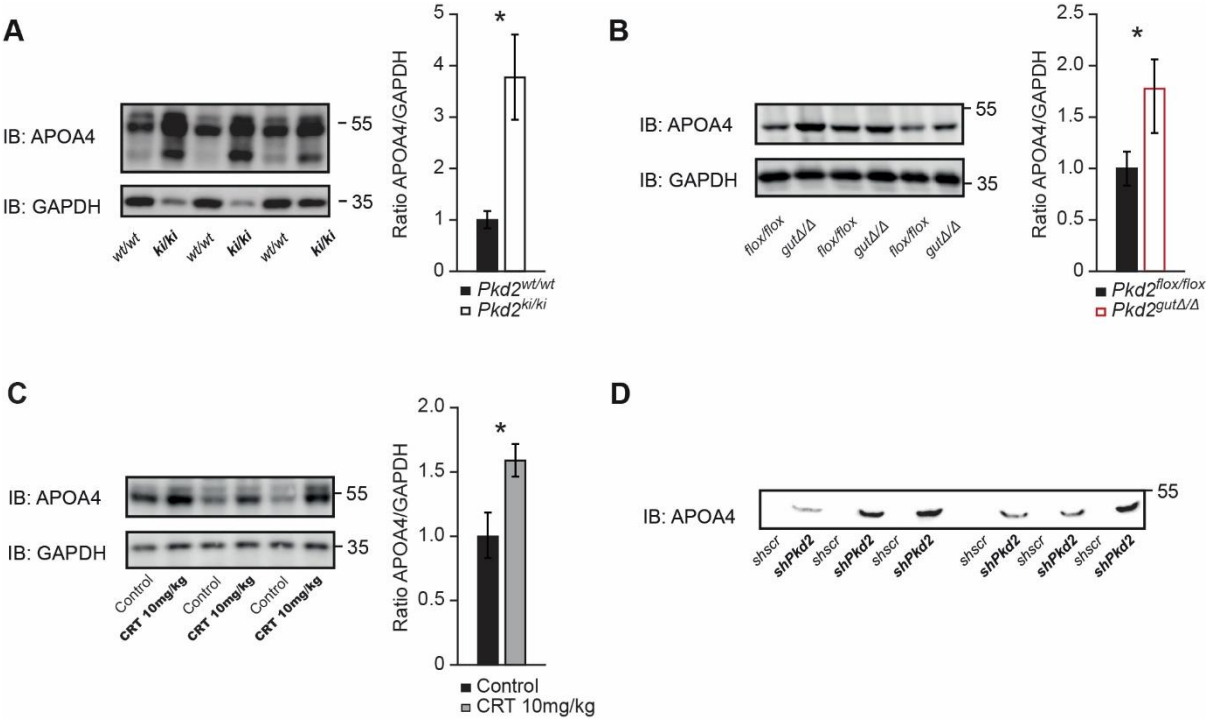

Fig 45. APOA4 levels increase under PKD2 inactivation, deletion or inactivation.

A. Western blot of ApoliproteinA4 in jejunum of *Pkd2*$^{wt/wt}$ and *Pkd2*$^{ki/ki}$ male mice after one week of HFD. Quantification of bands normalized to loading control and relative to *Pkd2*$^{wt/wt}$. n=3. B. WB of ApoliproteinA4 in jejunum of *Pkd2*$^{flox/flox}$ and *Pkd2*$^{gut\Delta/\Delta}$ male mice after one week of HFD. Quantification of bands normalized to loading control and relative to *Pkd2*$^{flox/flox}$ n=7. C. WB of Apolipoprotein A4 in jejunum of male C57BL/6 mice in HFD and treated with CRT0066101 or control for 13 weeks. Quantification of bands normalized to GAPDH and relative to control (water) n=6. D. WB of 20µL of basal medium of Caco2 cells expressing *shscramble* or *shPkd2* in transwell system after 12 hours stimulation with oleic acid. n=6.

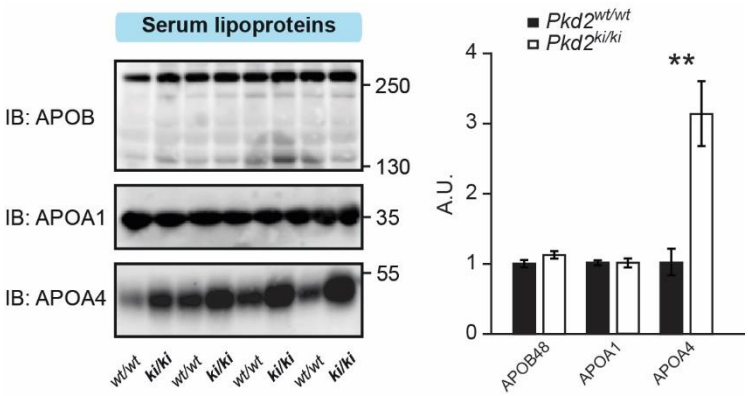

Fig 46. Chylomicron-associated apolipoproteins in serum of *Pkd2*$^{wt/wt}$ and *Pkd2*$^{ki/ki}$ mice.

Western blot analysis of specified apolipoproteins in 10µL of serum of overnight fasted, 2 hours refed male animals after 1 week in HFD. Quantification of bands relative to *Pkd2*$^{wt/wt}$. n=4.

Next, we hypothesized that PKD2 might regulate directly APOA4 by a posttranslational modification, presumably a phosphorylation. Consequently, we performed an in-vitro kinase assay by using recombinant PKD2 and APOA4 proteins in the presence or absence of the PKD inhibitor CRT0066101. After the incubation period, each sample was split into two runs for western blot. One of the membranes was incubated with PKD2 and APOA4 antibodies for loading control and the other was blotted with RxxS/T* antibody which recognizes the phosphorylation motif of PKDs. Fig 47 shows that PKD2 effectively phosphorylates APOA4 and this modification is absent when the PKD inhibitor is added to the reaction. Interestingly, autophosphorylation of PKD2 also seems to be increased by the presence of APOA4 and again reduced in the presence of CRT0066101.

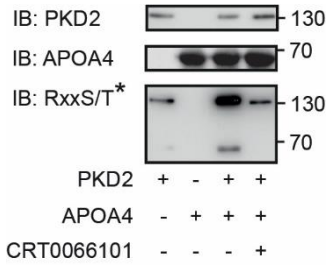

Fig 47. PKD2 phosphorylates APOA4.

Western blot against PKD2, APOA4 and RxxS/T* (phosphorylation motif of PKD2) after an in-vitro kinase assay with recombinant proteins and in the presence or absence of PKD inhibitor (CRT0066101).

Since APOA4 is a key component of chylomicrons and we had already proved a significant decrease in lipids absorption under a defective function of PKD2, the next step was to verify the size of chylomicrons under electron microscopy. With that purpose, we fasted mice overnight, gavaged them with olive oil, and collected their plasma two hours later. Representative pictures of chylomicrons from *Pkd2*$^{wt/wt}$ and *Pkd2*$^{ki/ki}$ mice (Fig 48A) show that the size of these lipoproteins is reduced under PKD2 inactivation. The quantification of the chylomicrons' size confirmed that the percentage of chylomicrons with higher size is increased in wild-type mice compared to *Pkd2*$^{ki/ki}$ mice (Fig 48B). Moreover, chylomicrons' size was also smaller in the plasma of *Pkd2*$^{gut\Delta/\Delta}$ mice as it can be appreciated in Fig 48C. Unfortunately, this result could not be quantified due to the lack of adequate replicates. Collectively, our data indicates that PKD2 phosphorylates APOA4 in order to increase chylomicron's size and, subsequently, to promote lipids' absorption. The discovery of this novel regulatory pathway open the possibility of using PKD2 inhibition as a target for decreasing lipids absorption for the treatment of obesity and comorbidities.

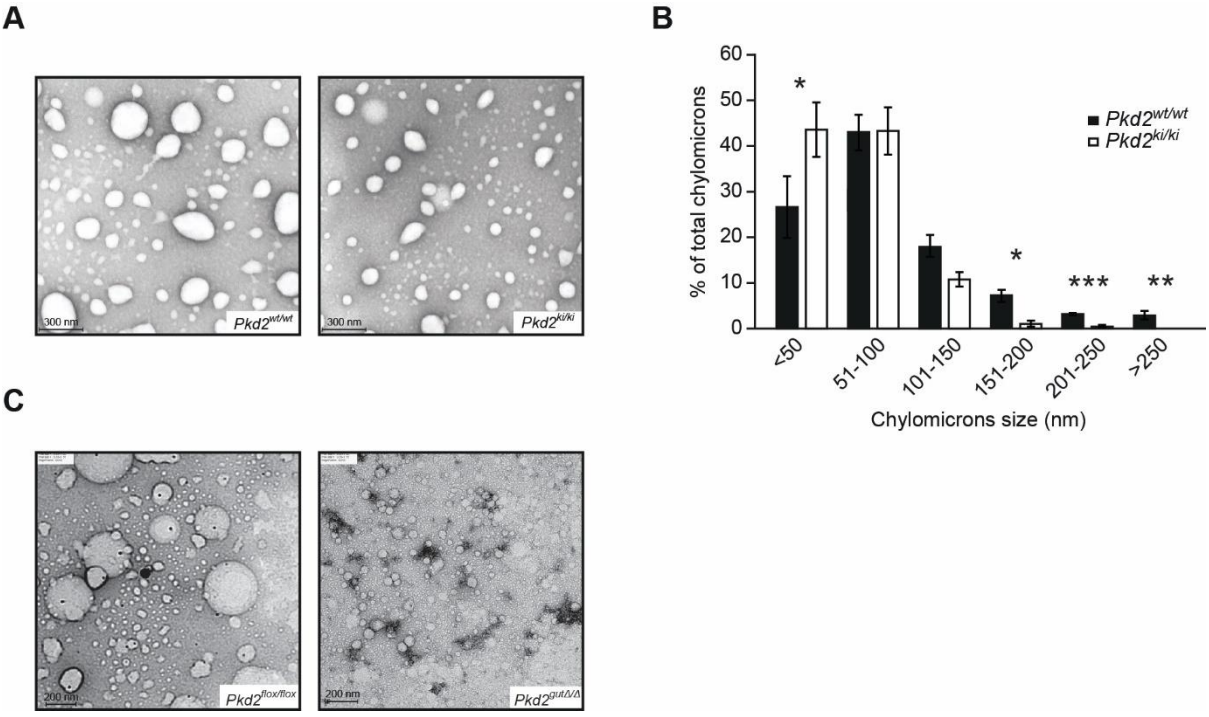

Fig 48. PKD2 inactivation or deletion reduces chylomicron size.

A. Electron microscopy pictures of chylomicrons obtained by ultracentrifugation of plasma from *Pkd2*$^{wt/wt}$ and *Pkd2*$^{ki/ki}$ male mice (magnification x50000). B. Quantification of the diameter the chylomicrons shown in A. n=3. C. Electron microscopy pictures of chylomicrons in plasma from *Pkd2*$^{flox/flox}$ and *Pkd2*$^{gut\Delta/\Delta}$ male mice (magnification x30000).

2.5. Reduced PKD2 activation in intestine of obese patient correlates with a healthier blood biochemical profile.

Our results in human Caco2 cells after PKD2 knockdown indicate that the in-vivo experiments in mice might have relevance also in a human context. Therefore, in an effort to find human significance to the results on PKD2 regulation of lipids absorption in the intestine, we studied the activation of PKD2 in the intestine of morbidly obese patients. Samples from jejunum of female human patients were obtained during Roux-en-Y gastric bypass. The lysates were run in a western blot by loading them according to the levels of fasting triglycerides, from lower to higher. The membrane was analyzed for phosphoPKD2 and normalized to GAPDH (Fig 49A). Then, by using scatter plots, we correlated the ratios of phosphorylated PKD2/GAPDH to several biochemical data obtained from fasted blood of the patients. Interestingly, activation of PKD2 in intestine displayed a positive and significant correlation with triglycerides levels (Fig 49B). Moreover, higher PKD2 phosphorylation also correlated with higher percentage of HbA1c; which indicates poor long-term glycemic control (Fig 49C). Fig 49D shows a negative correlation between PKD2 activation and HDL levels, which did not reach significance. Other parameters measured in these patients, including phosphoPKD2/GAPDH ratios are shown in Fig 49E. The correlations between increased PKD2 activation in intestine and a deteriorated blood profile indicate that our results might be of importance in a human framework and inhibition of this kinase might be considered for futures strategies in body weight management.

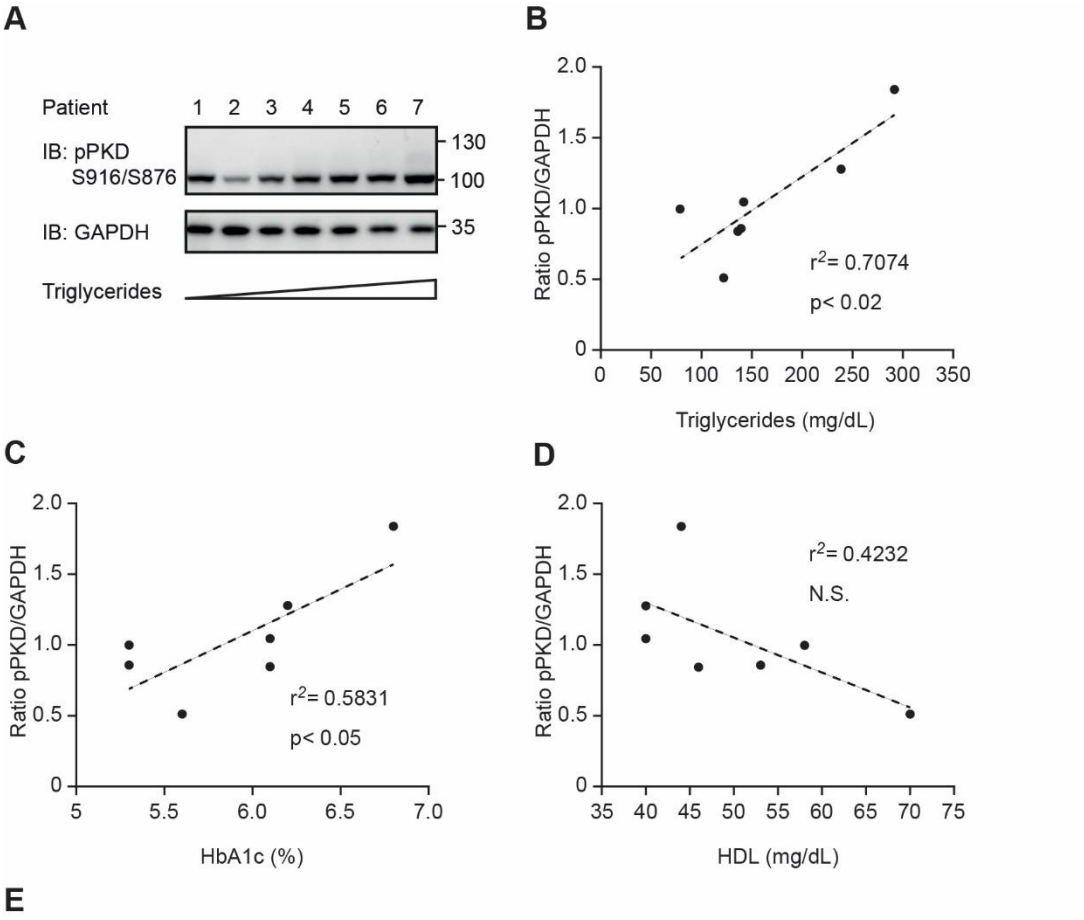

E

Patient	Weight (kg)	Height (cm)	BMI (kg/m^2)	T2D	Fasting glucose (mg/dL)	Cholesterol (mg/dL)	LDL (mg/dL)	HDL (mg/dL)	HbA1c (%)	Triglycerides (mg/dL)	pPKD/GAPDH (relative to patient 1)
1	158	175	51.7	No	90	181	107	58	5.3	79	1
2	128	161	49.6	No	99	221	127	70	5.6	122	0.52
3	112	162	42.7	No	97	210	137	46	6.1	136	0.85
4[a]	127	168	45	No	92	174	93	53	5.3	138	0.86
5	158	171	54	No	85	149	80	40	6.1	143	1.05
6[b]	137	170	47.4	Yes	86	269	181	40	6.2	238	1.28
7[b]	122	163	45.9	Yes	95	165	63	44	6.8	291	1.84

[a] Medicated with metformin for PCOS [b] Medicated with metformin for T2D

Fig 49. Decreased PKD2 activation in intestine correlates with a healthier blood profile in obese human patients.

Proximal jejunum and fasting blood samples were taken from morbidly obese female patients undergoing Roux-en-Y gastric bypass surgery. A. Western blot analysis of PKD phosphorylation in proximal jejunum. Samples are loaded from lower to higher triglyceride levels. B. Scatter plot of PKD phosphorylation in jejunum (normalized to GAPDH) vs. circulating triglycerides. C. Scatter plot of PKD phosphorylation in jejunum vs. percentage of glycated hemoglobin (HbA1c). D. Scatter plot of PKD phosphorylation in jejunum vs. high density lipoprotein levels. E. Anthropometric, metabolic and biochemical data from human female patients. n=7.

3. DISCUSSION

Certainly, increased body weight has become a major concern for the health systems all around the world. Administration of some medications or hormonal imbalances like hypothyroidism or leptin deficiency/resistance are partially responsible for this epidemic. However, the major roles in the development of obesity are played by increased food consumption and a sedentary life style.

Evidently, prevention in early stages would be the ideal goal in the fight against obesity. By limiting food intake and promoting physical activity, the surge of obesity would decline. However, as shown by increasing numbers in the last decades, that strategy is not properly working. Not only the availability of food has increased in most of the world, but also the quality has worsened over the years. Energy dense diets, which are rich in fats and sugars, provide high amounts of calories in small portions. As a result, a positive energy balance is generated and the excess is accumulated as lipids in the adipose depots.

Apart from the biomechanical disabilities of obesity, including osteoarthritis, there is an exponential increased risk of life-threatening diseases like hyperlipidemia, coronary heart disease, congestive heart failure, stroke and cancer. Moreover, increased body weight associates with disorders in the release and response to insulin, ghrelin, PYY, CCK, GLP-1, and leptin, among others. These signaling pathways control the cross-talk among organs and the nutrients´ consumption, storage and utilization.

The variety of signaling pathways and organs involved in the metabolic homeostasis, give us, on the one hand, a very complex and challenging network to unravel, but on the other hand, the opportunity to continue finding pathways and mechanisms that can be targeted in the treatment of obesity and comorbidities.

3.1. PKD2: a central kinase for the intestinal response to lipids.

Kinases are one of the largest groups of enzymes in eukaryotic organisms. They are highly important due to the fact that they control a plethora of cellular processes through phosphorylation of substrates. Kinases catalyze the transfer of phosphate

groups from ATP into their substrates and consequently induce the activation, deactivation, localization or stability of those. As previously described, PKD1 activity regulates adipose tissue biology by promoting lipids accumulation and decrease mitochondrial oxidation while PKD3 limits insulin signalling and lipids accumulation in liver. However, the role of PKD2 in metabolic homeostasis remains vastly unknown.

In this study, we aimed to explore the role of Protein Kinase D2 in metabolic homeostasis by using mice lacking the functionality of this kinase in all organs. Point mutations in serines 707 and 711 for alanines generated normal, viable, and fertile mice with no gross abnormalities. The use of total knockin mice has the advantage of performing the study in a model that shows a complete picture of the whole-body metabolic consequences of PKD2 inactivation. However, since no specific organ is targeted, the interpretation of the results demonstrated to be more challenging.

Pkd2$^{ki/ki}$ mice eating normal chow diet did not present any significant difference in body weight gain or metabolic tests compared to respective littermate controls. These results were expected, since only *ob/ob* and *db/db* mice develop morbid obesity in the absence of a metabolic challenge due the lack of production or receptor for leptin, respectively, and their defect in appetite satiety. In this case, we used a diet with 60% of caloric content coming from fat as a challenge to induce obesity. This stimuli induced body weight gain, localized to adipose depots, which was significantly lower in mice with inactive PKD2. As a consequence, wildtype animals performed poorly in several indicators of metabolic syndrome when compared to *Pkd2*$^{ki/ki}$ mice. Improved profiles for insulin sensitivity, glucose clearance and blood lipids levels also demonstrated that global deficiency of PKD2 activity is beneficial for metabolic fitness.

Since our model involved the inactivation of PKD2 in all organs, we performed studies that allowed to explore which organ might be involved in the development of the observed phenotype. We targeted the main metabolic organs which also have been correlated to be importantly regulated by members of the Protein kinase D family. PKD1 has been showed to regulate adipocytes biology by promoting lipogenesis and suppressing energy dissipation through mitochondria (Löffler, Mayer et al. 2018). However, our study of adipose tissue demonstrated that, more than obesity-related hypertrophy, there were no significant changes in the expression of proteins involved in adipocytes´ beiging and energy expenditure. We also studied circulating levels of

hepatic enzymes as an indicator of correct liver function and no differences were found between genotypes. Liver histology and triglycerides content after 22 weeks in HFD indicated higher lipids accumulation in liver of *Pkd2*$^{wt/wt}$ mice, however, as in the case of adipocytes, more than explaining the phenotype, this result is a consequence of the diet-induced obesity.

A previous study showed that global deletion of PKD2 in mice increased insulin levels, promoted insulin resistance and increased body weight under normal diet through a mechanism mediated by increased expression and activity of L-type Ca^{2+} channels in pancreatic β-cells (Xiao, Wang et al. 2018). However, the same study found improved glucose uptake in a glucose tolerance test under PKD2 deletion. This result is somehow contradictory after they proved insulin resistance in skeletal muscle and liver, because these organs, together with adipose tissue, are the main organs responsive to insulin and they regulate glucose uptake from circulation and storage. Similarly, in the case of *Pkd2*$^{ki/ki}$ mice, we also found an improved glucose uptake and a tendency to increased levels of insulin in unstimulated conditions. However, contrary to the previous observations, we observed increased islet area and, more importantly, improved insulin sensitivity in *Pkd2*$^{ki/ki}$ mice. The main reasons behind these discrepancies might be associated to the number of subjects used in the studies (more than 24 per group in their case and between 8-10 in our case); mechanistic differences under complete absence or only inactivation of PKD2; and very importantly, the lack of an obesogenic diet in their study which could trigger a stronger and more clear phenotype. It would have been also interesting to analyze their model for energy intake, expenditure and activity to clarify the missing connecting points of the phenotype. Since our results showed a significant decrease in body weight of *Pkd2*$^{ki/ki}$ mice, the observed responses to glucose and insulin are most probably a consequence of the diet-induced obesity. However, specific studies on insulin secretion and sensitivity mediated by PKD2 in our model could be of interest.

The difference in body weight and composition clearly indicated unequal energy balance between the *Pkd2*$^{ki/ki}$ mice and respective controls under HFD. However, analysis of these mice in metabolic cages revealed that such difference was not explained by variations in energy consumption or energy expenditure. This result led us to investigate into nutrients absorption as a possible explanation for the phenotype. Due to technical reasons, like sample collection, sample drying and coprophagy, it is

certainly not easy to find significant differences in the energy equation by analyzing feces content (Grobe 2017). However, in our case, a simple approach of separating the mice into individual cages and collecting the feces, resulted in obvious differences between the genotypes. Fatty feces from the knockin mice, characterized by a yellowish color and lower density, contained higher amount of lipids and were more energy dense. Not only, the chemical content of feces was different, but also the amount excreted was significantly more. As a result, after calculating the different components of the energy equation, *Pkd2*$^{ki/ki}$ mice were less efficient transforming food into body mass and the percentage of energy excreted almost doubled the control mice. After the study of the different components of metabolism, we could conclude that, even though the inactivation of PKD2 was global and PKD family members have been proved to control other metabolic pathways/organs, the phenotype observed in this case was due to decreased intestinal absorption of lipids, which resulted in increased excretion of consumed energy and decreased metabolizable energy.

Decreased intestinal absorption of lipids in *Pkd2*$^{ki/ki}$ mice was also proved in the short-term by challenging the mice with oral olive oil and directly measuring triglycerides levels in serum. This experiment demonstrated that decreased absorption is independent of obesity and other pathologies that can develop after long term feeding with HFD. Moreover, by using tyloxapol to inhibit lipoprotein lipase and as a result blocking TG degradation and uptake by tissues, we also concluded that the main mechanism responsible for the lower TG levels in *Pkd2*$^{ki/ki}$ mice after oil gavage involves absorption and not hydrolysis or uptake of triglycerides.

Defective nutrients absorption could be related to several pathologies or intestinal malfunctioning. However, intestinal histology did not show obvious affectation of intestinal anatomy and the intestinal length of *Pkd2*$^{ki/ki}$ mice did not differ from controls. PKD2 activity has been shown to be protective for epithelial barrier function and against colitis (Xiong, Zhou et al. 2016), therefore, we tested in several models for PKD2 inactivation, inhibition or deletion, in-vivo and in-vitro, but we found no differences in intestinal permeability that might be affecting nutrients absorption. That is most likely due to the lack of the chemically induced colitis used in the previous study which induces a strong inflammatory reaction and intestinal tissue damage.

We also developed organoids from stem cells obtained from the crypts of these mice´s intestine and that showed no affectation of organogenesis. We also performed immunofluorescence staining of these organoids for Villin as a marker of epithelial brush and Chromogranin A as a marker of endocrine cells but we did not find differences in the qualitative analysis. However, PKD2 decreased activity has been proved to downregulate trans Golgi transport and release of secretory granules containing Chromogranin A (von Wichert, Edenfeld et al. 2008). More profound studies and quantification of the organoids´ stainings might provide a better understanding of the in-vivo situation and to determine the significance in the context of lipids absorption.

Having identified the intestine as the responsible organ for the observed phenotype in *Pkd2*$^{ki/ki}$ mice, we proceeded to study PKD2 expression and activation in this organ. We found, by using qPCR and quantifying the total mRNA copy numbers, that *Pkd2* is the most expressed of the PKD members, followed by *Pkd3* and *Pkd1*, which showed very low expression. Moreover, by gavaging olive oil to mice, we found that PKD2 is being activated upon lipids ingestion, which supports our notions of an important role of PKD2 in lipids absorption by enterocytes.

We did not find significant differences in expression or protein levels of the three members of the PKD family in intestine of mice with the inactive version of PKD2. However, we found complete loss of activation of PKD2 in the intestine of *Pkd2*$^{ki/ki}$ mice as identified by a specific antibody recognizing autophosphorylation at serine 876. Decreased activity of PKD2 was also found with an antibody recognizing activation/autophosphorylation of PKD1 and PKD2 at serines 916 and 876, respectively. Interestingly, the reported molecular weights of PKD1 and PKD2 are 115 and 105 KDa, respectively (Guo, Gertsberg et al. 2011). However, we found PKD2 at a slightly higher molecular weight than PKD1 in our different models (Fig 23, Fig 24, Fig 25 and Fig 29). Given the reducing conditions in our western blots, this can be most likely due to post-translational modifications, like ubiquitination or glycosylation. This matter is still under study. Moreover, we found no differences in PKD1 activation in intestine of *Pkd2*$^{ki/ki}$ mice when compared to controls. Unfortunately, there is no available antibody to recognize PKD3 activation. However, in our in-vitro model of Caco2 cells in transwells, we determined that deletion of PKD1 or PKD3 by using *shRNA* did not alter the transport, retention or uptake of free-fatty acids. Conversely,

Caco2 cells expressing *shPkd2* demonstrated decreased release of triglycerides. Overall, these results demonstrated that: first, PKD2's mechanism of action is independent of other PKD members' activity, expression, and protein levels; and second, the central role in lipids transport and triglycerides release is specific for PKD2 among the PKD members.

In conclusion, we demonstrated that a challenge with high-fat nutrients activates Protein kinase D2 in the intestine and inactivation of this kinase's activity blocks the enterocytes' ability to transport lipids from the intestinal lumen into circulation. As a result, deficiency of PKD2 activity promotes lipids excretion in feces and protects against diet induced obesity and metabolic consequences. Importantly, even though PKD2 activity was globally impaired, we did not find significant changes in morphology or activity of other organs or in the other components of the energy balance equation.

3.2. Intestinal deletion of PKD2 reduces fat absorption and improves microbiota.

Previous results in our *Pkd2* knockin model led us to investigate in detail the intestinal involvement of Protein kinase D2 in the process of lipid absorption. For that purpose, we utilized Villin-Cre mice, which specifically express Cre recombinase in villus and crypts along the small and large intestine. By breeding these mice with PKD2-floxed mice in exons 15 and 16, we generated mice with specific deletion of PKD2 in intestinal epithelial cells.

As expected, these mice showed decreased expression and activation of PKD2, but more importantly, $Pkd2^{gut\Delta/\Delta}$ mice resembled the phenotype observed for $Pkd2^{ki/ki}$ mice when compared to the respective $Pkd2^{flox/flox}$ mice. Intestinal deletion of PKD2 decreased the absorption of lipids from intestinal lumen to circulation, which represented a decreased in body weight gain and adiposity. Consequently, after long-term HFD feeding, $Pkd2^{gut\Delta/\Delta}$ mice showed improved metabolic fitness regarding glucose tolerance and circulating levels of free-fatty acids and triglycerides.

Microbiota content is highly dependent on the diet but also the nutrients assimilation is affected by the microbiota diversity. Even more, microbiome composition has been correlated with obesity/leanness and its transplantation has been studied as a therapeutic tool for treatment of immune diseases and overweight (Niederwerder

2018, Stanislawski, Dabelea et al. 2019, Zhang, Mocanu et al. 2019). Therefore, in order to broaden our results on PKD2 regulation of intestine, we studied the duodenum, jejunum, ileum and cecum contents of *Pkd2*$^{gut\Delta/\Delta}$ mice and controls under HFD. Our results indicate that the bacterial contents of Jejunum and Illeum are comparable and therefore we analysed them together. Moreover, we found higher alpha diversity in the small intestine of *Pkd2*$^{gut\Delta/\Delta}$ mice, which indicates a healthier microbiome and the presence of more species in *Pkd2*$^{gut\Delta/\Delta}$ mice. Then we used beta diversity to compare the two different genotypes and we also found increased diversity in duodenum and jejunum/ileum but not in cecum. When specific OTUs (operational taxonomic units) were analysed, we found that members of *Bacteroides* were present only in duodenum of *Pkd2*$^{gut\Delta/\Delta}$ mice and completely absent in controls. *Bacteroides* have been reported to decrease upon high-fat diet feeding (Martinez-Guryn, Hubert et al. 2018) and are associated to weight loss (Turnbaugh, Ley et al. 2006). These results indicate that *Pkd2*$^{gut\Delta/\Delta}$ mice have a healthier and more diverse microbiota, which might be associated with less susceptibility to nutritional perturbations and weight loss. However, due to the symbiotic relation between diet, nutrients absorption, body weight and microbiota, the improved microbiome should not be completely credited to PKD2 deletion in enterocytes but more like a result of the interaction between these factors.

3.3. Pharmacological inhibition of PKD2 resembles phenotype and rescues from established obesity.

Because of their central role in cell biology, kinases are considered an important target for the treatment of a multiple pathologies. In fact, aberrant activation of kinases has largely proved to be involved in the development of several cancers, and efforts are being made to inhibit them as a therapeutic approach (Essegian, Khurana et al. 2020). However, in the subject of metabolic diseases, the research on kinases activation or inhibition as a therapeutic tool is more limited and possesses a big potential.

Some examples of kinases inhibition in the context of metabolism include inhibition of PKCβ for the treatment of cardiovascular complications associated to diabetes (Koya and King 1998). In addition, activation of AMPK by metformin is beneficial for glucose and fatty acid metabolism in liver, muscle and adipose tissue (Towler and Hardie 2007). Furthermore, the use of MK5 inhibitor GLPG0259 in mice promotes energy

dissipation as heat and protects against obesity (El-Merahbi, Viera et al. 2020). PKD inhibitor CRT0066101 reduces lipogenesis and increases oxygen consumption in human adipocytes in-vitro and it increases lipogenic gene expression in mice's liver (Löffler, Mayer et al. 2018, Mayer, Löffler et al. 2019). These studies demonstrate that kinases are not only key regulators of cells function, but also potential targets for the treatment of human diseases.

Firstly, we decided to make use of the PKD inhibitor CRT0066101 in the transwell in-vitro system. The results showed a dosage-dependent inhibition of triglycerides transport by CRT0066101, which is most likely dependent on PKD2 inhibition since the deletion of PKD2 by *shRNA* did not decrease further the triglycerides release into the basolateral side of the membrane. This inhibitor has been already used orally to block the growth of pancreatic mice in-vivo (Harikumar, Kunnumakkara et al. 2010). In this study, the authors used a dosage of 80mg/kg/day for 5 days in order to achieve a decreased in activation/autophosphorylation of PKD1/PKD2 about 50% in the tumors' tissue. They also found that the concentrations of the inhibitor in the tumors decreases over time from 12 µM, 2 hours after gavage, to 2 µM, 24 hours after gavage; showing a clearance of the inhibitor. In our case, we aimed for a local inactivation of PKD2 specifically in the intestine. For that purpose, we decided to use C57BL/6 mice and to administer once a day 10mg/kg/day of CRT0066101 dissolved in water or only water as control.

Our results proved that, at the specified dosage, there was an effective inhibition of PKD2 activity without affecting other organs like liver or EpiWAT, in which PKD inhibition might compromise our results. More importantly, we demonstrated that this inhibition at the intestinal level was able to reduce the lipids absorption from the lumen of the intestine to the circulation and, as a result, this led to increase excretion of energy in feces. This resemblance to the genetic inactivation and deletion of PKD2 promoted that mice receiving the inhibitor under high-fat diet also gained less body weight than the controls. Decreased body weight also came along with improved metabolic fitness in mice receiving CRT0066101 daily. These mice showed an improved glucose clearance from circulation and better insulin sensitivity, which was shown not only by the insulin tolerance test, but also by decreased levels of insulin. The brown adipose tissue also displayed a healthier multilocular architecture under treatment with the inhibitor. The usage of CRT0066101 did not affect liver function or

TG accumulation, nor parameters like energy intake, energy expenditure or activity from these mice.

Several mechanisms are altered during the development of obesity. Compensatory mechanisms in energy expenditure and food intake, misregulation of hormone signalling and aberrant activation of signalling pathways make the treatment of obesity a challenging process (Melanson, Keadle et al. 2013, Tanti, Ceppo et al. 2013, Kwon, Kim et al. 2016). Therefore, in a translational approach, we explored whether inhibition of PKD2 would improve metabolic parameters and decrease body weight gain after obesity had been induced by feeding C57BL/6 mice with high-fat diet. There are no standards to define at which point the mice are considered overweight or obese; however, we decided to start with the inhibitor treatment after 7 weeks in HFD and almost 15 grams of gained weight. Three weeks after the start of the treatment, the weight of mice under CRT0066101 treatment (10mg/kg/day) was significantly lower compared to the control group receiving water. The reduction in body weight was specific to the different adipose depots and carried out an improved glucose and insulin tolerance for the mice receiving the inhibitor. These results demonstrate that the usage of PKD inhibitor CRT00666101 could be of interest in the search for treatments or adjuvants in weight-loss therapies.

3.4. PKD2 controls CM size via APOA4 regulation.

Next, we directed our efforts into the characterization of the mechanisms involved in the decreased intestinal absorption of lipids under inactivation, deletion or inhibition of PKD2. In-vivo and in-vitro intestinal permeability did not display any changes that can affect lipids' absorption. In addition, we measured expression of genes involved in lipids digestion and bile acids production and metabolism. Expression of pancreatic lipase and colipase showed no difference between *Pkd2*$^{ki/ki}$ and *Pkd2*$^{wt/wt}$ mice. Interestingly, levels of pancreatic lipase in duodenum were measured after 1 hour of olive oil gavage and no differences were found between genotypes, but we noticed a time-dependent difference. This is most likely due to a circadian rhythm regulation which has already been explored (George, Lebenthal et al. 1985, Keller and Layer 2002). qPCR analysis of liver and ileum for genes involved in bile acid homeostasis showed no significant differences except for the expression levels of *Cyp7a1* in liver.

Pkd2$^{ki/ki}$ mice presented higher levels of *Cyp7a1,* which is considered the main and rate-limiting enzyme for the production of bile acids. High levels of CYP7A1 promote cholesterol catabolism into bile acids and elimination and protect from high-fat diet induced obesity and diabetes (Qi, Jiang et al. 2015). Increase in liver expression of *Cyp7a1* might be a consequence of the development of obesity (La Frano, Hernandez-Carretero et al. 2017), however, in this case *Pkd2*$^{ki/ki}$ and control mice were in HFD only for a week. Therefore, increased *Cyp7a1* levels in *Pkd2*$^{ki/ki}$ mice are most probably related to a feedback regulatory mechanism. Due the decreased lipids absorption, high amount of lipids are reaching the ileum of *Pkd2*$^{ki/ki}$ mice without being absorbed, as a response, *Cyp7a1* expression and bile acid synthesis are stimulated in order to promote absorption (Qi, Jiang et al. 2015).

Our results pointed to a specific regulation of enterocytes biology as the explanation for the phenotype. Therefore, we analyzed the expression levels of fatty acid-binding proteins and fatty acid-transport proteins, which are in charge of intracellular and transmembrane trafficking of fatty acids, respectively (Smathers and Petersen 2011). However, no changes were observed between *Pkd2*$^{ki/ki}$ and control mice. Another protein that might regulate free-fatty acids uptake is the membrane protein CD36, however, CD36 was also unchanged between genotypes in the qPCR and at the protein level. Next, we analyzed proteins involved in triglycerides re-esterification. Expression levels of *Dgat1* and *Mogat2*, as well as protein levels of the latter, were unaffected by PKD2 inactivation. This was also the case for MTTP, which main function consists in the packaging of TG into newly formed chylomicrons. From these results, we could conclude that the decreased transport of TG is not due to regulation in the protein levels of the cell machinery involved in the metabolism or repackaging of triglycerides.

We continued by analyzing the components of the lipoproteins in charge of lipids transport from the intestine to circulation: chylomicrons. Firstly, we analyzed APOB, which exists in 2 isoforms: APOB100 and APOB48, produced in liver and intestine, respectively. APOB48 corresponds to the 48% of the N-terminal of APOB100. However, while APOB100 is part of VLDL, Lp(a), IDL and LDL; APOB48 is unique to chylomicrons and it can be used to indicate the amount of chylomicrons in a sample, although not necessarily the diameter or lipid content of those chylomicrons (Reckless and Lawrence 2003, Nakajima, Nakano et al. 2011). We found that mRNA and protein

levels of APOB48 where not affected by inactivation of PKD2, which might indicate that the amount of chylomicrons produced are the same in *Pkd2*$^{ki/ki}$ and *Pkd2*$^{wt/wt}$ mice. It has been showed that Apolipoprotein A1 is also secreted with chylomicrons and rapidly transferred to HDL where it might help with the anti-atherosclerotic function of this lipoprotein (Glickman and Green 1977, Feingold 2021). Western blot analysis demonstrated no significant differences in the levels of this protein in the intestine of *Pkd2*$^{ki/ki}$ and *Pkd2*$^{wt/wt}$ mice. Lastly, we analyzed APOA4 and, even though the mRNA levels were unchanged, the protein levels were increased, indicating that PKD2 activity stabilizes APOA4 possibly by a post-translational modification.

Increased levels of APOA4 were found in the jejunum of mice under genetic inactivation or deletion of PKD2 as well as in those under PKD inhibitor. Moreover, cells expressing *shPkd2* in the transwell system also released more APOA4 into the basolateral medium. Higher levels of APOA4 were also found in the serum of *Pkd2*$^{ki/ki}$ mice. These results demonstrated solid and consistent evidence of PKD2 regulation of APOA4 levels. We verified this interaction in an in-vitro kinase assay, which demonstrated that PKD2 phosphorylates APOA4 and that this kinase is activated in the presence of APOA4. Sequence analysis and a prediction software (Wang, Xu et al. 2020) could identify several sites in APOA4 for potential phosphorylation by PKD2. In our opinion, the threonine T158 seems to meet the requirements for PKD2 phosphorylation. First, because it contains the sequence LxRxxT, characteristic for PKD phosphorylation motif, and second, because it is conserved between several species including mouse, rat and bull. However, this statement would need to be confirmed by other analysis and it is likely that there is not only one site for PKD2 phosphorylation.

Electron microscopy of chylomicrons after lipids administration made evident the main mechanism by which PKD2 controls lipids absorption in the intestine. Inactivation or intestinal deletion of PKD2 decreased substantially the size of chylomicrons, and therefore, this limits the amount of lipids absorbed. The evidence regarding APOA4 regulation of chylomicrons' size and metabolism is contradictory. In some studies, higher levels of APOA4 increased chylomicrons size and fat absorption. On the other hand, APOA4 knockout mice also secreted larger chylomicrons. Our results suggest, that phosphorylation of APOA4 by PKD2 might hold the chylomicrons inside the enterocyte and promote their maturation and growth. It is also likely that more

molecules of APOA4 are attached to the chylomicrons in a compensation for the lack of phosphorylation by PKD2 in the pursuit of increasing chylomicron size. Since APOA4 has demonstrated to sensitize LPL and promote lipoprotein uptake, we cannot rule out the possibility that increased levels of APOA4 induce a faster and more efficient uptake of this lipoprotein.

In conclusion, we have shown that PKD2 regulates chylomicron-mediated lipid absorption from the intestine by phosphorylating Apolipoprotein A4. Deletion or inactivation of PKD2 in enterocytes rises levels of APOA4 and decreases the size of chylomicrons, which, as a final consequence, increases fat excretion in feces.

3.5. Pharmacological approaches to combat obesity.

The epidemic of obesity and metabolic syndrome is an important concern for the health systems around the world and big efforts have been made in prevention and treatment. However, due to the complexity of this disease, the current strategies appear to be insufficient. Theoretically, the obvious and adequate procedure should involve prevention, education, diet, behavioral modifications and physical activity. But, in many cases, surgical or pharmacological interventions are necessary (Kos, Baker et al. 2005, Ruban, Stoenchev et al. 2019)

Several medications target specific components of the metabolic syndrome like hypercholesterolemia, type 2 diabetes and hypertension. However, the pharmacological treatments for the root problem, obesity, are more limited.

Available medications act in different organs and systems but they are mostly focus on decreasing food intake. Liraglutide, a GLP-1 receptor agonist, resembles the action of the GLP-1 produced by the intestine after food intake and it is one of the approved medicines for reducing food intake and delaying gastric emptying. Another medicine is the mixture of naltrexone and bupropion, which increases satiety and promotes energy expenditure by antagonizing the opioid receptor and inhibiting the reuptake of norepinephrine–dopamine. Lorcaserin also suppress appetite by a mechanism involving hypothalamic activation of 5-HT_{2C} receptor. Lastly, the combination of phentermine and topiramate also suppress appetite by increasing norepinephrine release. It is important to mention that, due to their effect on the central neural system,

these drugs bring along side effects involving nausea, dizziness, and vomiting among others (Williams, Nawaz et al. 2020).

Other drugs are still under studies. Those include SGLT-2 inhibitors, which promote glucose elimination through urine. Furthermore, analogues of signaling peptides produced by several organs are of interest. For example, analogues of amylin (which is produced by the pancreas) induce satiety. Also, supplements for leptin (normally produced by adipose tissue) increase satiety and promote energy expenditure. On the other hand, antagonists of orexigenic Ghrelin and Neuropeptide Y are under study. However, the efficacy of these drugs is still under debate, some of them are only effective in combination and some have been removed from the market due to serious side effects. One of them is rimonabat, a very effective weight-reducing agent (antagonist of cannabinoid-1 receptor) that inhibited appetite but increased the risk of suicide. Another example is Sibutramine which increased satiety and energy expenditure (inhibitor of serotonin and noradrenalin reuptake) but increased blood pressure and heart frequency (Finer 2002, Williams, Nawaz et al. 2020)

In the last years, several studies have proposed the beiging of white adipose tissue as a possibility to increase energy expenditure and decrease body weight. By inducing the expression of brown markers like PGC-1α and PRDM16, it is possible to transdifferentiate white adipocytes into beige adipocytes with thermogenic characteristics. Cold exposure or activation of PPARα, PPARγ, or AMPK have shown promising results in that field, however, it is still unknown their relevance in human biology (Kuryłowicz and Puzianowska-Kuźnicka 2020).

The previously described strategies focus on decreasing food intake and increasing energy expenditure. However, another alternative is orlistat. This drug has been used worldwide for a couple of decades and its mechanism of action involves binding to the serine residues of gastric and pancreatic lipases and their inactivation. By inactivating these lipases, orlistat decreases triglycerides hydrolysis and therefore, their absorption (Bansal and Al Khalili 2021). The treatment with orlistat reduces intestinal fat absorption by approximately 30% which is comparable to our findings for lipids excretion in the *Pkd2*$^{ki/ki}$ mice model. The side effects observed under orlistat treatment include steatorrhea, fecal urgency and hyper-defecation. We did not observe liquid oily fecal depositions from our mice models when placed in a white

paper under HFD (results not shown), however, we noticed increased amount of feces. Another disadvantage of orlistat is the necessity of administration with each meal due to the local and immediate effect of the drug. In our study, we administered CRT0066101 inhibitor once a day and it was enough to keep a sustained inhibition of PKD2 and a decreased lipid absorption. Even though, it is clear that orlistat and PKD2 inhibition have a common final effect, the mechanism of action by which they decrease lipid absorption is certainly different and the results are not necessarily comparable. It would be necessary to perform a parallel study to provide more insights into the suitability of PKD2 inhibition as an anti-obesity therapy.

Our findings on human intestinal samples indicate that our results in mice models might also be relevant for human biology. PKD2 activation correlated positively with TG levels in obese patients, which goes in line with our conclusions on PKD2 role in lipids absorption. Moreover, PKD2 activation was not only associated with increased TG levels but also with higher percentage of glycated hemoglobin, as an indicator of poor glucose homeostasis. Furthermore, even if it did not reach significance, probably due to the sample size, the levels of HDL correlated negatively with PKD2 activation. These results demonstrate that, also in a human context, PKD2 activation in intestine plays a major role in lipids and metabolic homeostasis.

4. GRAPHICAL ABSTRACT

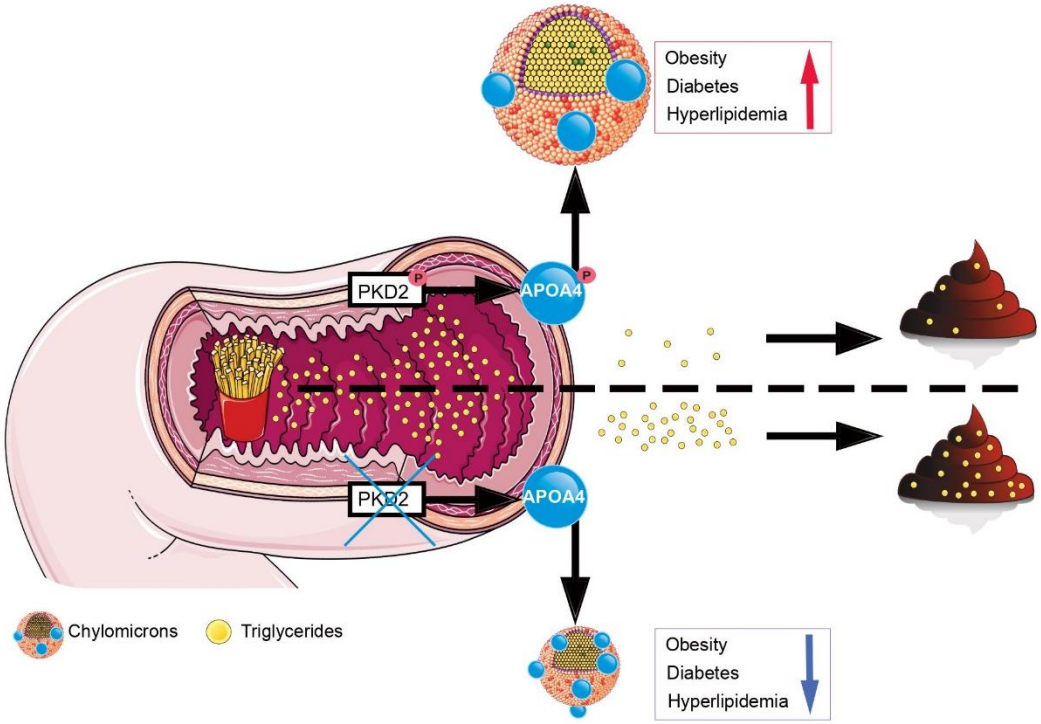

Fig 50. Graphical abstract: PKD2 regulates chylomicron size by APOA4 phosphorylation.

Under HFD stimuli, PKD2 activation phosphorylates APOA4 and promotes chylomicron's growth and fat absorption. PKD2 inactivation, deletion or inhibition limits chylomicron's size and promotes lipids excretion in feces.

5. MATERIALS

5.1. Oligonucleotides

Table 1. Primers

Gene	**Forward (5'-3')**	**Reverse (5'-3')**
Pnlip	CTGGGAGCAGTAGCTGGAAG	AGCGGGTGTTGATCTGTGC
Clps	GAACAGTATGCAGTGTAAGAGCA	GCAGATGCCATAGTTGGTGTTG
Cyp7a1	ATCAAAGAGCGCTGTCTGGGT	GCGTTAGATATCCGGCTTCAAAC
Cyp8b1	CTAGGGCCTAAAGGTTCGAGT	GTAGCCGAATAAGCTCAGGAAG
Abcg5	AGGGCCTCACATCAACAGAG	GCTGACGCTGTAGGACACAT
Abcg8	CTGTGGAATGGGACTGTACTTC	GTTGGACTGACCACTGTAGGT
Ehhadh	ATGGCTGAGTATCTGAGGCTG	GGTCCAAACTAGCTTTCTGGAG
Acaa1a	TCTCCAGGACGTGAGGCTAAA	CGCTCAGAAATTGGGCGATG
Cd36	ATGGGCTGTGATCGGAACT	GTCTTCCCAATAAGCATGTCTCC
Bacs	TCTATGGCCTAAAGTTCAGGCG	CTTGCCGCTCTAAAGCATCC
Baat	GGAAACCTGTTAGTTCTCAGGC	GTGGACCCCCATATAGTCTCC
Taat	GCACACGGCCTGAAGATGA	ATTTTTGTAGCAGAGGTACGGG
Csad	CCAGGACGTGTTTGGGATTGT	ACCAGTCTTGACACTGTAGTGA
Asbt	GTCTGTCCCCCAAATGCAACT	CACCCCATAGAAAACATCACCA
Osta	AGGCAGGACTCATATCAAACTTG	TGAGGGCTATGTCCACTGGG
Ostb	AGATGCGGCTCCTTGGAATTA	TGGCTGCTTCTTTCGATTTCTG
Pppara	AACATCGAGTGTCGAATATGTGG	CCGAATAGTTCGCCGAAAGAA
Acadl	TCTTTTCCTCGGAGCATGACA	GACCTCTCTACTCACTTCTCCAG
Fabp4	GGATGG444GTCGACCACAA	TGGAAGTCACGCCTTTCATA

Fabp2	GTGGAAAGTAGACCGGAACGA	CCATCCTGTGTGATTGTCAGTT
Fatp4	ACTGTTCTCCAAGCTAGTGCT	GATGAAGACCCGGATGAAACG
Fatp2	TCGTGGGACTGGTAGATTTTG	CGCGATGTGTTGAAAGAGTTT
Pkd1	GGGGGCATCTCGTTCCAT	GTGCCGAAAAAGCAGGATCTT
Pkd2	GCTGAGACACCTGCACTTCA	GGATCGGCTGATGCCAGTAA
Pkd3	GTCTGTCAAATGTATCTCTGCCA	GGTGAGTATGTGACTCTTCACTG
Mttp1	CTCTTGGCAGTGCTTTTTCTCT	GAGCTTGTATAGCCGCTCATT
Mogat2	TGGGAGCGCAGGTTACAGA	CAGGTGGCATACAGGACGGA
Dgat1	GCGCTACTTCCGAGACTACTT	GGGCCTTATGCCAGGAAACT
Apoa4	GCATCTAGCCCAGGAAACTG	ATGTATGGGGTCAGCTGGAG
Apoa1	GGCACGTATGGCAGCAAGAT	CCAAGGAGGAGGATTCAAACTG
ApoB	AAGCACCTCCGAAAGTACGTG	CTCCAGCTCTACCTTACAGTTGA
Ucp1	AGGCTTCCAGTACCATTAGGT	CTGAGTGAGGCAAAGCTGATTT
Cidea	TGACATTCATGGGATTGCAGAC	GGCCAGTTGTGATGACTAAGAC
Bmp7	ACGGACAGGGCTTCTCCTAC	ATGGTGGTATCGAGGGTGGAA
Adrb3	AGAAACGGCTCTCTGGCTTTG	TGGTTATGGTCTGTAGTCTCGG
Prdm16	CCACCAGCGAGGACTTCAC	GGAGGACTCTCGTAGCTCGAA
Cidec	ATGGACTACGCCATGAAGTCT	CGGTGCTAACACGACAGGG
Pgc1a	AGCGCCGTGTGATTTACGTT	CCGCAGATTTACGGTGCATT
Myh2	AAAGCTCCAAGGACCCTCTT	AGCTCATGACTGCTGAACTCAC
Ckm	CAGCACAGACAGACACTCAGG	GAACTTGTTGTGGGTGTTGC
Mck	GCAAGCACCCCAAGTTTGA	ACCTGTGCCGCGCTTCT
Slc6a8	TGCATATCTCCAAGGTGGCAG	CTACAAACTGGCTGTCCAGA
Slc27a2	TCCTCCAAGATGTGCGGTACT	TAGGTGAGCGTCTCGTCTCG
Ucp3	CTGCACCGCCAGATGAGTTT	ATCATGGCTTGAAATCGGACC
Myh1	TCTGCAGACGGAGTCAGGT	TTGAGTGAATGCCTGTTTGC

Genotyping	**Forward (5´- 3´)**	**Reverse (5´- 3´)**
Pkd2$^{ki/ki}$	AGTGGCACGTTCCCCTTCAATG	CTTTGCCCAATCCCTTACAGCCT
Vil-Cre/WT	GCCTTCTCCTCTAGGCTCGT	TATAGGGCAGAGCTGGAG GA
Vil-Cre/Tg	GCCTTCTCCTCTAGGCTCGT	AGGCAAATTTTGGTGTACGG
Pkd2-Flox	TGAAGGAAGTGTCTTGGGAGTCCCTGCTGTTTTAATAGC	TGTCTAGGAGGGGACATAACGAACCTGAGGAAACGGATCGGC
Absolute quantification	**Forward (5'-3')**	**Reverse (5'-3')**
Pkd1	TTTAACTCCCGTTGGAGCGA	CACTGTTGTTTGGTGGGGAAC
Pkd2	ATGTCACCTACTTTGTGGGCG	TGGGCGCATCTTGGAGGATA
Pkd3	AGGCAGTAACCCACACTGTTT	TCTGCGCCACATCTAGTCCC

Table 2. Plasmids

Name	Manufacturer	Identifier
MISSION® pLKO.1-puro Non-Target shRNA Control Plasmid DNA	Sigma Aldrich	SHC016
MISSION® pLKO.1-puro shRNA Protein Kinase D2 CCGGCTTCTACGGCCTTTACGACAACTCGAGTTGTCGTAAAGGCCGTAGAAGTTTTT	Sigma Aldrich	SHCLNG-NM_016457
MISSION® pLKO.1-puro shRNA Protein Kinase D3 CCGGCACTTCATTATGGCTCCTAATCTCGAGATTAGGAGCCATAATGAAGTGTTTTTTG	Sigma Aldrich	SHCLNG-NM_005813
Vector Builder pLV (shRNA)-Puro-U6> h Protein Kinase D1(shRNA#1) CAGGAAGAGATGTAGCTATTA	Vector Builder	VB201126-1100ute
pMD2.G	Addgene	12259
psPAX	Addgene	12260

5.2. Commercial kits, chemicals and reagents

Table 3. Commercial kits

Commercial kit	**Manufacturer**	**Identifier**
BCA Protein Assay Kit	Thermo Fisher Scientific	#23227
First Strand cDNA Synthesis Kit	Thermo Fisher Scientific	#K1612
Infinity ALT (GPT) liquid stable reagent	Thermo Fisher Scientific	TR71121
Infinity AST (GOT) liquid stable reagent	Thermo Fisher Scientific	TR70121
Mouse Insulin ELISA Kit	Crystal Chem	#90080
NEFA Kit: NEFA-HR(2) R1 Set; NEFA-HR(2) R2 Set	Wako	#434-91795; #436-91995
NucleoBond® Xtra Midi	Macherey-Nagel	#740410.50
NucleoSpin® Gel and PCR Clean-up	Macherey-Nagel	#740609.250
NucleoSpin® Plasmid	Macherey-Nagel	#740588.250
QBT Fatty Acid Uptake Assay Kit	Molecular Devices	#R6132
Serum TG Determination Kit	Sigma-Aldrich	#TR0100
Serum TG Kit> Free Glycerol Reagent	Sigma-Aldrich	#F6428
Serum TG Kit> Triglyceride Reagent	Sigma-Aldrich	#T2449
Taq DNA Polymerase	Thermo Fisher Scientific	#EP0282

Table 4. Chemicals and reagents

Chemicals and reagents	**Manufacturer**	**Identifier**
1,4-Dithiothreitol (DTT)	Sigma-Aldrich	#10197777001
2'-deoxynucleoside 5'-triphosphate (dNTP) mix (2 mM each):	Thermo Fisher Scientific	#R0242
Acetic acid	Roth	#3738.1
Acrylamide	AppliChem	#A4989
Agar	Sigma-Aldrich	#A1296
Agarose	Roth	#2267.4
Ampicillin	Sigma-Aldrich	#A0166
ATP	NEB	#P0756S
Bovine serum albumin (BSA)	Sigma-Aldrich	#A7030

Chemicals and reagents	**Manufacturer**	**Identifier**
Bromophenol blue	Roth	#A512.1
Butanol	Merck	#8222622500
Calcium chloride ($CaCl_2$)	Roth	#CN93.1
Chloroform ($CHCl_3$)	Roth	#Y015.1
Coomassie brilliant blue	Sigma-Aldrich	#B0770
CRT0066101	Tocris	#4975
DNA loading dye solution, 6x	Sigma-Aldrich	#G2526
Dry milk; fat-free	Roth	#T145.4
Earle's balanced salt solution (EBSS) (without Ca^{2+}/Mg^{2+})	Thermo Fisher Scientific	#14155048
Enhanced chemiluminescence (ECL) substrate	Bio-Rad	#170-5061
Eosin G solution	Roth	#3139.2
Ethanol; absolute	Roth	#5054.1
Ethanol; denatured	Roth	#K928.3
Ethyl acetate	Sigma-Aldrich	#34858
Ethylenediaminetetraacetic acid (EDTA)	Roth	#8040.1
Fluorescein Isothiocyanate Dextran	Sigma-Aldrich	#46944
Fluoromount-GTM with DAPI	Thermo Fisher Scientific	#00-4959-52
Formalin	Sigma-Aldrich	#HT501128
Free fatty acid (FFA) standard	Wako Diagnostics	#276-76491
GeneRuler 1 kbp DNA ladder	Thermo Fisher Scientific	#SM0311
GeneRuler 100 bp DNA ladder	Thermo Fisher Scientific	#SM0241
Glucose	Roth	#X997.2
Glycerol standard	Sigma-Aldrich	#G7793
Glycine	Roth	#3790.3
Goat serum	Sigma-Aldrich	#G9023

Chemicals and reagents	**Manufacturer**	**Identifier**
Hank's balanced salt solution (HBSS) (with Ca^{2+}/Mg^{2+})	Biochrom (Merck)	#L2035
Hexane	Sigma-Aldrich	#34859-M
Hoechst 33342 dye	Thermo Fisher Scientific	#62249
Hydrochloric acid (HCl)	Sigma Aldrich	#30721
Hydrogen peroxide (H_2O_2)	Sigma-Aldrich	#31642
Hydrophobic pen; Roti®-Liquid barrier marker	Roth	#AN91.1
Immersion liquid type G	Leica	#11513910
Insulin solution human	Sigma-Aldrich	#I9278
Isopropanol	Roth	#CP41.3
Magnesium chloride ($MgCl_2$)	Roth	#KK36.1
Mayer's hematoxylin solution	Sigma-Aldrich	#MHS16
Matrigel	Corning	#356231
Methanol (MeOH)	Sigma-Aldrich	#34860
Methanol (MeOH)	Roth	#4627.3
Midori green advance DNA stain	Nippon Genetics	#MG04
Mounting medium; Roti®-Mount	Roth	#HP68.1
NEBuffer for Protein Kinases	NEB	#B6022
Nonidet P-40 (NP-40)	Sigma-Aldrich	#74385
NuPAGE® *lithium dodecyl sulfate* (LDS) sample buffer	Thermo Fisher Scientific	#NP0007
Oleic acid	Sigma-Aldrich	#O1008
Oleic acid	Sigma-Aldrich	#O1383
Olive Oil	Filippo Berio	
PageRuler® prestained protein ladder	Thermo Fisher Scientific	#26619
C^{14}-Palmitic acid	Perkin Elmer	#NEC075H250UC
Paraformaldehyde (PFA)	Roth	#0335.2

Chemicals and reagents	**Manufacturer**	**Identifier**
Phosphate-buffered saline (PBS)	Sigma-Aldrich	#P3813
Pierce™ BCA™ Protein-Assay	Thermo Fisher Scientific	#23225
Pierce™ IP Lysis Buffer	Thermo Fisher Scientific	#87787
PowerUp™ SYBR™ green master mix	Thermo Fisher Scientific	#A25742
Protease and phosphatase inhibitor (PPI) cocktail (100x)	Thermo Fisher Scientific	#78442
QIAzol lysis reagent	Qiagen	#79306
Quick Start™ Bradford 1x dye reagent	Bio-Rad	#5000205
Scintillation fluid	Zinsser Analytic	#1008000
Sodium chloride (NaCl)	Roth	#3957.1
Sodium dodecyl sulfate (SDS) pellets	Roth	#CN30.2
Sodium hydroxide (NaOH)	Roth	#P031.1
Sulfuric acid (H_2SO_4)	Sigma-Aldrich	#30743-M
Taurocholic acid sodium salt hydrate	Sigma-Aldrich	#T4009
Tetramethylethylenediamine (TEMED)	Carl Roth	#2367.1
TRIS base	Roth	#AE15.4
Triton X-100	Roth	#3051.3
Trypanblue 0.4%	Thermo Fisher Scientific	#15250061
Tween 20	Roth	#9127.1
Tyloxapol (Triton WR1339)	Sigma-Aldrich	#T0307
UltraPure™ distilled water (Dnase/Rnase Free)	Thermo Fisher Scientific	#10977-035
Urea	Sigma-Aldrich	#U0631
Xylol	Roth	#9713.3
Yeast extract	AppliChem	#A1552.1
β-mercaptoethanol	Sigma-Aldrich	#M3148

5.3. Equipment and consumables

Table 5. Equipment

Equipment	**Specification**	**Manufacturer/source**
Animal ear punch	2 mm	Fine Science Tools
Autoclave	VX-120	Systec
Autoclave sterilizer	DX-100	Systec
Automated tissue processor	ASP200S	Leica
Bench-top homogenizer	PT 1600E	Polytron
Bomb calorimeter	6400 Automatic Isoperibol Calorimeter	Parr Instrument Company
Centrifuge	5424 R	Eppendorf
Centrifuge	5810 R; rotor: A-4-62	Eppendorf
Confocal microscope	TCS SP8	Leica
Electrode for TEER	Millicell ERS-2	Millipore
Electron Microscope	Zeiss EM 900	Zeiss
Electron Microscope	JEM-2100	JEOL
Electrophoresis cell	Sub-Cell GT	Bio-Rad
Erlenmeyer flask	1000 mL	Simax
Evaporator	Reacti-Vap™; 9-port; 27-port	Thermo Fisher Scientific
Fluorescence microscope	DM5500 B; illuminator: X-Cite 200DC; camera: Leica DFC365 FX; power supply: CTR HS	Leica
Freezer (-20°C)	profi line GG4310	Liebherr
Freezer (-20°C)	Comfort	Liebherr
Freezer (-80°C)	HERAfreeze HFU666 basic	Thermo Fisher Scientific
Freezing chamber		Thermo Fisher Scientific
Fridge	profi line FKS5000	Liebherr

Equipment	Specification	Manufacturer/source
Fridge-freezer	CP3523-21	Liebherr
Gas burner	Type CFH	A. Hartenstein
Glass bottles	2000 mL; 1000 mL; 500 mL; 250 mL; 100 mL	Duran
Glucometer	Accu-Chek	Roche
Homogenizing pestle	PP-pestle; cone-shaped; 70 mm	Roth
Ice machine		Ziegra
Imager for Gels	Typhoon TRIO	GE Healthcare
Imager for Proteins	Amersham Imager 680	GE Healthcare
Incubator	C150	Binder
Incubator	Heracell 240	Heraeus
Incubator shaker	ISF-1-W	Kuhner
Inverted microscope	CKX31	Olympus
Inverted microscope	IX71	Olympus
Laminar flow cabinet	SB-1200	BDK Luft- und Reinraumtechnik
Liquid scintillation counter	Tri-Carb 2910 TR	Perkin Elmer
Magnetic stirrer	MR Hei-Standard	Heidolph
Mass spectrometer	TOF/TOF™ 5800 System	SCIEX
Manual counter	T120	IVO
Metabolic cages	Indirect calorimetry system PhenoMaster	TSE systems
Mice cage	GM500PFS; lid: for water bottles; water bottle: 300 mL; lid: full length	Tecniplast
Mice cage rack system	Green Line IVC	Tecniplast
Micro scale	AB265-S	Mettler Toledo
Microcentrifuge	Galaxy Ministar	VWR
Microwave		Dynamic

Equipment	Specification	Manufacturer/source
MilliQ water purification system	X-CAD	Millipore
Multi-channel pipette	Transferpette S12 (20 – 200 µL)	Brand
Multimode microplate reader	Spark™ 10M	Tecan
Multiplex ELISA reader	Bio-Plex® MAGPIX™ Multiplex reader	Bio-Rad
Neubauer chamber	0.1 mm Depth	Hecht-Assistant
Nitrogen cell storage tank	Cryosytem 4000	MVE
Nitrogen storage tank	Cryotherm	Apollo
Nuclear magnetic resonance (NMR) analyzer	The minispec LF50	Bruker
pH-meter	FiveEasy	Mettler Toledo
Photometer	BioPhotometer	Eppendorf
Pipette	Transferpette S (0.5 – 10 µL)	Brand
Pipette boy		Gilson
Pipette controller	Accu-Jet Pro	Brand
Power supply	PowerPac HC	Bio-Rad
Real-time PCR system	QuantStudio 5 real-time PCR system	Thermo Fisher Scientific
Repetitive pipet	Repetman	Gilson
Rotation microtome	RM2255	Leica
Scissors (standard)	Blunt; 13 cm	Fine Science Tools
Scissors (tissue)	Spiky; 10.5 cm	Fine Science Tools
Thermal cycler	T100	Bio-Rad
Thermo block	Thermomixer Comfort	Eppendorf
Tweezer (fine)	Tip: 0.8 mm x 0.7 mm	Fine Science Tools
Tweezer (standard)	15.5 cm	Fine Science Tools

Equipment	Specification	Manufacturer/source
Ultracentrifuge	Optima MAX-XP Ultracentrifuge MLA-130	Beckam Coulter
UV-/Vis-spectral photometer	Nanodrop 2000c	Thermo Fisher Scientific
UV-transilluminator	UVT-28 ME; camera: EASY 440K	Herolab
Vacuum pump	BVC 21	Vacuubrand
Volumetric flask	2000 mL; 1000 mL; 250 mL; 100 mL	Vitlab
Vortexer	RS-VA 10	Phoenix Instrument
Water bath	TW8	Julabo
Water bath	WB20	P-D Industriegesellschaft
X-ray film processor	Cawomat 2000 IR	CAWO

Table 6. Consumables

Consumable	Specification	Manufacturer/source
384-well plate	MicroAmp Optical	Thermo Fisher Scientific
96-well plate	Nunc-Immuno; MaxiSorp	Thermo Fisher Scientific
Adhesive film	PCR compatible	Thermo Fisher Scientific
Aluminium foil	15 µm	A. Hartenstein
Cell Culture Insert	1.0 µm pore size REF 353103	Corning
Cell scraper	24 cm	Techno Plastic Products
Cell strainer	100 µm	Corning
Collagen type I-coated plate	6-well; 12-well, 96-well	Corning
Cover slips	Round; 20 mm diameter	Roth
Cover slips	24 x 60 mm	Roth
Cryo tube	1.8 mL	Sarstedt
Cuvette	10 x 4 x 45 mm	Sarstedt

Consumable	Specification	Manufacturer/source
Filter papers	185 mm	Macherey-Nagel
Glucometer stripes	ACCU-CHEK Inform II test strips (50)	Roche
Immobilon-P transfer membrane (*polyvinylidene fluoride* (PVDF))	0.45 µm	Millipore
Microscope slide	26 x 76 mm	Roth
Microscope slide	Superfrost; 26 x 76 mm	Thermo Fisher Scientific
Needles		BD Microlane
Petri dish	92 x 16 mm	Sarstedt
Pipette	Serological; 2 mL; 5 mL; 10 mL; 25 mL	Sarstedt
Pipette filter tips	Biosphere; 20 µL; 200 µL; 1250 µL	Sarstedt
Pipette syringes	500 µL; 1250 µL; 2500 µL	VWR
Pipette tips	20 µL; 200 µL; 1000 µL	Sarstedt
Reaction tube	Conical; 15 mL, 50 mL	Sarstedt
Reaction tube	1500 µL; 2000 µL; 5000 µL	Sarstedt
Reaction tube	Multiply-µStrip; Pro8; 200 µL	Sarstedt
Reagent reservoir	Disposable; Pre-sterile; 50 mL	VWR
Repetitive pipette tips	0.1 mL; 0.5 mL; 1.25 mL; 2.5 mL; 5 mL; 12 mL	VWR
Scintillation vial	Pony Vial, 6 mL	Perkin Elmer
Seal foil	Parafilm	Roth
Sterile filter	Filtropur; pore size: 0.2 µm; 0.45 µm	Sarstedt
Syringe	Omnifix; 1 mL; 5 mL; 10 mL; 20 mL	B. Braun

Consumable	Specification	Manufacturer/source
Syringe	Omnican; U-100 Insulin; 1 mL/100 I.U.; 30 G x 1/2“; 0.3 mm x 12 mm	B. Braun
Syringe	Tuberculin; 1 mL	Chirana T. Injecta
Tissue culture dishes	10 cm; 6 cm	Sarstedt
Well plates	6-well; 12-well, 96-well	Sarstedt
X-ray films	Super RX-N	Fujifilm

5.4. Antibodies and recombinant proteins

Table 7. Primary Antibodies

Antibodies		
Rabbit anti-GAPDH	Sigma-Aldrich	Cat# G9545, RRID:AB_796208
Rabbit Anti-APOA4/Apo-AIV	Abcam	Cat# AB_231660
Mouse anti-apolipoprotein A4	Cell Signaling Technology	Cat# 5700, RRID:AB_10859038
Rabbit anti-apolipoproteinB	Proteintech	Cat# 20578-1-AP, RRID:AB_10732938
Rabbit anti-apolipoprotein A1	Abcam	Cat# ab20453, RRID:AB_445592
Rabbit Anti-MOGAT2	Abcam	Cat# ab63156, RRID:AB_956147
Rabbit Anti-DGAT1	Abcam	Cat# ab54037, RRID:AB_869453
Rabbit Anti-MTTP	Abcam	Cat# ab63467, RRID:AB_10672035
Rabbit Anti-PKD3/PKC,clone (D57E6)	Cell Signaling Technology	Cat# 5655, RRID:AB_10695917
Rabbit Anti-Protein Kinase D2, clone (EP1495Y)	Abcam	Cat# ab51250, RRID:AB_882058

Rabbit Anti-Protein Kinase D2, clone (D1A7)	Cell Signaling Technology	Cat# 8188, RRID:AB_10829368
Rabbit Anti-PKD/PKCμ	Cell Signaling Technology	Cat# 2052 RRID:AB_2800149
Rabbit Anti-Phospho-PKD/PKCμ (Ser744/748)	Cell Signaling Technology	Cat# 2054 RRID:AB_2172539
Rabbit Anti-Phospho-PKD/PKCμ (Ser916)	Cell Signaling Technology	Cat# 2051 RRID:AB_330841
Rabbit Anti-PKD2 (phospho S876), clone (EP1496Y)	Abcam	Cat# ab51251 RRID:AB_882060
Rabbit Anti-Phospho-Akt Substrate (RXXS*/T*) (110B7E)	Cell Signaling Technology	Cat# 9614 RRID:AB_331810
Mouse anti-β-actin	Sigma-Aldrich	Cat# A5441 RRID:AB_476744
Rabbit anti-α-Tubulin	Cell Signaling Technology	Cat# 2144 RRID:AB_2210548
Rabbit anti-Pancreatic Lipase	Abcam	Cat# ab2287737 RRID:AB_2889168
Goat Anti-Villin, clone (C-19)	Santa Cruz Biotechnology	Cat# sc-7672, RRID:AB_2215973
Rabbit Anti-Chromogranin A, clone (H-300)	Santa Cruz Biotechnology	Cat# sc-13090, RRID:AB_2080982
Mouse Anti-E-Cadherin	BD Biosciences	Cat# 610182, RRID:AB_397581
Gpig Anti-Insulin	Abcam	Cat# ab7842 RRID:AB_306130

Table 8. Secondary antibodies

Antibody	**Manufacturer**	**Reference no.**
Donkey anti-mouse Alexa Flour® 555	Thermo Fisher Scientific	#A-31570
Donkey anti-rabbit Alexa Flour® 647	Thermo Fisher Scientific	#A-31573
Donkey anti-Goat IgG Alexa Flour® 555	Thermo Fisher Scientific	#A-21447

Antibody	Manufacturer	Reference no.
Goat anti-Rabbit IgG-HRP	GE Healthcare	#RPN4301
Sheep anti-Mouse IgG-HRP	GE Healthcare	#RPN4201

Table 9. Recombinant Proteins

Recombinant Protein	Manufacturer	Reference no.
Recombinant Human APOA4/Apo-AIV protein	Abcam	ab132653
Recombinant human PKD2 protein	Abcam	ab60875

5.5. Cell culture reagents and cell lines

Table 10. Cell culture reagents

Cell culture reagents and media	Manufacturer	Identifier
Bovine serum albumin (BSA)	Sigma-Aldrich	#A8806
DharmaFECT duo	Thermo Fisher Scientific	#T-2010-03
Dimethyl sulfoxide (DMSO)	Sigma-Aldrich	#D8418
DMEM (4.5 g/L D-glucose, 1 mM sodium pyruvate, 4.0 mM glutamine)	Gibco	#31966-021
Dulbecco's modified eagle media (DMEM) (1 g/L D-glucose) (no phenol red)	Gibco	#11054-020
Dulbecco's phosphate-buffered saline (DPBS)	Gibco	#14190-094
Foetal bovine serum (FBS)	Gibco	#10270-106
Gentamicin (10mg/mL)	Gibco	#15710-049
GlutaMAX (100x)	Gibco	#35050-061
Nonessential amino acids (NEAA) (100x)	Gibco	#11140-035
Oleic acid-Albumin from bovine serum	Sigma-Aldrich	#O3008
OptiMEM	Gibco	#31985-047
Sodium pyruvate (100 mM)	Gibco	#11360-039
Trypsin (0.05%)-EDTA	Gibco	#25300-054

Table 11. Cell lines

Cell lines	**Source**	**Identifier**
HEK293T	ATCC	CRL-3216
One Shot™ TOP10 Chemically Competent E. coli	Thermo Fisher Scientific	#C404003
Caco2	ATCC	# HTB-37

5.6. Mice and diets

Table 12. Mice

Mouse line	**Origin**	**Identifier**
Pkd2$^{S707A/S711A}$	The Jackson Laboratory	#017285
Pkd2$^{flox/flox}$	Lab. Professor Yamasaki	
Mouse: B6.Cg-Tg(Vil1-cre)1000Gum/J	The Jackson Laboratory	#021504
C57BL/6JRj	Janvier Labs	

Table 13. Diets

Experimental diets	**Manufacturer**	**Identifier**
High-fat diet (HFD) with 58 kcal% fat with sucrose	ResearchDiets	#D12331i
Normal diet (ND)	sniff Spezialdiäten	#V1125-3

5.7. Buffers

Table 14. Buffers and solutions

Buffer/Solution	**Content**
TBS	20 mM Tris, 150 mM NaCl.
TBST	TBS, 0.1% Tween 20.
Blocking for WB	5% BSA or fat-free dry milk in TBST.
Blocking for IF	PBS, 0.5% BSA, 10% normal goat serum.
50x Tris-Acetate-EDTA (TAE)	2 mM TRIS, 5.7% acetic acid, 10% EDTA (0.5 M stock).
Running Buffer for WB	25 mM TRIS, 192 mM Glycine, 0.5% SDS (20% stock).
Transfer buffer for WB	25 mM TRIS, 192 mM Glycine, 20% methanol.
5x Laemmli buffer	300 mM TRIS, 10% SDS, 50% Glycerol, 25% β-mercaptoethanol, spatula tip Bromophenol blue.
Lysis buffer	20 mM TRIS (pH 7.5 (1 M stock)), 150 mM NaCl (5 M stock), 20 mM β-glycerophosphate, 5 mM $MgCl_2$, 5% Glycerol, 0.2% NP-40, 0.2% Triton X-100, 1x PPI (before usage).
10% separating gel	9.8 mL ddH_2O, 5 mL TRIS (pH 8.6 (1.5 mM stock)), 5 mL Acrylamide (40% stock), 100 µL SDS (20% stock), 200 µL APS (10% stock), 20 µL TEMED.
4% stacking gel	8.2 mL ddH_2O, 620 µL TRIS (pH 8.6(1.5 mM stock)), 946 µL Acrylamide (40% stock), 50 µL SDS (20% stock), 100 µL APS (10% stock), 10 µL TEMED.

5.8. Softwares

Table 15. Softwares

Software and algorithms	**Manufacturer**	**Identifier**
Illustrator CS6	Adobe	
ImageJ	NIH	https://imagej.nih.gov/ij/
LAS X	Leica	
QuantStudio™ Design & Analysis Software	Thermo Fischer Scientific	

6. METHODS

6.1. Mice Experiments

6.1.1. Animals description

Animal experiments performed in this thesis were approved by the local institutional animal care (Regierung von Unterfranken, Germany) and conducted according to the guidelines and state regulations. Experiments were performed under animal protocol numbers AK 55.2-2531.01-124/13 and 55.2-2532-2-741. Mice were maintained in a specific-pathogen-free facility with the ambient temperature set at 23°C and 55% humidity, following a 12-h light-dark cycle and given ad libitum access to water and standard chow diet which was exchanged under indicated experimental conditions to High-fat diet (HFD). Mice were kept in groups of up to 5 mice per cage. Euthanasia was performed by cervical dislocation, in a separate area, away from other animals and all efforts were made to minimize suffering. No animals died or became ill during the development of this research.

After each experiment, the mice were subjected to regular check-ups as specified in the animal permissions.

Pkd2 knockin mice were generated in the laboratory of Prof. Cantrell (Matthews, Navarro et al. (2010)). These mice presented point mutations of Ser^{707} and Ser^{711} into alanines ($Pkd2^{ki/ki}$) by the homologous recombination of the PGK-NeoR cassette in C57BL/6 embryonic stem cells which were microinjected into C57BL/6 blastocysts. Mice were maintained in a C57BL/6 background.

The generation of mice bearing a specific deletion of intestinal PKD2 was achieved by crossbreeding Villin-Cre mice (B6.Cg-Tg(Vil1-cre)1000Gum/J) with *Pkd2* flox/flox mice (courtesy of Prof. Yamasaki, Osaka University) (Ishikawa, Kosako et al. 2016).

All the experiments were performed in male mice.

6.1.2. Mice genotyping

6.1.2.1. DNA extraction

Ears of mice were clipped and the tissue was lysed in 500 µL of buffer containing 10 mM Tris pH 8, 100 mM EDTA pH 8, 0.5% SDS and 0.1 mg/mL Proteinase K. After overnight digestion at 55°C, 100 µL of 5 M NaCl were added and centrifuged at 13000 rpm for 10 min at 4°C. DNA is precipitated from the supernatant by addition of 300 µL of isopropanol, cooling at -20°C for 30 min and centrifugation. The pellet is washed with 70% ethanol, air-dried and resuspended in 50 µL of ultra pure water.

6.1.2.2. PCR for genotyping

The components for one PCR reaction are 1,5 µL of DNA and:

Component	Amount in µL
Thermo 10x Buffer with KCl	2,5
Each primer (10 µM)	1
Thermo dNTPs (5 µM)	2
Thermo $MgCl_2$ (10x)	2,5
Thermo taq Polymerase (5U/ µL)	0,5
Total amount (to complete with H_2O)	23,5

Genotyping was performed for indicated mice models using primer sets from Table 1.

The PCR cycling conditions are:

a) *Pkd2* $^{ki/ki}$ genotyping

Step 1	94°C	3 min
Step 2	94°C	30 sec
Step 3	65°C	20 sec
Step 4	68°C	40 sec
Step 5	go to Step 2, repeat 10x	

Step 6	94°C	30 sec	
Step 7	50°C	20 sec	
Step 8	70°C	40 sec	
Step 9	go to Step 6, repeat 25x		
Step 10	72°C	2 min	
Step 11	10°C	hold	

b) *Pkd2*$^{flox/flox}$ genotyping

Step 1	94°C	2 min
Step 2	94°C	30 sec
Step 3	60°C	30 sec
Step 4	68°C	30 sec
Step 5	go to Step 2, repeat 40x	
Step 6	72°C	10 min
Step 7	4°C	hold

c) Villin Cre genotyping

Step 1	94°C	2 min	
Step 2	94°C	20 sec	
Step 3	65°C	15 sec	-0,5°C per cycle decrease
Step 4	68°C	10 sec	
Step 5	go to Step 2, repeat 10x (Touchdown)		
Step 6	94°C	15 sec	
Step 7	60°C	15 sec	
Step 8	72°C	10 sec	
Step 9	go to Step 6, repeat 28x		
Step 10	72°C	2 min	
Step 11	10°C	hold	

6.1.2.3. Agarose gel electrophoresis

The PCR product is mixed with 6x loading dye and loaded into an agarose gel 2%. The gel was prepared by adding 6 g of agarose into 300 mL of TRIS-acetate-EDTA buffer, boiled in a microwave and adding 30 µL of Midori Green for DNA staining.

For running the gel, DNA samples and 100 bp DNA ladder are run at 120 V for 1 h. Bands are visualized under ultraviolet light.

The resulting bands for each genotyping are:

a) *Pkd2* $^{ki/ki}$ genotyping: wildtype = 280 bp knockin = 340 bp
b) *Pkd2*$^{flox/flox}$ genotyping: wildtype = 350 bp flox = 450 bp
c) Villin Cre genotyping: transgene = 150 bp internal positive control = 182 bp

6.1.3. Body weight and composition

Body weight was measured by using a balance once per week for as long as shown for each individual experiment/diet. Fat mass, lean mass and free fluids were measured for body composition by using a Bruker's Minispec LF50 which utilizes nuclear magnetic resonance (NMR) technology. The weight of different organs is taken directly during the dissection process in an analytic balance. The length of the intestine is measured with a ruler.

6.1.4. Glucose and insulin tolerance tests

Glucose tolerance test was performed in overnight (16h) fasted mice. Zero time-point was measured short before the intraperitoneal administration of glucose (2g/kg). In the case of insulin tolerance test, the intraperitoneal injection contains 0.5U/kg of human insulin (Sigma) and the fasting period is reduced to 4h.

In both experiments, a drop of blood is collected from the tail directly onto a glucometer strip inserted into a glucometer for glucose concentration measurement (Accu-Chek). Measurements were performed at 15, 30, 60 and 90 minutes after injection.

6.1.5. Serum composition and liver triglycerides

Triglycerides, free-fatty acids, glycerol, aspartate aminotransferase and alanine aminotransferase in circulation were determined in serum samples using mentioned kits and according to their manufacturers' instructions.

Free-fatty acids were measured in 5µL of serum. 200µL of Reagent A were added and measured. Directly afterwards, 100µL of Reagent B were added and measured. Each time, providing 5min incubation at 37°C and measuring absorption at 546nm a 660nm (background). A standard curve was used.

Glycerol and triglycerides were measured in 2 or 3µL of serum. Firstly, free glycerol is measured by addition and incubation with 200µL of Free Glycerol reagent. A second measure is taken after addition of 50µL of Triglyceride reagent which hydrolyse triglycerides into glycerol. Before measuring and after addition of each reagent, 5min incubation at 37°C is provided. Absorption is measured at 540nm and triglyceride concentration is determined after subtracting the initial value corresponding to free glycerol.

The quantification of AST and ALT were performed in 7µL of serum of mice that were starved for 4h and gavaged with olive oil (10µL/g of body weight). Then blood samples were taken 1h (AST) and 2h (ALT) after gavaging. Sample was mixed 1:10 with the respective reagent and concentration was calculated by measuring the changes in absorption per minute during 8 minutes. Absorption was measured at 340nm.

Liver triglycerides were measured by homogenization of 50 mg of liver in 500 uL of lysis buffer and lipids extraction in methanol:chloroform, phase extraction and evaporation. The lipids were redissolved in DMSO and triglycerides quantified with the mentioned kit and according to the manufacturers' instructions.

6.1.6. Metabolic measurements

The measurements of food and water intake, activity (photobeam breaks), energy expenditure, respiratory exchange rate, oxygen consumption and CO_2 production were performed by indirect calorimetry in a PhenoMaster system (TSE Systems). Mice were kept in individual cages under specified diet in a 12h light/dark cycle. Measurements were recorded every 10 min for 7 days (after 2 days of adaptation).

6.1.7. Feces analysis

Feces were manually collected with tweezers from the bedding of single-caged mice in a daily basis. Feces were desiccated in an oven at 60°C overnight and subsequently weighted and stored. In order to analyze feces/energy excreted vs. food/energy ingested, the feces collection was performed while the food ingestion and body weight were monitored.

Lipids were extracted from feces with a few modifications from a stablished protocol (Kraus, Yang et al. 2015). Briefly, 500mg of dried and grinded feces were suspended in 2 mL of NaCl 0,9% and lipids extracted in 6mL of 2:1 Chloroform:Methanol. The organic phase is removed and evaporated with the help of an evaporator on a previously weighted tube. The weight of lipids is calculated after subtracting initial from final weight.

Calorie content from feces was analyzed by bomb calorimetry. About 3g of dried feces were pulverized and 1g was pressed into a tablet which was accurately weighted and burned into a 6400 Automatic Isoperibol Calorimeter (Parr Instrument Company). Duplicates were measured. Metabolizable energy was calculated from intake minus excreted and assuming a urinary excretion of 2% (Kless, Rink et al. 2017)

6.1.8. Lipids tolerance test

Intestinal lipids absorption was measured as previously described (Wang, Rong et al. 2016). Mice were overnight fasted and a defined dosage of olive oil (10µL/g of body weight) administered by gavage into the stomach. Blood samples were withdrawn before gavage and 1h, 2h, 3h and 4h afterwards. Serum was analysed for triglycerides as described previously in this thesis.

This experiment was performed after feeding the mice HFD: one week in the *Pkd2*$^{ki/ki}$ mouse model, 6 weeks for *Pkd2*$^{gut\Delta/\Delta}$ and 9 weeks in the case of C57BL/6j mice receiving either water or CRT0066101 (10mg/kg).

6.1.9. Intestinal permeability assay

To test intestinal barrier integrity, FITC-Dextran solution (40mg/mL) was gavaged to overnight fasted mice (10µL/g of body weight). Blood samples were taken 4h after gavage and fluorescence measured (Ex:490nm/Em:530nm). Concentration was

calculated from a standard curve of known concentrations subtracting the blank (serum from water-gavaged mice)(Woting and Blaut 2018).

6.1.10. Chylomicrons isolation

Chylomicrons were isolated according to a stablished protocol (Wang, Rong et al. 2016). After 3 weeks in HFD, mice were overnight fasted and given a defined dosage of olive oil (10µL/g of body weight). 2h later, blood samples were taken and plasma collected after centrifugation. Plasma of three mice with the same genotype were pooled together and 200µL mixed with 600µL of NaCl 0.9%. The samples were centrifuged at 50.000rpm at 4°C for 3h in a Optima MAX-XP Ultracentrifuge MLA-130. 60 µL of the upper layer containing the chylomicrons were taken for microscopy.

6.1.11. Oral administration of PKD inhibitor CRT0066101

PKD inhibitor CRT0066101 (Tocris) was dissolved in mice drinking water to a concentration of 1mg/mL and administered by daily gavage at 2:00 p.m. The reported dosage (80mg/kg) (Harikumar, Kunnumakkara et al. 2010) was decreased to promote a local effect in the intestine instead of the systemic distribution of the inhibitor. Mice were kept in groups of up to five per cage without separation between control and treated groups. Mice were only separated in order to collect feces or to analyze them in Phenomaster for metabolic parameters.

In order to stablish the minimum effective dosage of the inhibitor, two oral dosages were tested (3mg/kg and 10 mg/kg). For that purpose, mice were gavaged daily with 3mg/kg, 10mg/kg or water while they had unlimited access to HFD and water. After two weeks, a lipids tolerance test was performed and 10mg/kg was chosen as the dosage to continue with the experiments. The experiment had a total duration of 13 weeks in which body weight, lipids tolerance, GTT and ITT were measured and feces collected for further analysis.

In the rescue experiment, mice were kept in HFD for seven weeks while the body weight was monitored. After that period, mice were randomly assigned to two groups: one receiving the inhibitor and the other receiving water. Mice continued in HFD during the treatment, which lasted for 11 weeks.

6.2. Microscopy studies

6.2.1. H&E Staining

The specified organs were dissected and directly placed into paraformaldehyde 4% for fixation during a period of 24h at 4°C. Tissues were dehydrated and paraffin infiltrated in an automatic processor Leica ASP200S. Samples were embedded in paraffin and cut into 5µm sections. Standard Hematoxylin-Eosin staining was performed including deparaffinization with xylol, rehydration in alcohol gradient, 10 min hematoxylin and 2 min eosin staining. Digital pictures were taken in a Leica light microscope DM4000B at 20x for adipose tissue, 40x for liver sections and 10x for intestine. A blinded experiment was performed to measure adipocyte size. 6 specimens per genotype and about 400-500 adipocytes per specimen were measured with ImageJ for that purpose.

6.2.2. Immunofluorescence

Mice organoids were collected and fixed with 4% paraformaldehyde for 1h at 4°C and resuspended in Histogel^{TM} drops, then, they were embedded in paraffin, sectioned and deparaffinized. Antigen retrieval was performed with a steamer and blocking with 5% normal serum. Organoids were then incubated with primary antibodies against indicated antigens followed by fluorescent labelling with appropriate secondary antibodies. Samples were mounted using Fluoromount-G^{TM} with DAPI. Slides were visualized using Leica TCS SP8 confocal microscope (Sato, Vries et al. 2009).

For pancreatic islets stainings and quantification, the pancreas was dissected and directly embedded into OCT. 3 different sections (7 µm) per subject were taken with a distance of 50 µm. Sections were fixed (4% PFA) and blocked (5% BSA, 0.2% Triton in PBS) before overnight incubation (4°C) with the primary antibody. Then, the sections were washed and incubated with the secondary antibody (1 hour at RT) before mounting with DAPI.

6.2.3. Electron Microscopy of chylomicrons

5µL of the chylomicrons after ultracentrifugation were applied to carbon-coated copper grids for 5 min, then, 20µL of uranyl acetate 2% was applied for staining for 15min.

Pictures of chylomicrons from *Pkd2*$^{ki/ki}$ mouse model were taken with an electron microscope Zeiss EM 900 and 80 kV (50,000x magnification). Pictures of chylomicrons from *Pkd2*$^{gut\Delta/\Delta}$ mouse model were taken with an electron microscope JEM-2100 and 200 kV (30,000x magnification). Particle size was quantified with ImageJ from 4 different pictures per genotype.

6.3. Immunoblotting

Tissues and cells were lysed in lysis buffer supplemented with Protease and Phosphatase inhibitor. For tissues, one frozen piece was homogenized with a pestle and for cells with the help of a syringe needle. After lysis, samples were subjected to centrifugation (13000rpm, 10 min at 4°C) and the supernatant containing the lysate was recovered and quantified with Pierce™ BCA Protein Assay Kit. Equal amounts of protein (either 50 or 100µg) were adjusted to volume with lysis buffer, mixed with 5x Laemmli buffer, boiled at 95°C for 5 min and loaded into a SDS-PAGE gel (8% or 10%).

Serum lipoproteins were analyzed in western blot after overnight fasting and 2 hours refeeding of mice that previously were in HFD for a week. Blood was withdrawn and centrifuged (13000rpm, 10 min at 4°C) and 10µL of serum was mixed with 2.5µL of 5x Laemmli buffer, boiled at 95°C, 5 min and loaded in a SDS-PAGE gel.

For the study of proteins released into the medium, Caco2 cells were differentiated onto a transwell and overnight stimulated with oleic acid (as explained in the in-vitro studies section). The basolateral medium was collected and 20µL were mixed with 5µL of 5x Laemmli buffer, boiled at 95°C, 5 min and loaded in a SDS-PAGE gel.

SDS-PAGE gels were run overnight at 40V (RT). Transfer into PVDF membranes was performed at 220mA and 4°C for 4h. Membrane was blocked in 5% milk in TBST (1h, 4°C) and incubated at 4°C overnight with primary antibodies (1:3000 in 5%BSA in TBST). The membrane was washed three times with TBST and then incubated with HRP-conjugated secondary antibody for 1h at 4°C (1:3000 in 5% milk in TBST). After three more washes with TBST and one with TBS, the membrane was developed with ECL by using X-ray films or digitally in Amersham Imager 680.

6.4. Real-time qPCR

Extraction of total RNA was performed with 1 mL of QIAzol lysis reagent and following the instructions of its manufacturer with the help of an homogenizer. After quantification, 1 µg of RNA was reversely transcribed with First cDNA Synthesis Kit according to manufacturer's protocol. cDNA was diluted 1:15 before running the qPCR with SYBR Green Master mix.

The mix for the RT-qPCR contained:

2 µL of diluted cDNA

0.4 µL of each primer (forward and reverse) (10 pmol/µL)

5 µL PowerUp SYBR Green

2.2 µL UltraPure water

RT-qPCR conditions:

Step 1	95°C	10 min	
Step 2	95°C	15 s	
Step 3	60°C	1 min	
go to step 2, 40x			
Step 4	95°C	15 s	
Step 5	60°C	1 min	
Step 6	95°C	15 s	(step 4-6 for melting curve)

Comparative C_T method was used to quantify relative amounts of mRNA of specified genes, using *Rpl13a* or *18S* for normalization.

Absolute quantification was performed according to a standard protocol from Applied Biosystems. Briefly, primers were designed to be located within same exons and genomic DNA of known concentration was used for creating a standard curve reflecting copy numbers.

6.5. In-vitro studies

6.5.1. Plasmids transformation, culture and purification

Plasmids were transformed into One-Shot TOP10 chemically competent *E. coli*. For that purpose, 50 µL of competent cells were thaw on ice and 1-2 µL of plasmid were added. The mixture was kept on ice for 30 min and then put for heat shock at 42°C for 30 sec. The tube was cooled down on ice and 250 µL of SOC medium was added. The tube was incubated for 1 h at 37°C while shaking at 200 rpm. Afterwards, the bacteria was plated into agar plates containing the respective antibiotic an incubated at 37°C overnight. Single colonies were picked for plasmid production and purification.

Mini-prep kit was used for confirmation of successful cloning with sequencing (performed by Eurofins). Positive cultures were used for incubation of Midi-prep cultures for plasmid production. Kits for mini-prep and midi-prep were both purchased from Macherey-Nagel (NucleoSpin Plasmid and NucleoBond Midi, respectively). Briefly, the cells are pelleted by centrifugation, resuspended and lysed in the specified buffers. The lysis process is stopped by a neutralization buffer. Proteins and cell debris are removed either by centrifugation (mini-prep) or filtration (midi-prep). The supernatant containing the plasmid, is loaded into a column. The column is washed and the plasmid eluted. The plasmid is also washed and finally reconstituted in water.

6.5.2. HEK293T culture, transfection and generation of viral particles

HEK293T cells were cultured in Dulbecco's modified eagle's medium (DMEM) High Glucose, 10% fetal bovine serum (FBS), 1x non-essential amino acids (NEAA) and 40 µg/mL gentamycin. The medium was changed every 2 days and they were splitted before they reached more than 80% confluence.

Lentiviral vectors were transfected together with packaging vectors psPAX and pMD2.G (Addgene) with the help of transfection reagent DharmaFECT™ Duo. Medium from transfected HEK293T cells was collected 48 and 72 h after transfection. Then, the medium was centrifuged and filtered (40 µm) and mixed with polybrene (4 µg/mL, Sigma). Target cells (Caco2) were spinfected with that medium and selected for 72-96 h with Puromycin (5 µg/mL, ThermoFisher).

6.5.3. Generation of stable cell lines expressing *shRNA*

Caco2 cells were spinfected with viral particles generated in HEK293T cells as specified before. The cells were infected with lentiviral particles from pLKO.1 vector containing either *shRNA* targeting *Pkd2* or scramble (non-targeting) (both acquired from MISSION *shRNA* library) and the deletion efficiency verified by western blot with an specific antibody against PKD2.

6.5.4. Caco2 cells culture and freezing

Caco2 cells were cultured in Dulbecco's modified eagle's medium (DMEM) 4,5 g/L glucose, 10% fetal bovine serum (FBS), 1x non-essential amino acids (NEAA), 1 mM sodium piruvate and 40µg/mL gentamycin. Medium was changed every two days and the cells were splitted before reaching 80% confluence by detaching the cells with 0.05% Trypsin.

Lipids transport by Caco2 cells was assessed in a transwell system . For that purpose, Caco2 cells were detached, resuspended and counted under the light microscope in a Neubauer chamber with the help of Trypan blue. 3 x 10^5 cells were seeded into a 12-well cell culture insert (transwell) in a volume of 500 µL. The insert was placed into a 12-well plate but the basolateral remains empty overnight during the first night after seeding the Caco2 cells. The day after seeding, apical medium is changed and 1 mL medium is added to the basal side. Medium was changed every two days and kept for 14 days to promote tight junction formation and polarization.

Cells were frozen before reaching 80% confluence in freezing medium containing 50% DMEM (4,5 g/L glucose), 40% FBS and 10% DMSO. Cells were centrifuged, resuspended, aliquoted into freezing vials (1 mL) and placed in a freezing chamber that was maintained at -20°C for 1 h before being transferred to -80°C or liquid nitrogen.

6.5.5. Caco2 lipids transport in transwell inserts

Caco2 cells were seeded and polarized in transwell inserts as previously described. In order to verify tight junctions development and barrier integrity, Transepithelial electrical resistance (TEER) was measured (Srinivasan, Kolli et al. 2015, Tan, Trier et al. 2018). Briefly, after 14 days of differentiation, the electrical resistance of the Caco2 monolayer was measured by chop stick hand-electrode in 3 different points of the

membrane and the average was taken as the value per well. The resistance is expressed as Ω*cm².

For lipids transport and release, cells in the transwell system were incubated in the apical compartment with 500 µL of DMEM, 10% FBS, 1 mM Oleic acid (#O1383, Sigma), 2 mM sodium taurocholate and 0.2 µCi of C^{14}-palmitic acid. The basolateral compartment contained 1 mL of DMEM 0.1% FBS. After 24 h stimulation, apical, basolateral and cell lysates were collected and aliquots were placed into scintillation vials. 5 mL of scintillation cocktail were added and radioactivity quantified. This experiment was also performed in Caco2 cells after treatment with CRT0066101 inhibitor. In that case, the inhibitor was added at 3 or 5 µM concentration in regular Caco2 medium, 24 h before the stimulation and added also in the stimulation cocktail.

Lipids transport was also measured by using QBT Fatty Acid Uptake Assay Kit (Molecular Devices). Briefly, DMEM medium (low glucose, 0,1% FBS, no phenol red) was mixed with fluorescent QBT Fatty Acids (70:30). 500 µL of the medium was added to the apical side and 1 mL of DMEM (low glucose, 0,1% FBS, no phenol red) added to the basolateral side. Aliquots from the basal medium were taken at different time points and measurement expressed as RFU/µg of protein. Fluorescence was measured at Ex:485 nm and Em:530 nm.

6.5.6. Intestinal Epithelial cells isolation and organoids culture

For generation of mice organoids, 1-2 cm of jejunum from *Pkd2*$^{wt/wt}$ and *Pkd2*$^{ki/ki}$ mice were washed with HBSS and cut open. Mucus and villi were removed with HBSS by scraping with glass slides. Then, a series of 6 washings with cold HBSS and shaking (in order: vortex 5 sec, rotation 30 min, inversion and 3x manual shaking) ensured the removal of the villi and extraction of the crypts. After centrifugation, crypts are seeded in Matrigel™ (5000 crypts/mL) in 50 µL drops. After an incubation period of 10-20 min at 37°C, 300µL culture medium was added to cover the solidified drops. Basal medium, for resuspension of pellets, contains DMEM-F12 Advanced complemented with 1x N2, 1x B27 w/o vitamin A, 1x Anti-anti, 10 mM HEPES, 2mM GlutaMAX-I, 1 mM N-acetylcystein. The organoids were maintained in basal medium supplemented with 500 ng/mL hR-Spondin 1, 100 ng/mL rec Noggin, 50 ng/mL hEGF, 3 µM

CHIR99021 and 1mM valproic acid (also 10 µM Y-27632 only the first day after splitting). Medium was changed every 2 days.

6.5.7. In-vitro kinase assay

In-vitro kinase assay was performed with recombinant human PKD2 protein (ab60875) and recombinant human APOA4 (ab132653) both purchased from Abcam. The phosphorylation reaction takes place in 1x NEBuffer for Protein Kinases and 10 µM ATP. 50 ng of PKD2 and 10 µg of APOA4 were used per reaction. In case it is indicated, CRT0066101 (10 µM) was added to inhibit PKD2.

The assay lasts for 30 min at 30°C. Time after which, 5x loading dye was added to the mixture to stop the reaction. Samples were immediately boiled at 95°C for 5 min and loaded into a SDS-PAGE gel for western blot. In-vitro kinase assay was performed by duplicates in the same tube and splitted in two for western blot analysis. Primary antibody recognizing the phosphorylation motif of Protein Kinase D was used to verify phosphorylation. Primary antibody against APOA4 was used to verify equal loading and correspondence between the APOA4 band and the phosphorylated band.

6.6. Human samples

Fasting blood samples were collected from 7 morbidly obese (BMI 42.7-54 kg/m2) female patients aged 33-57 years prior to Roux-en-Y gastric bypass (RYGB) surgery for standard biochemical analysis. A whole-wall segment of proximal jejunum (5cm) was collected from fasted patients during the surgery and gently rinsed in ice-cold PBS before rapidly snap-freezing in liquid nitrogen. At the time of surgeries, two patients were on metformin medication for type 2 diabetes and one patient for polycystic ovary syndrome. Prior to surgeries, all patients observed a standard 2-4 week very low calorie diet (1, 000 kcal per day) which comprised 2 daily liquid meals (such as egg white shakes or vegetable soup) and 1 daily solid meal (such as tuna fish or chicken breast salads) that were low in fat and carbohydrates and rich in protein (100g). Informed, written consent was obtained from all patients and usage of human material was approved by the Ethics Committee of the Medical Faculty of the University of Würzburg (approval number EK AZ 188/17 - MK).

6.7. Statistical analysis

The results are presented as mean values ± standard error of the mean (SEM). Significances were assessed by using a two-tailed Student's t -test for independent groups. P values of 0.05 or lower were considered as statistically significant (*$p<0.05$, **$p<0.01$, and ***$p<0.001$).

For microbiota studies, analysis of alpha diversity was performed with GraphPad prism v6 using the non-parametric Mann-Whitney U test. We visualized beta diversity using non-metric multi-dimensional scaling based on generalized UniFrac and tested for significance using PERMANOVA. Differences in OTUs were determined using Fisher`s Exact test with adjustments for multiple testing using the Benjamini & Hochberg method.

For scatter plots of human samples, r2= square of the Pearson product-moment correlation coefficient and p was determined for Pearson correlation coefficient for the given degrees of freedom.

7. REFERENCES

Azoitei, N., M. Cobbaut, A. Becher, J. Van Lint and T. Seufferlein (2018). "Protein kinase D2: a versatile player in cancer biology." Oncogene **37**(10): 1263-1278.

Azoitei, N., A. Kleger, N. Schoo, D. R. Thal, C. Brunner, G. V. Pusapati, A. Filatova, F. Genze, P. Möller and T. Acker (2011). "Protein kinase D2 is a novel regulator of glioblastoma growth and tumor formation." Neuro-oncology **13**(7): 710-724.

Bäckhed, F., R. E. Ley, J. L. Sonnenburg, D. A. Peterson and J. I. Gordon (2005). "Host-bacterial mutualism in the human intestine." Science **307**(5717): 1915-1920.

Bagchi, D. and H. G. Preuss (2007). Obesity: Epidemiology, Pathophysiology, and Prevention, CRC Press.

Bansal, A. B. and Y. Al Khalili (2021). Orlistat. StatPearls. Treasure Island (FL), StatPearls Publishing Copyright © 2021, StatPearls Publishing LLC.

Bass, L. and B. K. Wershil (2016). "Anatomy, histology, embryology and developmental anomalies of the small and large intestine." Sleisenger and Fordtran's gastrointestinal and liver disease. 10th ed. Philadelphia, PA: Saunders, Elsevier Inc: 1649.

Bergeron, V., J. Ghislain, K. Vivot, N. Tamarina, L. H. Philipson, J. Fielitz and V. Poitout (2018). "Deletion of Protein Kinase D1 in Pancreatic β-Cells Impairs Insulin Secretion in High-Fat Diet–Fed Mice." Diabetes **67**(1): 71-77.

Bradley, W. D., C. Zwingelstein and C. M. Rondinone (2011). "The emerging role of the intestine in metabolic diseases." Archives of Physiology and Biochemistry **117**(3): 165-176.

Brahmbhatt, M. (2017). "Social and physical determinants of obesity in adults." Adv Obes Weight Manag Control **6**(1): 17-23.

Brainkart. (2021). "Essentials of anatomy and physiology." from http://www.brainkart.com/article/Anatomy-of-the-Small-intestine.

Charles, M. M., II (2009). "The Formation and Intracellular Transport of Chylomicrons." Immunology, Endocrine & Metabolic Agents in Medicinal Chemistry (Under Re-organization) **9**(1): 55-59.

Coughlan, K. A., R. J. Valentine, B. S. Sudit, K. Allen, Y. Dagon, B. B. Kahn, N. B. Ruderman and A. K. Saha (2016). "PKD1 Inhibits AMPKα2 through Phosphorylation of Serine 491 and Impairs Insulin Signaling in Skeletal Muscle Cells." The Journal of biological chemistry **291**(11): 5664-5675.

Cummings, B. (2001).

de Andrade Júnior, M. C. (2018). "iMedPub Journals."

Demignot, S., F. Beilstein and E. Morel (2014). "Triglyceride-rich lipoproteins and cytosolic lipid droplets in enterocytes: Key players in intestinal physiology and metabolic disorders." Biochimie **96**: 48-55.

DeSesso, J. M. and C. F. Jacobson (2001). "Anatomical and physiological parameters affecting gastrointestinal absorption in humans and rats." Food Chem Toxicol **39**(3): 209-228.

El-Merahbi, R., J. T. Viera, A. L. Valdes, K. Kolczynska, S. Reuter, M. C. Löffler, M. Erk, C. P. Ade, T. Karwen, A. E. Mayer, M. Eilers and G. Sumara (2020). "The adrenergic-induced ERK3 pathway drives lipolysis and suppresses energy dissipation." Genes & Development **34**(7-8): 495-510.

Essegian, D., R. Khurana, V. Stathias and S. C. Schürer (2020). "The Clinical Kinase Index: Prioritizing Understudied Kinases as Targets for the Treatment of Cancer." bioRxiv: 2020.2002.2014.943886.
Feingold, K. (2021). "Introduction to Lipids and Lipoproteins."
Ferrer, F., E. Bigot-Corbel, P. N'Guyen, M. Krempf and J. M. Bard (2002). "Quantitative measurement of lipoprotein particles containing both apolipoprotein AIV and apolipoprotein B in human plasma by a noncompetitive ELISA." Clin Chem **48**(6 Pt 1): 884-890.
Finer, N. (2002). "Sibutramine: its mode of action and efficacy." International Journal of Obesity **26**(4): S29-S33.
George, D. E., E. Lebenthal and M. Landis (1985). "Circadian rhythm of the pancreatic enzymes in rats: Its relation to small intestinal disaccharidase." Nutrition Research **5**(6): 651-662.
Glickman, R. M. and P. H. Green (1977). "The intestine as a source of apolipoprotein A1." Proceedings of the National Academy of Sciences **74**(6): 2569-2573.
Gonzalez-Vallina, R., H. Wang, R. Zhan, H. M. Berschneider, R. M. Lee, N. O. Davidson and D. D. Black (1996). "Lipoprotein and apolipoprotein secretion by a newborn piglet intestinal cell line (IPEC-1)." American Journal of Physiology-Gastrointestinal and Liver Physiology **271**(2): G249-G259.
Gotto, A. M., Jr. (1990). "Interrelationship of triglycerides with lipoproteins and high-density lipoproteins." Am J Cardiol **66**(6): 20a-23a.
Grobe, J. L. (2017). "Comprehensive Assessments of Energy Balance in Mice." Methods in molecular biology (Clifton, N.J.) **1614**: 123-146.
Guo, J., Z. Gertsberg, N. Ozgen, A. Sabri and S. F. Steinberg (2011). "Protein kinase D isoforms are activated in an agonist-specific manner in cardiomyocytes." The Journal of biological chemistry **286**(8): 6500-6509.
Hankir, M. K., F. Seyfried, A. D. Miras and M. A. Cowley (2018). "Brain Feeding Circuits after Roux-en-Y Gastric Bypass." Trends Endocrinol Metab **29**(4): 218-237.
Hao, Q., R. McKenzie, H. Gan and H. Tang (2013). "Protein kinases D2 and D3 are novel growth regulators in HCC1806 triple-negative breast cancer cells." Anticancer research **33**(2): 393-399.
Harikumar, K. B., A. B. Kunnumakkara, N. Ochi, Z. Tong, A. Deorukhkar, B. Sung, L. Kelland, S. Jamieson, R. Sutherland and T. Raynham (2010). "A novel small-molecule inhibitor of protein kinase D blocks pancreatic cancer growth in vitro and in vivo." Molecular cancer therapeutics **9**(5): 1136-1146.
Harikumar, K. B., A. B. Kunnumakkara, N. Ochi, Z. Tong, A. Deorukhkar, B. Sung, L. Kelland, S. Jamieson, R. Sutherland, T. Raynham, M. Charles, A. Bagherzadeh, C. Foxton, A. Boakes, M. Farooq, D. Maru, P. Diagaradjane, Y. Matsuo, J. Sinnett-Smith, J. Gelovani, S. Krishnan, B. B. Aggarwal, E. Rozengurt, C. R. Ireson and S. Guha (2010). "A Novel Small-Molecule Inhibitor of Protein Kinase D Blocks Pancreatic Cancer Growth In vitro and In vivo." Molecular Cancer Therapeutics **9**(5): 1136-1146.
Hayashi, H., D. F. Nutting, K. Fujimoto, J. A. Cardelli, D. Black and P. Tso (1990). "Transport of lipid and apolipoproteins A-I and A-IV in intestinal lymph of the rat." J Lipid Res **31**(9): 1613-1625.
Hesse, D., A. Jaschke, B. Chung and A. Schürmann (2013). "Trans-Golgi proteins participate in the control of lipid droplet and chylomicron formation." Bioscience reports **33**(1).

Hidalgo, I. J., T. J. Raub and R. T. Borchardt (1989). "Characterization of the human colon carcinoma cell line (Caco-2) as a model system for intestinal epithelial permeability." Gastroenterology **96**(2): 736-749.
Hurt, R. T., C. Kulisek, L. A. Buchanan and S. A. McClave (2010). "The obesity epidemic: challenges, health initiatives, and implications for gastroenterologists." Gastroenterology & hepatology **6**(12): 780-792.
Hussain, M. M. (2014). "Intestinal lipid absorption and lipoprotein formation." Current opinion in lipidology **25**(3): 200.
Hussain, M. M., N. Nijstad and L. Franceschini (2011). "Regulation of microsomal triglyceride transfer protein." Clinical lipidology **6**(3): 293-303.
Iqbal, J. and M. M. Hussain (2009). "Intestinal lipid absorption." American Journal of Physiology-Endocrinology and Metabolism **296**(6): E1183-E1194.
Ishikawa, E., H. Kosako, T. Yasuda, M. Ohmuraya, K. Araki, T. Kurosaki, T. Saito and S. Yamasaki (2016). "Protein kinase D regulates positive selection of CD4+ thymocytes through phosphorylation of SHP-1." Nature Communications **7**(1): 12756.
Kahn, B. B. and J. S. Flier (2000). "Obesity and insulin resistance." The Journal of Clinical Investigation **106**(4): 473-481.
Kalogeris, T. J., K. Fukagawa and P. Tso (1994). "Synthesis and lymphatic transport of intestinal apolipoprotein A-IV in response to graded doses of triglyceride." J Lipid Res **35**(7): 1141-1151.
Kalogeris, T. J. and R. G. Painter (2001). "Adaptation of intestinal production of apolipoprotein A-IV during chronic feeding of lipid." Am J Physiol Regul Integr Comp Physiol **280**(4): R1155-1161.
Keller, J. and P. Layer (2002). "Circadian pancreatic enzyme pattern and relationship between secretory and motor activity in fasting humans." Journal of Applied Physiology **93**(2): 592-600.
Kellett, G. L., E. Brot-Laroche, O. J. Mace and A. Leturque (2008). "Sugar Absorption in the Intestine: The Role of GLUT2." Annual Review of Nutrition **28**(1): 35-54.
Keohane, P. P., G. K. Grimble, B. Brown, R. C. Spiller and D. B. Silk (1985). "Influence of protein composition and hydrolysis method on intestinal absorption of protein in man." Gut **26**(9): 907-913.
Kersten, S. (2014). "Physiological regulation of lipoprotein lipase." Biochim Biophys Acta **1841**(7): 919-933.
Kim, J. B. (2016). "Dynamic cross talk between metabolic organs in obesity and metabolic diseases." Experimental & Molecular Medicine **48**(3): e214-e214.
Kless, C., N. Rink, J. Rozman and M. Klingenspor (2017). "Proximate causes for diet-induced obesity in laboratory mice: a case study." European Journal of Clinical Nutrition **71**(3): 306-317.
Kohan, A. B., F. Wang, X. Li, S. Bradshaw, Q. Yang, J. L. Caldwell, T. M. Bullock and P. Tso (2012). "Apolipoprotein A-IV regulates chylomicron metabolism-mechanism and function." American journal of physiology. Gastrointestinal and liver physiology **302**(6): G628-G636.
Kohan, A. B., F. Wang, X. Li, A. E. Vandersall, S. Huesman, M. Xu, Q. Yang, D. Lou and P. Tso (2013). "Is apolipoprotein A-IV rate limiting in the intestinal transport and absorption of triglyceride?" American Journal of Physiology-Gastrointestinal and Liver Physiology **304**(12): G1128-G1135.
Kolczynska, K., A. Loza-Valdes, I. Hawro and G. Sumara (2020). "Diacylglycerol-evoked activation of PKC and PKD isoforms in regulation of glucose and lipid metabolism: a review." Lipids in Health and Disease **19**(1): 1-15.

König, J., J. Wells, P. D. Cani, C. L. García-Ródenas, T. MacDonald, A. Mercenier, J. Whyte, F. Troost and R.-J. Brummer (2016). "Human intestinal barrier function in health and disease." Clinical and translational gastroenterology **7**(10): e196.
Kos, K., C. Baker and S. Kumar (2005). "Current treatment strategies for obesity." Therapy **2**: 955-967.
Koya, D. and G. L. King (1998). "Protein kinase C activation and the development of diabetic complications." Diabetes **47**(6): 859-866.
Kraus, D., Q. Yang and B. B. Kahn (2015). "Lipid Extraction from Mouse Feces." Bio Protoc **5**(1).
Kronenberg, F., M. Stühlinger, E. Trenkwalder, F. S. Geethanjali, O. Pachinger, A. von Eckardstein and H. Dieplinger (2000). "Low apolipoprotein A-IV plasma concentrations in men with coronary artery disease." Journal of the American College of Cardiology **36**(3): 751-757.
Kuryłowicz, A. and M. Puzianowska-Kuźnicka (2020). "Induction of Adipose Tissue Browning as a Strategy to Combat Obesity." Int J Mol Sci **21**(17).
Kwon, O., K. W. Kim and M.-S. Kim (2016). "Leptin signalling pathways in hypothalamic neurons." Cellular and Molecular Life Sciences **73**(7): 1457-1477.
La Frano, M. R., A. Hernandez-Carretero, N. Weber, K. Borkowski, T. L. Pedersen, O. Osborn and J. W. Newman (2017). "Diet-induced obesity and weight loss alter bile acid concentrations and bile acid–sensitive gene expression in insulin target tissues of C57BL/6J mice." Nutrition Research **46**: 11-21.
Lea, T. (2015). Caco-2 cell line. The impact of food bioactives on health, Springer, Cham**:** 103-111.
Ley, R. E., P. J. Turnbaugh, S. Klein and J. I. Gordon (2006). "Microbial ecology: human gut microbes associated with obesity." Nature **444**(7122): 1022-1023.
Li, Q. Q., I. Hsu, T. Sanford, R. Railkar, N. Balaji, C. Sourbier, C. Vocke, K. Balaji and P. K. Agarwal (2018). "Protein kinase D inhibitor CRT0066101 suppresses bladder cancer growth in vitro and xenografts via blockade of the cell cycle at G2/M." Cellular and Molecular Life Sciences **75**(5): 939-963.
Liu, M., L. Shen, Y. Liu, S. C. Woods, R. J. Seeley, D. D'Alessio and P. Tso (2004). "Obesity induced by a high-fat diet downregulates apolipoprotein A-IV gene expression in rat hypothalamus." Am J Physiol Endocrinol Metab **287**(2): E366-370.
Liu, Y., Y. Wang, S. Yu, Y. Zhou, X. Ma, Q. Su, L. An, F. Wang, A. Shi, J. Zhang and L. Chen (2019). "The Role and Mechanism of CRT0066101 as an Effective Drug for Treatment of Triple-Negative Breast Cancer." Cell Physiol Biochem **52**(3): 382-396.
Löffler, M. C., A. E. Mayer, J. Trujillo Viera, A. Loza Valdes, R. El-Merahbi, C. P. Ade, T. Karwen, W. Schmitz, A. Slotta and M. Erk (2018). "Protein kinase D1 deletion in adipocytes enhances energy dissipation and protects against adiposity." The EMBO journal **37**(22): e99182.
Löffler, M. C., A. E. Mayer, J. T. Viera, A. L. Valdes, R. El-Merahbi, C. P. Ade, T. Karwen, W. Schmitz, A. Slotta and M. Erk (2018). "Protein kinase D1 deletion in adipocytes enhances energy dissipation and protects against adiposity." The EMBO journal **37**(22).
Mansbach, C. M. and S. Siddiqi (2016). "Control of chylomicron export from the intestine." American Journal of Physiology-Gastrointestinal and Liver Physiology **310**(9): G659-G668.
Martinez-Guryn, K., N. Hubert, K. Frazier, S. Urlass, M. W. Musch, P. Ojeda, J. F. Pierre, J. Miyoshi, T. J. Sontag, C. M. Cham, C. A. Reardon, V. Leone and E. B. Chang (2018). "Small Intestine Microbiota Regulate Host Digestive and Absorptive Adaptive Responses to Dietary Lipids." Cell Host Microbe **23**(4): 458-469.e455.

Matthews, S. A., M. N. Navarro, L. V. Sinclair, E. Emslie, C. Feijoo-Carnero and D. A. Cantrell (2010). "Unique functions for protein kinase D1 and protein kinase D2 in mammalian cells." The Biochemical journal **432**(1): 153-163.
Mayer, A. E., M. C. Löffler, A. E. L. Valdés, W. Schmitz, R. El-Merahbi, J. T. Viera, M. Erk, T. Zhang, U. Braun and M. Heikenwalder (2019). "The kinase PKD3 provides negative feedback on cholesterol and triglyceride synthesis by suppressing insulin signaling." Science signaling **12**(593): eaav9150.
Mazmanian, S. K., C. H. Liu, A. O. Tzianabos and D. L. Kasper (2005). "An immunomodulatory molecule of symbiotic bacteria directs maturation of the host immune system." Cell **122**(1): 107-118.
Mazzawi, T., D. Gundersen, T. Hausken and M. El-Salhy (2015). "Increased chromogranin a cell density in the large intestine of patients with irritable bowel syndrome after receiving dietary guidance." Gastroenterology research and practice **2015**.
Melanson, E. L., S. K. Keadle, J. E. Donnelly, B. Braun and N. A. King (2013). "Resistance to Exercise-Induced Weight Loss: Compensatory Behavioral Adaptations." Medicine & Science in Sports & Exercise **45**(8): 1600-1609.
Merkel, M., R. H. Eckel and I. J. Goldberg (2002). "Lipoprotein lipase genetics, lipid uptake, and regulation." Journal of lipid research **43**(12): 1997-2006.
Meunier, V., M. Bourrie, Y. Berger and G. Fabre (1995). "The human intestinal epithelial cell line Caco-2; pharmacological and pharmacokinetic applications." Cell biology and toxicology **11**(3-4): 187-194.
Mihailovic, T., M. Marx, A. Auer, J. Van Lint, M. Schmid, C. Weber and T. Seufferlein (2004). "Protein kinase D2 mediates activation of nuclear factor κB by Bcr-Abl in Bcr-Abl+ human myeloid leukemia cells." Cancer Research **64**(24): 8939-8944.
Nakajima, K., T. Nakano, Y. Tokita, T. Nagamine, A. Inazu, J. Kobayashi, H. Mabuchi, K. L. Stanhope, P. J. Havel, M. Okazaki, M. Ai and A. Tanaka (2011). "Postprandial lipoprotein metabolism: VLDL vs chylomicrons." Clinica Chimica Acta **412**(15): 1306-1318.
Niederwerder, M. C. (2018). "Fecal microbiota transplantation as a tool to treat and reduce susceptibility to disease in animals." Veterinary immunology and immunopathology **206**: 65-72.
Nordskog, B. K., C. T. Phan, D. F. Nutting and P. Tso (2001). "An examination of the factors affecting intestinal lymphatic transport of dietary lipids." Advanced Drug Delivery Reviews **50**(1): 21-44.
Obert, J., M. Pearlman, L. Obert and S. Chapin (2017). "Popular Weight Loss Strategies: a Review of Four Weight Loss Techniques." Curr Gastroenterol Rep **19**(12): 61.
Pelaseyed, T., J. H. Bergström, J. K. Gustafsson, A. Ermund, G. M. H. Birchenough, A. Schütte, S. van der Post, F. Svensson, A. M. Rodríguez-Piñeiro, E. E. L. Nyström, C. Wising, M. E. V. Johansson and G. C. Hansson (2014). "The mucus and mucins of the goblet cells and enterocytes provide the first defense line of the gastrointestinal tract and interact with the immune system." Immunological reviews **260**(1): 8-20.
Qi, Y., C. Jiang, J. Cheng, K. W. Krausz, T. Li, J. M. Ferrell, F. J. Gonzalez and J. Y. Chiang (2015). "Bile acid signaling in lipid metabolism: metabolomic and lipidomic analysis of lipid and bile acid markers linked to anti-obesity and anti-diabetes in mice." Biochim Biophys Acta **1851**(1): 19-29.
Qu, J., C. W. Ko, P. Tso and A. Bhargava (2019). "Apolipoprotein A-IV: A Multifunctional Protein Involved in Protection against Atherosclerosis and Diabetes." Cells **8**(4).

Rao, R., A. Roche, G. Febres, M. Bessler, P. Tso and J. Korner (2017). "Circulating Apolipoprotein A-IV presurgical levels are associated with improvement in insulin sensitivity after Roux-en-Y gastric bypass surgery." Surgery for Obesity and Related Diseases **13**(3): 468-473.
Ravussin, Y., C. Xiao, O. Gavrilova and M. L. Reitman (2014). "Effect of intermittent cold exposure on brown fat activation, obesity, and energy homeostasis in mice." PLoS One **9**(1): e85876.
Reckless, J. P. D. and J. M. Lawrence (2003). HYPERLIPIDEMIA (HYPERLIPIDAEMIA). Encyclopedia of Food Sciences and Nutrition (Second Edition). B. Caballero. Oxford, Academic Press**:** 3183-3192.
Renton, M. C., S. L. McGee and K. F. Howlett (2020). "The role of protein kinase D (PKD) in intracellular nutrient sensing and regulation of adaptive responses to the obese environment." Obesity Reviews.
Rozman, J., M. Klingenspor and M. Hrabě de Angelis (2014). "A review of standardized metabolic phenotyping of animal models." Mamm Genome **25**(9-10): 497-507.
Ruban, A., K. Stoenchev, H. Ashrafian and J. Teare (2019). "Current treatments for obesity." Clinical medicine (London, England) **19**(3): 205-212.
Sambuy, Y., I. De Angelis, G. Ranaldi, M. Scarino, A. Stammati and F. Zucco (2005). "The Caco-2 cell line as a model of the intestinal barrier: influence of cell and culture-related factors on Caco-2 cell functional characteristics." Cell biology and toxicology **21**(1): 1-26.
Sato, T., R. G. Vries, H. J. Snippert, M. van de Wetering, N. Barker, D. E. Stange, J. H. van Es, A. Abo, P. Kujala, P. J. Peters and H. Clevers (2009). "Single Lgr5 stem cells build crypt-villus structures in vitro without a mesenchymal niche." Nature **459**(7244): 262-265.
Sharlow, E. R., K. V. Giridhar, C. R. LaValle, J. Chen, S. Leimgruber, R. Barrett, K. Bravo-Altamirano, P. Wipf, J. S. Lazo and Q. J. Wang (2008). "Potent and Selective Disruption of Protein Kinase D Functionality by a Benzoxoloazepinolone *." Journal of Biological Chemistry **283**(48): 33516-33526.
Simon, T., V. R. Cook, A. Rao and R. B. Weinberg (2011). "Impact of murine intestinal apolipoprotein A-IV expression on regional lipid absorption, gene expression, and growth." Journal of Lipid Research **52**(11): 1984-1994.
Smathers, R. L. and D. R. Petersen (2011). "The human fatty acid-binding protein family: Evolutionary divergences and functions." Human Genomics **5**(3): 170.
Srinivasan, B., A. R. Kolli, M. B. Esch, H. E. Abaci, M. L. Shuler and J. J. Hickman (2015). "TEER Measurement Techniques for In Vitro Barrier Model Systems." Journal of Laboratory Automation **20**(2): 107-126.
Stahl, A., D. J. Hirsch, R. E. Gimeno, S. Punreddy, P. Ge, N. Watson, S. Patel, M. Kotler, A. Raimondi, L. A. Tartaglia and H. F. Lodish (1999). "Identification of the Major Intestinal Fatty Acid Transport Protein." Molecular Cell **4**(3): 299-308.
Stanislawski, M. A., D. Dabelea, L. A. Lange, B. D. Wagner and C. A. Lozupone (2019). "Gut microbiota phenotypes of obesity." npj Biofilms and Microbiomes **5**(1): 18.
Stein, O., Y. Stein, M. Lefevre and P. S. Roheim (1986). "The role of apolipoprotein A-IV in reverse cholesterol transport studied with cultured cells and liposomes derived from an ether analog of phosphatidylcholine." Biochimica et Biophysica Acta (BBA) - Lipids and Lipid Metabolism **878**(1): 7-13.

Steinmetz, A., R. Barbaras, N. Ghalim, V. Clavey, J. C. Fruchart and G. Ailhaud (1990). "Human apolipoprotein A-IV binds to apolipoprotein A-I/A-II receptor sites and promotes cholesterol efflux from adipose cells." J Biol Chem **265**(14): 7859-7863.
Sturany, S., J. Van Lint, F. Müller, M. Wilda, H. Hameister, M. Höcker, A. Brey, U. Gern, J. Vandenheede, T. Gress, G. Adler and T. Seufferlein (2001). "Molecular Cloning and Characterization of the Human Protein Kinase D2: A NOVEL MEMBER OF THE PROTEIN KINASE D FAMILY OF SERINE THREONINE KINASES*." Journal of Biological Chemistry **276**(5): 3310-3318.
Sumara, G., I. Formentini, S. Collins, I. Sumara, R. Windak, B. Bodenmiller, R. Ramracheya, D. Caille, H. Jiang and K. A. Platt (2009). "Regulation of PKD by the MAPK p38δ in insulin secretion and glucose homeostasis." Cell **136**(2): 235-248.
Sumara, G., I. Formentini, S. Collins, I. Sumara, R. Windak, B. Bodenmiller, R. Ramracheya, D. Caille, H. Jiang, K. A. Platt, P. Meda, R. Aebersold, P. Rorsman and R. Ricci (2009). "Regulation of PKD by the MAPK p38delta in insulin secretion and glucose homeostasis." Cell **136**(2): 235-248.
Sun, H., E. C. Y. Chow, S. Liu, Y. Du and K. S. Pang (2008). "The Caco-2 cell monolayer: usefulness and limitations." Expert Opinion on Drug Metabolism & Toxicology **4**(4): 395-411.
Tan, H.-Y., S. Trier, U. L. Rahbek, M. Dufva, J. P. Kutter and T. L. Andresen (2018). "A multi-chamber microfluidic intestinal barrier model using Caco-2 cells for drug transport studies." PLOS ONE **13**(5): e0197101.
Tanti, J.-F., F. Ceppo, J. Jager and F. Berthou (2013). "Implication of inflammatory signaling pathways in obesity-induced insulin resistance." Frontiers in endocrinology **3**: 181-181.
Torres-Marquez, E., J. Sinnett-Smith, S. Guha, R. Kui, R. T. Waldron, O. Rey and E. Rozengurt (2010). "CID755673 enhances mitogenic signaling by phorbol esters, bombesin and EGF through a protein kinase D-independent pathway." Biochemical and Biophysical Research Communications **391**(1): 63-68.
Towler, M. C. and D. G. Hardie (2007). "AMP-Activated Protein Kinase in Metabolic Control and Insulin Signaling." Circulation Research **100**(3): 328-341.
Tschöp, M. H., J. R. Speakman, J. R. S. Arch, J. Auwerx, J. C. Brüning, L. Chan, R. H. Eckel, R. V. Farese, J. E. Galgani, C. Hambly, M. A. Herman, T. L. Horvath, B. B. Kahn, S. C. Kozma, E. Maratos-Flier, T. D. Müller, H. Münzberg, P. T. Pfluger, L. Plum, M. L. Reitman, K. Rahmouni, G. I. Shulman, G. Thomas, C. R. Kahn and E. Ravussin (2012). "A guide to analysis of mouse energy metabolism." Nature Methods **9**(1): 57-63.
Tso, P., A. Nauli and C. M. Lo (2004). "Enterocyte fatty acid uptake and intestinal fatty acid-binding protein." Biochem Soc Trans **32**(Pt 1): 75-78.
Turnbaugh, P. J., R. E. Ley, M. A. Mahowald, V. Magrini, E. R. Mardis and J. I. Gordon (2006). "An obesity-associated gut microbiome with increased capacity for energy harvest." Nature **444**(7122): 1027-1031.
Venardos, K., K. A. De Jong, M. Elkamie, T. Connor and S. L. McGee (2015). "The PKD inhibitor CID755673 enhances cardiac function in diabetic db/db mice." PloS one **10**(3).
von Wichert, G., T. Edenfeld, J. von Blume, H. Krisp, D. Krndija, H. Schmid, F. Oswald, U. Lother, P. Walther, G. Adler and T. Seufferlein (2008). "Protein kinase D2 regulates chromogranin A secretion in human BON neuroendocrine tumour cells." Cellular Signalling **20**(5): 925-934.
Wang, B., X. Rong, M. A. Duerr, D. J. Hermanson, P. N. Hedde, J. S. Wong, T. Q. d. A. Vallim, B. F. Cravatt, E. Gratton, D. A. Ford and P. Tontonoz (2016). "Intestinal

Phospholipid Remodeling Is Required for Dietary-Lipid Uptake and Survival on a High-Fat Diet." Cell metabolism **23**(3): 492-504.
Wang, C., H. Xu, S. Lin, W. Deng, J. Zhou, Y. Zhang, Y. Shi, D. Peng and Y. Xue (2020). "GPS 5.0: An Update on the Prediction of Kinase-specific Phosphorylation Sites in Proteins." Genomics Proteomics Bioinformatics **18**(1): 72-80.
Wang, F., A. B. Kohan, C. M. Lo, M. Liu, P. Howles and P. Tso (2015). "Apolipoprotein A-IV: a protein intimately involved in metabolism." J Lipid Res **56**(8): 1403-1418.
Webb, K. E., Jr. (1990). "Intestinal absorption of protein hydrolysis products: a review." Journal of Animal Science **68**(9): 3011-3022.
Wei, N., E. Chu, P. Wipf and J. C. Schmitz (2014). "Protein kinase d as a potential chemotherapeutic target for colorectal cancer." Molecular cancer therapeutics **13**(5): 1130-1141.
Weinberg, R. B., J. W. Gallagher, M. A. Fabritius and G. S. Shelness (2012). "ApoA-IV modulates the secretory trafficking of apoB and the size of triglyceride-rich lipoproteins." Journal of lipid research **53**(4): 736-743.
WHO. (2020). "Obesity and overweight." from https://www.who.int/en/news-room/fact-sheets/detail/obesity-and-overweight.
Williams, D. M., A. Nawaz and M. Evans (2020). "Drug Therapy in Obesity: A Review of Current and Emerging Treatments." Diabetes Therapy **11**(6): 1199-1216.
Woting, A. and M. Blaut (2018). "Small Intestinal Permeability and Gut-Transit Time Determined with Low and High Molecular Weight Fluorescein Isothiocyanate-Dextrans in C3H Mice." Nutrients **10**(6): 685.
Wren, A. M. and S. R. Bloom (2007). "Gut hormones and appetite control." Gastroenterology **132**(6): 2116-2130.
Xiao, Y., C. Wang, J.-Y. Chen, F. Lu, J. Wang, N. Hou, X. Hu, F. Zeng, D. Ma and X. Sun (2018). "Deficiency of PRKD2 triggers hyperinsulinemia and metabolic disorders." Nature communications **9**(1): 1-11.
Xiong, J., M.-f. Zhou, Y.-d. Wang, L.-p. Chen, W.-f. Xu, Y.-d. Wang and F. Deng (2016). "Protein kinase d2 protects against acute colitis induced by dextran sulfate sodium in mice." Scientific reports **6**: 34079.
Zhang, Z., V. Mocanu, C. Cai, J. Dang, L. Slater, E. C. Deehan, J. Walter and K. L. Madsen (2019). "Impact of Fecal Microbiota Transplantation on Obesity and Metabolic Syndrome-A Systematic Review." Nutrients **11**(10): 2291.
Zhu, Y., Y. Cheng, Y. Guo, J. Chen, F. Chen, R. Luo and A. Li (2016). "Protein kinase D2 contributes to TNF-α-induced epithelial mesenchymal transition and invasion via the PI3K/GSK-3β/β-catenin pathway in hepatocellular carcinoma." Oncotarget **7**(5): 5327.
Zhu, Z., Y. Zhang, X. Wang, X. Wang and S.-D. Ye (2020). "Inhibition of protein kinase D by CID755673 promotes maintenance of the pluripotency of embryonic stem cells." Development **147**(16): dev185264.
Zietek, T., E. Rath, D. Haller and H. Daniel (2015). "Intestinal organoids for assessing nutrient transport, sensing and incretin secretion." Scientific reports **5**(1): 1-10.
Zou, Z., F. Zeng, W. Xu, C. Wang, Z. Ke, Q. J. Wang and F. Deng (2012). "PKD2 and PKD3 promote prostate cancer cell invasion by modulating NF-κB-and HDAC1-mediated expression and activation of uPA." Journal of cell science **125**(20): 4800-4811.
Zugaza, J. L., J. Sinnett-Smith, J. Van Lint and E. Rozengurt (1996). "Protein kinase D (PKD) activation in intact cells through a protein kinase C-dependent signal transduction pathway." The EMBO journal **15**(22): 6220-6230.

8. ANNEX

8.1. List of abbreviations

µg	Microgram
µm	Micrometer
Abcg5	ATP Binding Cassette Subfamily G Member 5
Abcg8	ATP Binding Cassette Subfamily G Member 8
Acaa1	Acetyl-CoA Acyltransferase 1
Acad1	Acyl-CoA Dehydrogenase Medium Chain
ACAT	Acyl-CoA cholesterol acyltransferase
ADRB3	Adrenoceptor Beta 3
AKT	Protein kinase B
ALT	Alanine transaminase
AMPK	AMP-activated protein kinase
APOA1	Apolipoprotein A1
APOA4	Apolipoprotein A4
APOB48	Apolipoprotein B48
APOC	Apolipoprotein C
APOE	Apolipoprotein E
APS	Ammonium peroxidisulphate
ARFRP1	ADP Ribosylation Factor Related Protein 1
ARL1	ADP Ribosylation Factor Like GTPase 1
Asbt	Apical Sodium Dependent Bile Acid Transporter
AST	Aspartate transaminase
ATP	Adenosine Triphosphate
Baat	Bile acid-CoA:amino acid N-acyltransferase
Bacs	Bile acyl-CoA synthetase
BAT	Brown Adipose Tissue
BMI	Body Mass Index
BMP7	Bone Morphogenetic Protein 7
BSA	Bovine Serum Albumin
$CaCl_2$	Calcium chloride
Caco2	Human colon epithelial cancer cell line
CAK	CDK-activating kinase
CAMK	Calcium/calmodulin-dependent protein kinase
CCK	Cholecystokinin
CD36	Cluster of differentiation 36
cDNA	Complementary DNA
CID755673	2,3,4,5 tetrahydro-7-hydroxy-1H-benzofuro(2,3-c) azepin-1-one
CIDEA	Cell Death Inducing DFFA Like Effector A
CIDEC	Cell Death Inducing DFFA Like Effector C
CKM	Creatine kinase M-type
Clps	Colipase

cm	Centimeter
CPM	Counts per minute
CREB	cAMP-response element-binding protein
CRT	CRT0066101
CRT0066101	2 (4 (((2R) 2 aminobutyl)amino) 2 pyrimidinyl) 4 (1 methyl 1H pyrazol 4 yl) phenol dihydrochloride
Csd	Cysteine sulfonic acid decarboxylase
Cyp7a1	Cholesterol 7α-hydroxylase
Cyp8b1	Sterol 12-Alpha-Hydroxylase
DAG	Diacylglycerol
DAPI	Prolong Gold Antifade Mountant with 4’,6-Diamidino-2-Phenylindole
DGAT1	Diacylglycerol O-Acyltransferase 1
dL	Deciliter
DMEM	Dulbecco's Modified Eagle Media
DMSO	Dimethyl Sulfoxide
DNA	Deoxyribonucleic acid
DNTP	2'-Deoxynucleoside 5'-Triphosphate
DPBS	Dulbecco's Phosphate-Buffered Saline
DTT	1,4-Dithiothreitol
ECL	Enhanced Chemiluminescence
EDTA	Ethylenediaminetetraacetic Acid
Ehhadh	Enoyl-CoA Hydratase And 3-Hydroxyacyl CoA Dehydrogenase
ELISA	Enzyme-linked immunosorbent assay
EPIWAT	Epididymal white adipose tissue
ER	Endoplasmic reticulum
FABP	Fatty Acid Binding Protein
FATP	Fatty Acid Transport Protein
FBS	Foetal Bovine Serum
FFA	Free Fatty Acid
G	grams
GAPDH	Glyceraldehyde 3-phosphate dehydrogenase
GLP-1	Glucagon-Like Peptide-1
GLUT	Glucose Transporter
GPCRS	G-Protein Coupled Receptors
GSIS	Glucose stimulated insulin secretion
GTT	Glucose Tolerance Test
gutΔ/Δ	Villin-Cre flox/flox
h	Hour
H&E	Hematoxylin and eosin
HCl	Hydrochloric acid
HDAC	Histone deacetylase
HDL	High density lipoprotein
HFD	High-Fat Diet

HRP	Horseradish peroxidase
Hypoth.	Hypothalamus
i.p.	Intraperitoneal
IF	Immunofluorescence
IgG	Immunoglobulin G
IHC	Immunohistochemistry
ITT	Insulin Tolerance Test
ki/ki	Knockin/knockin
KJ	KiloJoules
LDL	Low density lipoprotein
LDS	Lithium Dodecyl Sulfate
LP(a)	Lipoprotein a
LPL	Lipoprotein lipase
LTT	Lipids Tolerance Test
M	Molar
MeOH	Methanol
mEq	miliequivalent
MFI	Mean fluorescent intensity
mg	Miligram
MG	Monoglycerides
$MgCl_2$	Magnesium chloride
min	Minute
MK5	Map Kinase-Activated Protein Kinase 5
mL	mililiter
MOGAT2	Monoacylglycerol acyltransferase 2
MTTP	Microsomal triglyceride transfer protein
Myh1	Myosin Heavy Chain 1
MYH2	Myosin Heavy Chain 2
NaCl	Sodium chloride
NaOH	Sodium hydroxide
ND	Normal Diet
NEAA	Nonessential Amino Acids
NEFA	Non-Esterified Fatty Acids
ng	nanogram
NMR	Nuclear Magnetic Resonance
NP-40	Nonidet P-40
NPC1L1	Niemann-Pick C1-Like 1
OA	Oleic acid
Ostα	Organic solute transporter alpha
Ostβ	Organic solute transporter beta
OTU	Operational taxonomic unit
P/S	Penicillin/Streptomycin
PBS	Phosphate-Buffered Saline
PCK1	Phosphoenolpyruvate Carboxykinase

PCR	Polymerase Chain Reaction
PCTV	Prechylomicron transport vesicles
PEPT1	Peptide transporter 1
PFA	Paraformaldehyde
PGC-1a	Peroxisome Proliferator-Activated Receptor Gamma Coactivator 1-Alpha
pH	potentia hydrogenii
PKA	Protein Kinase A
PKC	Protein kinase C
PKD	protein kinase D
PKD2	Protein Kinase D2
PLA2	Phospholipase A2
PLK1	Serine/Threonine-Protein Kinase PLK1
Pnlip	Pancreatic Lipase
PPARα	Peroxisome Proliferator-Activated Receptor-Alpha
PPARγ	Peroxisome Proliferator-Activated Receptor-Gamma
PPI	Protease and Phosphatase Inhibitor
pPKD	Phospho Protein Kinase D
PRAK	P38-Regulated/Activated Protein Kinase
PRDM16	PR Domain Containing 16
PYY	Peptide YY
RER	Respiratory exchange rate
Rpl13a	Ribosomal protein L13a
RT	Room temperature
RT-qPCR	Quantitative Reverse Transcription PCR
SDS	Sodium Dodecyl Sulfate
SDS-PAGE	Sodium Dodecyl Sulphate-Polyacrylamide Gel Electrophoresis
SEM	Standard error of the mean
SGLT1	Na+-dependent glucose transporter
shNTC	shrna-Non-Targeting Control
shRNA	short Hairpin RNA
SLC6A8	Solute Carrier Family 6 Member 8
SR-B1	Scavenger Receptor Class B Member 1
SubWAT	Subcutaneous white adipose tissue
T2D	Type 2 Diabetes Mellitus
TAE	Tris-Acetate-Edta
Taut	Solute Carrier Family 6 Member 6 / Taurine transporter
TBST	Tris Buffered Saline with Tween
TEER	Transepithelial electric resistance
TEMED	Tetramethylethylenediamine
TG	Triglycerides
UCP1	Uncoupling Protein 1
UCP3	Uncoupling Protein 3
VLDL	Very-Low-Density Lipoproteins

WB	Western Blot
WHO	World Health Organization
wt/wt	wildtype/wildtype

8.2. List of figures

8.3. List of tables

8.4. Publications and presentations

8.4.1. Research articles

Trujillo-Viera J*, El-Merahbi R*, Schmidt V, Karwen T, Loza-Valdés A, Strohmeyer A, Reuter S, Noh M, Wit M, Hawro I, Mocek S, Fey C, Mayer AE, Löffler MC, Wilhelmi I, Metzger M, Ishikawa E, Yamasaki S, Hankir M, Seyfried F, Rau M, Geier A, Klingenspor M and Sumara G. Protein kinase D2 drives chylomicron-mediated lipid transport in the intestine and promotes obesity. EMBO Molecular Medicine. 2021.

Loza-Valdes A. Mayer A. Kassouf T. Trujillo-Viera J. Schmitz W. Dziaczkowski F. Leitges M. Schlosser A. Sumara G. A phosphoproteomic approach reveals that PKD3 controls PKA-mediated glucose and tyrosine metabolism. Life Science Alliance. 2021.

El-Merahbi R*, Trujillo-Viera J*, Loza-Valdes A, Kolczynska K, Reuter S, Löffler MC, Erk M, Ade CP, Karwen T, Mayer AE, Eilers M and Sumara G. Adrenergic-induced ERK3 pathway drives lipolysis and suppresses energy dissipation. Genes and Development. 2020.

Mayer AE , Löffler MC, Loza Valdes A, Schmitz W, El-Merahbi R, Trujillo-Viera J, Erk M, Zhang T, Braun U, Heikenwalder M, Leitges M, Schulze A, Sumara G. The kinase PKD3 provides negative feedback on cholesterol and triglyceride synthesis by suppressing insulin signaling. Science signaling. 2019.

Löffler MC, Mayer AE, Trujillo-Viera J, Loza Valdes A, El-Merahbi R, Ade CP, Karwen T, Schmitz W, Slotta A, Erk M, Janaki-Raman S, Matesanz N, Torres JL, Marcos M, Sabio G, Eilers M, Schulze A, Sumara G. Protein kinase D1 deletion in adipocytes enhances energy dissipation and protects against adiposity. EMBO J. 2018.

Trujillo-Viera J*, El-Merahbi R*, Nieswandt B, Stegner D, Sumara G. Phospholipases D1 and D2 suppress appetite and protect against overweight. PLOS ONE. 2016.

* Equal contribution

8.4.2. Oral presentations

Protein Kinase D2 promotes intestinal fat absorption and contributes to diet induced obesity. 3rd Central European Biomedical Congress. Krakow, Poland. September 2018.

Protein Kinase D2 promotes intestinal fat absorption and contributes to diet induced obesity. RVZ Retreat. Bad Brückenau, Germany. September 2018.

8.4.3. Posters

Unravelling ubiquitin-dependent signaling regulating function of adipocytes. EMBO practical course: New approaches to study Ubiquitin and Ubiquitin-like modifications. Alghero, Italy. September 2016.

Unravelling ubiquitin-dependent signaling regulating function of adipocytes. EUREKA. GSLS. University of Wuerzburg. October 2016.

Protein Kinase D2 promotes fat accumulation with detrimental metabolic consequences. EUREKA. GSLS. University of Wuerzburg. October 2017.

Protein Kinase D2 promotes intestinal fat absorption and contributes to diet induced obesity. EMBO Workshop: Organ crosstalk in energy balance and metabolic disease. Chiclana de la Frontera, Spain. April 2019.

Protein Kinase D2 promotes intestinal fat absorption and contributes to diet induced obesity. Mechanisms of metabolic syndrome. CSH. New York, USA. May 2019.

Targeting Protein Kinase D2 inhibits fat absorption and counteracts obesity. EUREKA. GSLS. University of Wuerzburg. October 2019.

8.5. Acknowledgments

I would like to express my gratitude towards the people and institutions that made possible the development of this thesis.

Firstly, I would like to thank the University of Wuerzburg and the master's program "FOKUS Life Sciences" for opening the doors for me to come to Germany and continue with my studies in the first place. Also to the GSLS for the big efforts they do to help all of us, PhD students, during this time.

Big thanks to Dr. Grzegorz Sumara, who accepted me in his laboratory from my master thesis and offered me a position to continue with my PhD. Thank you for believing in me and for your scientific support through the last years. His constant and hard work have built a solid group always expanding and trying to solve important scientific questions in the field of metabolism. I am proud to have been part of AG Sumara.

I would like to thank Prof. Dr. Hermann Schindelin, who always supported and advised my work even when there were unexpected changes or delays. Also thanks to Dr. Alexandros Vegiopoulos, who unfortunately could not supervise my thesis until the end but gave me great input during the beginning of my thesis. Special thanks to Dr. Mohamed Hankir for accepting to be my supervisor and always being very helpful when I need him. Thank you for offering me your expertise and also important samples necessary for developing this thesis. For these samples, I would also like to thank Prof. Dr. Geier, Dr. Rau and Dr. Seyfried.

This work would not have been possible without the help of our collaborators who offered me tools and expertise. From the Imaging Core Facility of the Biozentrum University of Wuerzburg, Prof. Dr. C. Stigloher and especially to Claudia Gehrig-Höhn. From the German Institute of Human Nutrition Postdam, thanks to Dr. Annette Schuermann and Dr. Ilka Wilhelmi for teaching me one of the main in-vitro techniques used during this thesis. All the kind people in the laboratory of Dr. Marco Metzger in the Fraunhofer Institute for Silicate Research, Wuerzburg. From the University of Osaka, I would like to thanks Prof. Dr. S. Yamasaki and Dr. Eri Ishikawa for sharing the mice model with us and doing all the work implied in the export process.

Thanks to the people in the ZIEL Core Facility Microbiome/NGS at the Technical University of Munich for their help with the microbiota analysis. Also to Prof. Dr. M. Klingenspor and the members of his team: Akim and Sabine. It has been a very successful collaboration, which hopefully continues over time.

This study was possible due to the funds from European Research Council (ERC), the German Research Foundation (DFG), and the Dioscuri Centre of Scientific Excellence. Thank you very much.

The process of my PhD was not only a journey through science but also through life. Several years have brought many important people in my life. Some of them transitory and some others for life. For all of them I feel immense gratitude.

My gratitude to my colleagues and friends. Mona, Manuela, Alexander, who not only offered support and expertise but also many enjoyable times out of work in BBQs, trips and parties. Thanks to Till for standing with me as the last members of AG Sumara in Germany and becoming a friend to me, we have made the best out of the last year. Of course, thanks a lot to my friend Rabih, who started as my mentor and has become like a brother to me. We have had great times together and there are more to come. Thanks to Angel for being a great support as a scientist but also as a friend. Having you in the lab makes me feel a bit closer to home. I miss you here. Finally to Vanessa who was literally my left hand in one of the most intense parts of this project. Thanks to my students, especially Minhee. I think we learned from each other.

I will always be thankful for being part of the FOKUS family. Thanks to Mano and David, and especially to Xidi and Ramon for being my family in Germany and my “accomplices” in life. There will always be a space in my heart and life for you.

I am also grateful to my friends out of the lab. Daniel, Camila, Carla, Hanaa, Raluca, Steffi, Philipp, Albert, Gali, Beatriz, Cristina and others that I might forget at this moment. Special thanks to Carito, I pray for your recovery.

To Alejandro, thanks for being part of my life, for your daily support, for comforting me when I lose hope and enthusiasm. You have made this process much easier. I hope I can pay back.

Lastly, thanks to my family. Especially to my siblings and my parents. They are behind all I have done and all I will do with my life. They have always supported me in all the

possible and impossible ways. From my parents I learnt to work hard, to believe in myself, to be responsible and to have goals in life. They also taught me to follow all my dreams, even if that implies having them thousands of kilometres apart. It is not easy to be far from you but all of this has been worthy. This thesis is dedicated to both of you.

8.6. Curriculum Vitae

8.7. Affidavit

I hereby confirm that my thesis entitled “Protein kinase D2 drives chylomicron-mediate lipid transport in the intestine and promotes obesity” is the result of my own work. I did not receive any help or support from commercial consultants. All sources and/or materials applied are listed and specified in the thesis.

Furthermore, I confirm that this thesis has not yet been submitted as part of another examination process neither in identical nor in similar form.

Würzburg, July 2021 _____

Jonathan Trujillo Viera

8.8. Eidesstattliche Erklärung

Hiermit erkläre ich an Eides statt, die Dissertation "Die Proteinkinase D2 treibt den Chylomicron-vermittelten Lipidtransport im Darm an und fördert Fettleibigkeit“ eigenständig, d.h. insbesondere selbstständig und ohne Hilfe eines kommerziellen Promotionsberaters, angefertigt und keine anderen als die von mir angegebenen Quellen und Hilfsmittel verwendet zu haben.

Ich erkläre außerdem, dass die Dissertation weder in gleicher noch in ähnlicher Form bereits in einem anderen Prüfungsverfahren vorgelegen hat.

Würzburg, Juli 2021 _____

Jonathan Trujillo Viera